Towards Environmentally friendly Wastewater Treatment - Photocatalytic Degradation of Reactive Blue-19 under visible light

A thesis submitted in partial fulfillment of the requirements for the degree of

Masters of Science

in

Chemistry

at University of Canterbury

by

Muhammad Sikander Hussain

2016

ACKNOWLEGMENTS

All praises to Almighty Allah, the most Gracious and Merciful and Creator of the universe. Many thanks to Him who bestowed us the perfect code of life through His last Prophet Muhammad (S.A.W).

I would like to take this opportunity to express my sincere gratitude to many people who helped me with this project. First and foremost, my thanks go to my supervisors, **Dr. Vladimir Golovko** for his gaudiness, help and financial support. I consider myself very fortunate to work under the kind supervision and his valuable guidance, scholarly inputs and consistent encouragement during my research work are very much appreciated, without which I would surely never have completed this task. It would have been next to impossible to finish this thesis writing without their continual guidance and commitment.

Thank you to Higher Education Department Govt. of Punjab Pakistan and British Council for collaborative scholarship, by which I have had the experiences of studying and living here in Christchurch, New Zealand. I would also be thankful to University of Canterbury for their Master scholarship for thesis.

I would especially like to thank Mr. Rohan Hudson for providing me the XPS results and Mr. Julion for TEM. Nick Oliver and Danny Leonard from the Mechanical Workshop, Wayne Mackay for Electronics Workshop, Alistair Duff lab manger**,** and Steven Graham from the West Precinct Electronic Workshop, as well as Robert McGregor from the Glassblowing workshop, for their excellent collaboration in maintaining the photocatalytic chamber, without which the project would not have been possible. Thanks also go to Dr. Matthew Polson for helping me in all instrumentation facilities. My thanks go to Mr. Thomas van Workum, Mr. Iman Hashemi and Mr. Vivek Balachandran, my fellows and senior colleagues, who helped me during my critical times.

I am greatly appreciative of academic, technical, and administration staff of the Department of Chemistry at the University of Canterbury, for being so helpful and friendly in taking care of my academic welfare.

My heartfelt appreciation goes to my friends, Mr. Rendy, Mr. Faiz and Mr. Sana for their friendship showing me New Zealand and their moral support especially during this challenging time. Last but not the least, I remember with gratitude my family members especially my dad and mom who were always a source of strength, support and inspiration.

LIST OF ABBREVIATIONS

µm	Micrometre
AAS	Atomic absorption spectroscopy
AATCC	Association of American textile chemists and colourists
AFM	Atomic Force Microscopy
AOP	Advance oxidative process
Au	Gold
a.u	Atomic units
BET	Brunauer–Emmett–Teller
cm	Centimetre
DLS	Dynamic Light Scattering
DSSC	Dye sensitized solar cell
EM	Electron microscopy
EPR	Electron paramagnetic resonance
HBP	High binding-energy peak
HOMO	Highest occupied molecular orbital
HRTEM	High resolution transmission electron microscopy
IC	Inorganic carbon
LBP	Low binding-energy peak
LED	Light emitting device
LUMO	Lowest unoccupied molecular orbital
M	Molar
mg	Milligram
ml	Millilitre
mm	Millimetre
mM	Millimolar
MS	Mass spectrometry
m/z	Mass to charge ratio
nm	Nanometre

NMR	Nuclear Magnetic Resonance
NPs	Nanoparticles
P-25	Aeroxide P-25 commercially available TiO_2
PXRD	Powder X-ray diffraction
RB-19	C.I Reactive Blue 19 industrial dye
SDC	Society of dyers and colorists
SEM	Scanning Electron Microscopy
SPR	Surface Plasmon Resonance
TC	Total carbon
TEM	Transmission Electron Microscopy
TGA	Tharmogavimetric analysis
TOC	Total organic carbon
UHR-TOF	Ultra-high resonance –time of flight
UHV	Ultra-high vacuum
UV/Vis	Ultra Violet and Visible
UV-DRS	UV-vis diffuse reflectance spectroscopy
v/v	volume by volume
XPS	X-ray photo electron spectroscopy
XRD	X-Ray Diffraction

LIST OF ILLUSTRARIONS

LIST OF TABLES

Abstract

The presence of noble metals such gold have been reported to activate the photocatalytic performance of TiO_2 in the visible light. It is important because pristine TiO_2 alone can only be activated by UV light which comprises only 8% of the irradiation reaching Earth. To degrade pollutants discharge by the textile industries in waste water by light is essential for clean environment.

One of primary aims of this thesis is to test the hypothesis that augmenting standard TiO_2 photocatalysts with Au nanoclusters could show performance of a catalyst under blue light. For this, the photocatalytic activity of several Au_9 clusters based on Titanium dioxide (P-25-TiO_2) materials were evaluated by using photo degradation of an industrial dye Reactive Blue 19 (RB-19) as a model reaction. Three different loadings (0.17, 0.34 and 0.5 wt%) of (Au) gold nanoclusters $Au_9(PPh_3)_8(NO_3)_3$ were deposited on pristine P-25 TiO_2 and sulfuric acid washed P-25 TiO_2 as heterogeneous photocatalysts under UV and blue light. Post treatment was done to remove the ligands characterised by TEM, XPS. 30 mg of each catalyst was sonicated and dispersed in 100 ml of 0.08 g/L of RB-19 and subjected to UV and blue light.

It was found that the effect of Au_9 increased the photo catalytic degradation under blue irradiation (78%) while the only pristine P-25 was totally inactive in that wavelength. Interestingly, not only the rate of degradation increased but also the percentage degradation increased when acid washed P-25 TiO_2 used as catalyst. Au_9 with ligands clusters were loaded on acid washed P-25, the highest degradation was observed under the blue light with the 0.5 wt% highest percentage of loading during the study. While the degradation was lowered down in the case of, with respect to same loadings, Au_9 *as made* or *calcined* clusters when deposited on the support pristine P-25 TiO_2. It is infer that SO_4^{2-} on TiO_2 has 26% degradation under blue light.

Chapter 1 - Introduction

Pollutants discharge by the textile industries requires significant attention because some of the dyes typically used in the industry are difficult to degrade and constitute persistent pollutants in waste water. It is estimated that 80 kg of water are required to produce only 0.5 kg of textile product.[1,2] The process of dyeing is a major concern for this particular industry. Different types of dyes belong to various chemical classes are used in dyeing operation, resulting in an effluent containing a complex mixture of colour and potentially toxic chemicals. Approximately, during the colouring process, about 1- 20% of dyes are released as textile effluent.[3] To limit this environmental impact, the textile industries are required to minimize release of hazards chemicals which produce as a result of dyeing.[4] It is also important for dye developers to optimize dyes and dyeing conditions that increase adhesion of dyes on the textile fibres, and hence reduce the amount in effluent. In spite of the preventive measures, the effluent cannot be dye free. Hence treatment methods are required to remove waste products from water. In general, biological, physical or chemical traditional methods for cleaning are in practiced. These methods have been widely used in textile industries, but are still plagued with further secondary problems. Biological treatment are usually resistant to aerobic bio-degradation but are somewhat beneficial due to its low cost and simplicity [5,6,7] Physical treatment (such as filtration, adsorption or coagulation/flocculation) are on the other hand are effective, but bears from high operational costs for post treatment of solid and coagulated wastes.[7,8,9] UV light photo degradation is alternative but penetration of UV light compared to visible is much low in water.[10] Since all applied systems are currently in practice have their limitations. Development of a significantly improved method for wastewater treatment is of paramount challenge in long-term environmental viability of the textile industry.

The most applicable methods for decolouration is generally involve the oxidative degradation. Collectively these methods are known as advanced oxidation processes (AOPs). TiO_2-mediated photocatalysis is one example of an AOP. [6,11] In this process dye molecules are firstly adsorbed on the surface of TiO_2, photo-activated and degraded.

Titanium dioxide (TiO_2) has been assumed to be a promising heterogeneous photocatalyst due to its low-cost, capable of photocatalysing under mild operating

conditions and is able to degrade a wide spectrum of organic contaminants without side-reactions.[9,12] The most important property of titania is its inertness towards living things, chemically stable and non-toxic.[7] Due to theses remarkable characteristics, TiO_2 is consider one of the very few substances those are appropriate for the industrial application of AOP-mediated dye degradation.[10,13,14,15]

Additionally, the presence of noble metals such as silver,[16] platinum,[17] palladium,[17] and gold[17,18] have been reported to activate the photocatalytic performance of TiO_2 in the visible light. It is important because pristine TiO_2 alone can only be activated by UV light which comprises only 8% of the irradiation reaching Earth.[1] It is believed that photo-generated electron in the TiO_2 is trapped by the noble metal particles, leading to high efficiency of charge separation between conduction and valance band.[18,19,20] Among different noble metals, gold is believed to be one of the promising dopant in terms of increasing the photocatalytic activity of TiO_2 and enhancing dye degradation. Gold nanoparticles have been shown to possess the ability to activate oxygen from air, and thus they could potentially be used to decompose organic colourants.[21] Consequently, the use of toxic oxidants can be voided, which is environmentally beneficial. Therefore, the photocatalytic study of dye degradation catalysed by gold nanoparticles deposited on the surface of titania is important part of this study.

1.1 Effluent and the Environment

The main target of this thesis is to explore the development and application of photocatalysts for the decolourization of textile industry dyes in waste water through gold deposited titania. However, a complete understanding of the problem cannot be accomplished without enough knowledge about the chemistry of dyes and the colouration in textiles. This section, therefore introduces some of the basic chemical principles linked with coloured compounds, and a summary of the ways in which the chemical structure of a molecule shows its colour properties. This is then followed by a description of how dyes and pigments are classified. The discussion then will focus on the features of textile effluent, with a closer look at coloured effluent resulting from the dyeing process and its environmental effects.

1.1.1 An Introduction to Dyes and Colour

"Colours, are the smiles of nature" according to Leigh Hunt a 19th-century poet. Our

moods and emotions are directly influenced by both natural and synthetic colours. In contrast, the presence of colour can be problematic in some cases where nature does not allow like colour in an effluent. In scientific terms, colour is actually light.[22] Colour is a psychological process of human sensation, read in the brain when light of a particular wavelength (see Figure 1) stimulates by the retina of our eyes. An object will appear coloured if it selectively absorbs some wavelengths of light, and reflects or transmits others, within the visible region.[23] Table 1 presents a list of colours that result from light absorption and reflection of a substrate within the visible light spectral region.

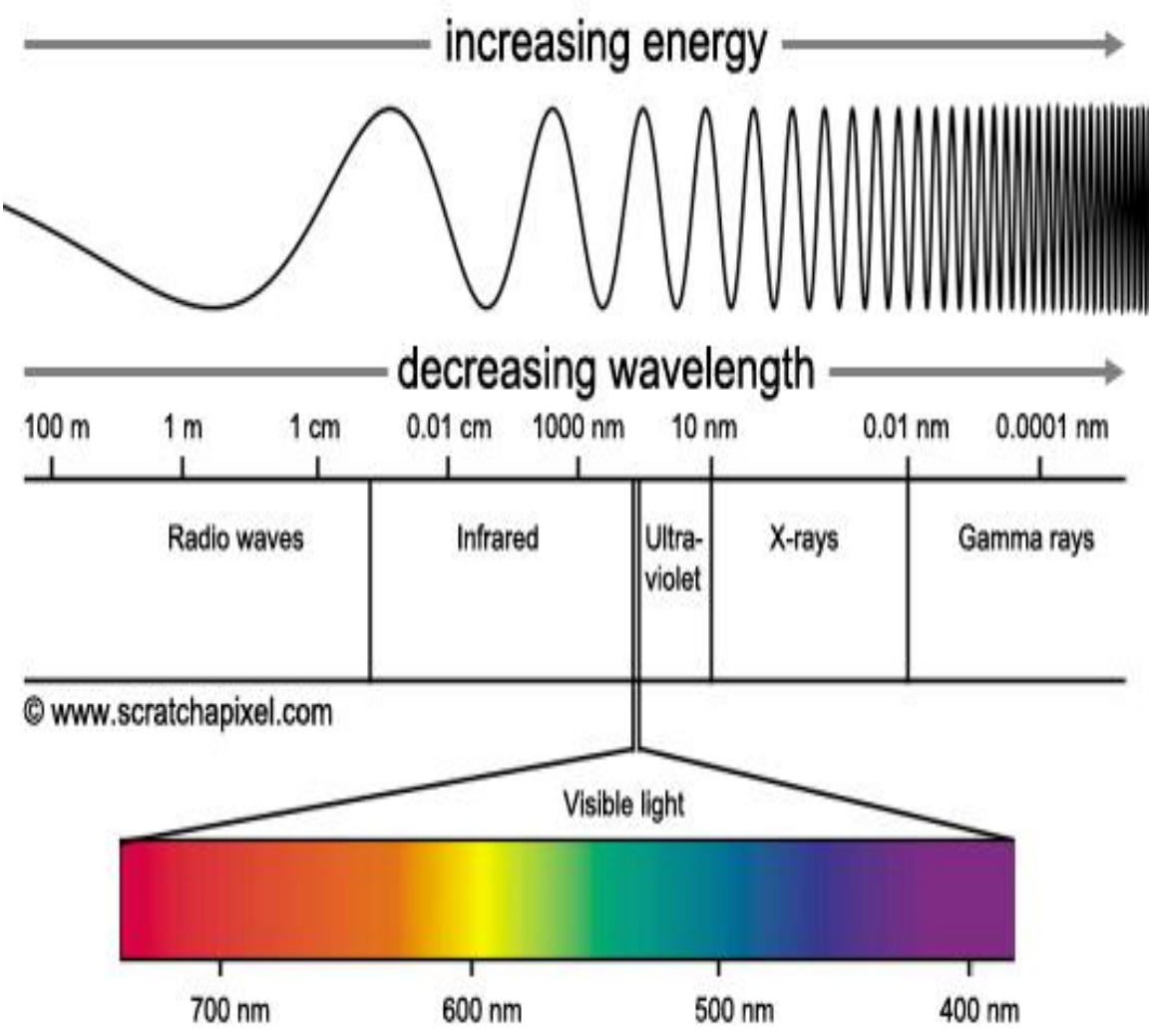

Figure 1: Visible Light Spectrum[1]

[1]Image was taken from http://www.scratchapixel.com/old/lessons/3d-basic-lessons/lesson-14-interaction-light-matter/light-as-a-wave/

Table 1: Spectral bands with colours absorption and reflections by a material viewed in white light [23]

Wavelength absorbed bands (nm)	Colour of the light absorbed	Visible colour of the reflected light (complementary colour)
400-440	Violet	Greenish-yellow
440-480	Blue	Yellow
480-510	Blue-green	Orange
510-540	Green	Red
540-570	Yellowish-green	Magenta
570-580	Yellow	Blue
580-610	Orange	Greenish-blue (cyan)
610-700	Red	Blue-green

There are fifteen specific causes of colour according to Nassau.[24] He arranged the colours on the basis of the physical and chemical principals that govern them into four categories:

(1) Colours cause by simple excitations and vibrations, that include incandescence, gas excitation, vibrations and rotations;

(2) Colours cause by ligand field effects as observed in transition metal compounds and impurities;

(3) Colours from transitions involving energy bands, as is the case with metals, semiconductors and colours from geometrical and physical optics, which include those generated from dispersion, scattering, interference and diffraction;

(4) Colours from transitions between molecular orbitals, which are generated by organic compounds such as dyes and pigments and by charge transfer.

In textile industries, colours are introduced into the materials as dyes or to a much lesser extent as pigments. Dyes and pigments can be classified by types of colourants – the substances capable of selectively change the reflection or transmission properties of a substrate. However, dyes and pigments show different type of behaviours when applied to different materials, and therefore have different toxicological and environmental features.[25] A dye, that is soluble in the solvent used in the application process and may be incorporated into a substrate through either physical or chemical (ionic, coordinative, or covalent) bonding. However, a pigment, is insoluble and has no substantively adhere to the matrial.[23,25] Sometimes these definitions are not true: for example, disperse and vat dyes are not soluble in water, but are consider as dyes due to the method in which they are introduced onto the textile fibres. Therefore, in addition to their solubility properties, it is always necessary to take into account the actual use to which the colourants are being put into.[11]

Previously, novel organic dyes were generally developed by the method of hit and trials. The dye manufacturers who attempted to synthesize organic dyes were tried the structures that were mimic to natural dyes.[25] Moreover, the association between colour and the chemical structure of a molecule had been considered of great concern until O. N. Witt proposed his dynamic approach in 1876, which was later followed by the others.[11,23] According to the Witt theory of colour, a molecule of dye must comprise both a *chromophore* (colour bearing) and an *auxochrome* (colour enhancer) centres attached to an aryl ring. Mitchell and Hewitt (1907) proposed that electronic conjugation in a system plays a vital role to develop the colour. In 1928, Dilthey and Witzinger combined all these concepts, suggesting that the auxochrome and chromophore are electron-donating groups and electron-withdrawing respectively, which are joined together through a conjugated system.[11,23]

UV-Visible spectroscopy is a useful analytic technique in determining the colour and concentration of a compound. Molecules containing non-binding valence electrons, such as pi-bonds, have unique properties that emit colour when excited by light. These light absorbing groups, chromophores, have energy difference between the higher and lower-occupied orbital, is directly related to a wavelength of light ($\lambda=h*c/\Delta E$). The wavelength that excites the electrons into a higher orbital is absorbed and gives the molecule its colour. Most dyes and pigments contain many chromophores conjugated together in order

to a molecule to absorb light in the visible spectrum. Auxochromes are functional groups attached to chromophores that modify the wavelength of absorbance of the chromophores but auxocrhromes do not produce any colours themselves. Often auxochromes are charged altering the electron cloud of the chromophores. Azo dyes contain many delocalized electrons and differing structures of the azo dyes yield unique colours. Colours seen by the eye are actually the wavelengths first absorbed and release back from the compound. So the colour seen is the complimentary colour of the colour absorbed. The detector uses UV light as well as visible light because not all absorbance occurs in the visible spectrum. [26]

A spectrophotometer uses these mentioned properties to determine the colour and concentration of compounds in a solution. For the spectrophotometer, a sample is prepared by placing a small amount of the solution in a cuvette. The cuvette has clear walls that allows light from the spectrophotometer to pass through the sample. The spectrophotometer then shines a range of wavelengths on the sample measuring the amount of light absorbed once it has passed through the sample. The amount of absorbance to the wavelength of light produces a plot with large peaks at wavelengths where the electrons raise to their excited state. That peak wavelength can be used to identify the compounds. If the concentration of the sample is known in the solution, the absorbance can be corrected to the molar absorbance. [26]

Chromophores are normally unsaturated groups like common chromophores include the thio (>C=S), azo (-N=N-), nitroso (-N=O) and nitro ($-NO_2$) and methano (R_1-CH=R_2), groups. To produce colour, it is necessary for an organic compound to have at least one center of chromophore on an aryl ring forming conjugating system.[25] For instant, introducing a nitro group into a benzene ring (colourless) gives a pale yellow substance, however the colour of azobenzene is orange-red. In addition, p-quinones are yellow, but o-quinones are orange or red both show different colours.

While commonly used auxochromes include -OR (alkoxy), $-NH_2$ (amino), -OH (hydroxyl) and - N-R (alkylated amino) groups. Through greater absorption of quantum yield these groups are all able to intensify the colour of the dye in a molecule. Nitroanilines, for instant, are more strongly coloured (deep yellow to orange) than nitrobenzene and aniline. An increasing ability of electron withdrawing or donating

power, or by the possibility of conjugation through auxochrome causes the absorption band to shift slightly towards longer wavelength. Such shift is referred to as a *bathochromic* shift, or a red shift. While a shift in the shorter wavelength is termed a *hypsochromic* shift, or a blue shift. Generally this applies to the most chemical classes of organic dyes, except for those that are not of the donor-acceptor type such as phthalocyanines.[11,25]

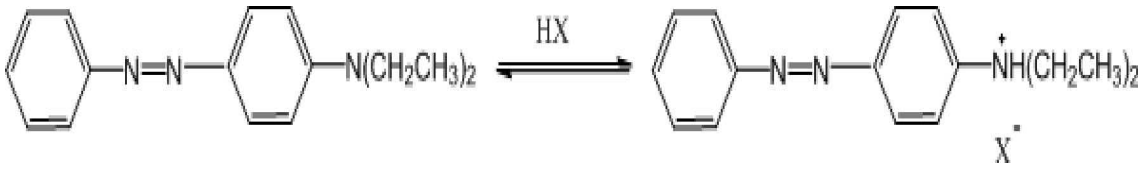

Figure 2: Protonation of N-N, diethylaminoazobenzene.

A more accurate agreement of the arrangement between colour and molecular structure is given by various modern electronic structure theories.[27] These theories are able to anticipate the transition energies of organic molecules by using mathematical equations and computer simulation. The molecular orbital method can provide precise understanding of the interaction between colour and chemical composition. Significantly, it also permits to predict the physical properties like colour without the synthesizing the dye itself.[11] For example, the azonium cation from N,N- diethylaminoazobenzene (Figure 2) can be a predict with specific intensity and colour to make by modifying the PPP-MO (PPP-MO is a self-consistent molecular orbital method specifically taking into account anti-symmetrisation and electron repulsion effects developed by Parises, Parr and People in 1953) parameters of the protonated N atoms. The analysed results in a bandwidth that are in agreement to experimental values.[25] The molecular orbital approach also useful for the analysis of halochromism (change in colour due to change in pH) like a complex bis-azonium ions with insulated chromogens.[28]

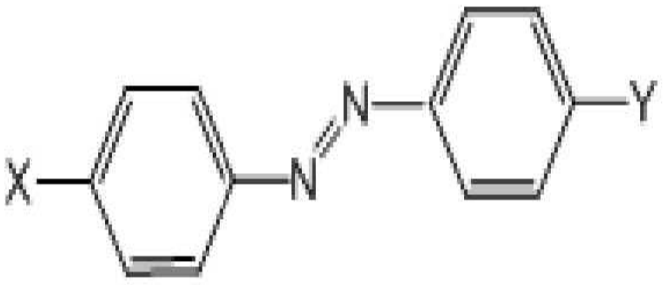

Figure 3: A molecule of azobenzene with two substituents X and Y.

Table 2: The effect of different substituent groups of azobenzene to its values[11]

Substituent X	Substituent Y	Wavenumber (nm)
H	H	320
NO_2	H	332
H	NH_2	385
H	NMe_3	407
H	NEt_2	415
NO_2	NEt_2	486

The difference in the energy between an excited and ground bands of a molecule determines the wavelength of light absorbed or quantized. The larger the difference between two states (HOMO and LUMO gap), the shorter the wavelength of comparatively high energy of the light absorbed and vice versa (Bohr-Einstein frequency relationship, AE=hc/X). Molecules in conjugation can stabilize the excitation state by delocalizing the excited electrons between bonded atoms.[29] Higher the conjugations will result in an increase in the wavelength of absorbed light by the molecule, changing the colour of the molecule. Hence, the resonance or conjugating system in a molecule of dyes determine its physical properties like colour. [11]

1.1.2 Classification of Dyes

Classification of dyes is usually based on the Colour Index (CI). It has been the most popular and well- known classification system of organic pigments and dyes since 1924. The second and third revised editions of Colour Index, compiled jointly by the Society of Dyers and Colourists (SDC) and the Association of American Textile Chemists and Colourists (AATCC), is considered as a leading standard reference for colour classification internationally for industries and importing authorities.[23, 25]

The CI identification contains the class name, chromaticity, and a specific number for a molecule: for instant, CI Disperse Red 1, the first red dye in the disperse class. The name of the dye class is given in accordance with the different properties of the dyes.

Reactive dyes are named because the presence of reactive groups and consequently their excellent reactivity to form covalent bonding with cellulosic and protein fibres. Normally, reactive groups include: (1) an activated halogen substituents (Cl or F) that

undergo nucleophilic substitution reaction with a *cellulosate* anion; and (2) an activated unsaturated vinyl group that reacts with cellulose through an addition reaction.

Figure 4 presents CI Reactive Red 1 and CI Reactive Blue 19 as examples of different reactive groups.[30] The latter is mainly used in this study.

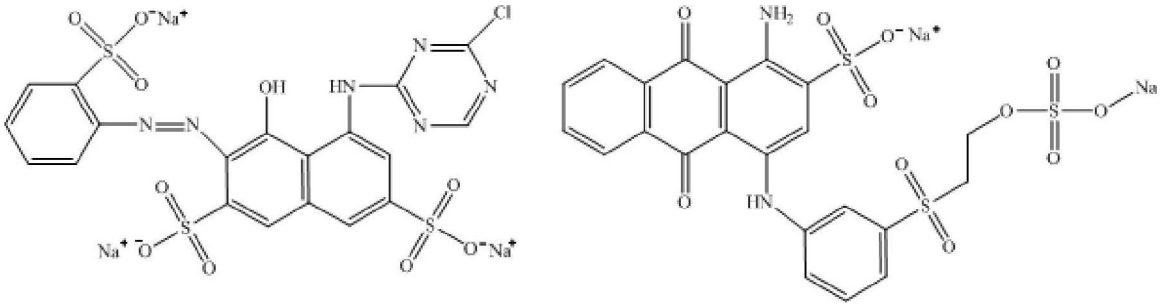

CI Reactive Red 1 CI Reactive Blue 19

Figure 4: Example of reactive dyes with triazinyl (left) and vinyl sulfone (right) reactive groups.

Some dyes are called as disperse dyes because they are applied onto fabrics in the form of dispersion in water. These dyes are generally used for polyester (a hydrophobic fibre). Other are basic and acidic dyes, named because having positive and negative charges.[31] Acidic dyes usually contain sulphonic groups in them having negative charges that attach to the protein fibres such as silk and wool that contain positive charge under acidic conditions. While basic dyes are classified by a delocalized positive charges and attract fibres such as polyacrylic and nylon.

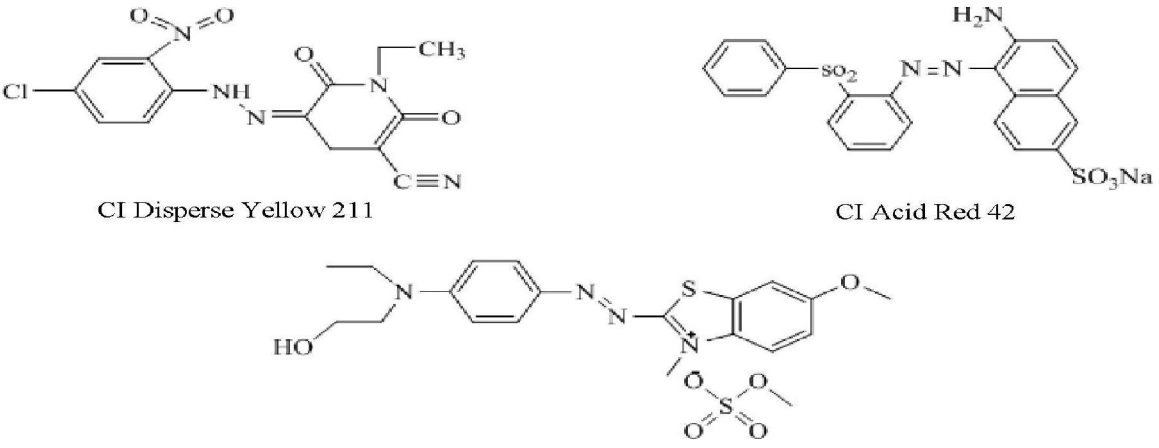

CI Disperse Yellow 211 CI Acid Red 42

CI Basic Blue 9

Figure 5: Yellow 211, CI Acid Red 42 and CI Basic Blue 9.

In addition to that, dyes can also arranged on the basis of their chemical components in the CI classification system. Azo dyes are considered as the largest chemical class of dyes, and account around 75-80% of all dyes produced by the industries around the globe. These dyes are globally in use, irrespective of their broad usage has been a questioned in the recent years due to safety concerns.

Colour Index recorded that there are 19 groups of generic-name and 25 structural classes of colourants.[25] The main classes of dyes based on method of application (generic name) and chemical constitutions are given in table 3.

Table 3: Classification of dyes according to application and chemical constitution

Classification according to method of application		**Classification according to chemical constitution**	
Generic name groups	Percentage of availability in commercial use	Chemical classes	Composition of total
CI Acid dyes	55%	Azo	~80%
CI Direct dyes	40%	Anthraquinone	15%
CI Disperse dyes	60%	Triarylmethane	3%
CI Reactive dyes	75% (continue to progress)	Phthalocyanine	2%
CI Basic dyes	60% (continue to progress)	Other minor classes (e.g. indigoid, quinophthalone, aminoketone, formazan, nitro, nitroso, etc.)	Less than 1%
CI Solvent dyes	60% (continue to progress)		
CI Pigments	60% (continue to progress)		
CI Vat dyes	45% (in decline)		
CI Mordant dyes	33% (in decline)		
Other minor groups (e.g. CI food dyes, CI fluorescent, brighteners etc.)			

1.1.3 Colour in Dyeing Effluent and Its Effect on the Environment

During the colouration process, a proportion of the dye or the pigment may discharged into surrounding waters because of not properly affixation onto the textile fibres. Thus, some degree of high intense colour in the dye can even a minor exhaust cause to show an obvious appearance of colour in discharged water bodies. A typical limit of visibility of coloured release in a water bodies varies between 0.1 to 1 g/L of dye, depends on colour, degree and illumination of clarity of water. In pure water, a reactive dye solution with a concentration of as small as 0.005 mg/L may be obvious, particularly if the dye is red or violet in colour. [25]

The effluent depends mainly on the dye used in the process and the intensity of shade.[32] For example, various textile industries in Pakistan have seen with the product of deep-coloured (e.g. dark red, navy blue and maroon) on cotton materials, polyester or percentage combination of both cotton-polyester. Thus high concentrations of reactive and disperse dyes result in high concentrations of dyes in discharged wastewater bodies.

The colour intensity for reactive dyes is comparable with other dyes in the effluent, because of their low rates of attachment on the textile fibre *(ca.* 50%-70%,[33]). Due to high solubility and reactivity of these dyes towards water, the fixation rate for reactive dyes is low during the dyeing process. This dynamic process of fixation and hydrolysis results in a low affinity for the fibres.

Technological and economic elements may also play a crucial role in the textile effluent.[32] Modern textile dyes are synthesized to increase their chemical stability, which gives them a good glow in water, soap, sunlight exposure and other environmental conditions such as bleach and perspiration. Now a days, antimicrobial agents are in practice for natural fibres such as cotton and wool can normally resist degradation, ultimately, hinder the process of removing dyes from textile wastewater.

In presence of other pollutants and chemicals in the coloured wastewater may become a source of other dangerous by-products through oxidation, hydrolysis, or other chemical reactions.[32] The major questions regarding the environmental impact of dyes and their hazardous residues have been putting on the table since industrial revolution. The question like at what possible concentration in wastewater possess a minimal hazard for the marine and aquatic life? A Debate is carry on concerning the issue because of organic

dyes have demonstrated toxicity to fish and other organisms. The toxicity is represented in terms of the value of LC_{50} - the concentration of substance required to kill half of the organisms exposed. It is reported that many types of dyes are observed as non-toxic within 24 hours LC_{50} > 100 mg/L, whereas the other dyes containing Cu element are considered to be toxic (24 hours LC_{50} > 6.0 mg/L and 48 hours LC_{50} > 3.6-6.0 mg/L).[34,35] Other researchers also suggest that biological toxicity in wastewater originates mainly from those dyes containing copper element.[36] However, it has been studied that wastewater containing dye has a substantial effect on algae, an aquatic life-form vital to the marine ecosystem. It is evidence that the presence of dyes colour in effluent suppresses the growth of algae even at concentrations as low as 1 mg/L.[25]

Textile dyes fixed to fibres are considered non-toxic and simply safe for general public because consumers have no direct contact with the free dyes. However this is not the case for farmers- for those people related to agriculture, dyes cause a high risk of severe toxicity such as skin irritation and sensitization during irrigation. Furthermore, it is reported that high incidences of bladder cancer found in plant workers due to the long-term effects of certain textile dyes (containing benzidine and 2- naphthylamine). A report published that indicates about long time contact with these dyes is more harmful and can also be fatal for living things. That study was conducted on 414 workers involved in a dye manufacturing at different departmental sections and it was found that 21 of them were facing severe allergic reactions as well as occupational asthma.[37,38] For the common citizens, exposure will more likely occur through discharge of unattached dyes into waterbodies.

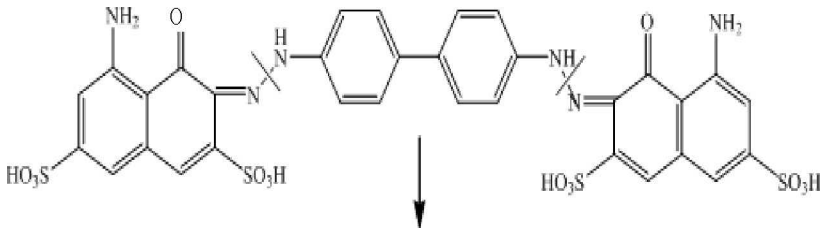

"':n^O~O_nhj

Figure 6: A typical example of water-soluble azo dyes that converts into metabolites dyes adopted from Gregory *et al.*[37]

The mechanism of N-hydroxylation, which can cause the carcinogenicity is shown in figure 6.[37] Benzidine and 2-naphthylamine, its metabolites may also cause cancer. The azo class of dyes, is an example of potential toxic dye that can cause cancer. They are not only biologically active because of the dye itself, but also due to their metabolites have potential for cancer.[39,40]

1.2. Titanium Dioxide and Photocatalysis

This section presents an introduction of titanium dioxide and its physical modification in association with photocatalytic activity. This will conclude with an overview of past reports on the photocatalytic decolourization of dyes in wastewater. These topics are introduced to lay the foundation for advance work and also for preliminary to the more detailed and comprehensive background to account of the deposition on titania and its application for the decolourization of wastewater dyes.

1.2.1 Characteristics of Titanium Dioxide

Titanium dioxide (TiO_2) is a semiconducting material and chemically activated towards light. It has a band gap of energy 3.0-3.2 eV, which is the same energy of near UV radiation (< 400 nm).[41] Since it is reported as a photocatalyst for the photo-splitting of water by Fujishima and Honda,[42] The photoactivity of titanium dioxide has been investigated in detail for its potential usage in different applications, ranging from photo-electrochromics and sensors to photovoltaics and photocatalysis. [42,43,44] Not only due to its prominent properties in photocatalysis, but also due to its low cost, high stability, and non-toxicity makes it an appropriate photocatalyst for commercial use.

TiO_2 commonly is also known as titania and P-25 Aeroxide, a commercially available form, that is efficient, harmless, stable and inexpensive, thus limiting the choice of convenient alternatives. [45] For catalytic purpose, titania has demonstrated promising results in photo oxidation [46], electrochemical applications [47], thermal catalytic decomposition [48] water gas shift [49], hydrodesulphurization [50] hydrogenation [51,52] and photo degradation. [53] TiO_2 exhibits in three major crystalline phases: rutile, anatase and brookite. Rutile is the most stable phase among these with small crystals < 11nm, anatase with relatively lager crystals size > 35nm and brookite in between these two.[44]

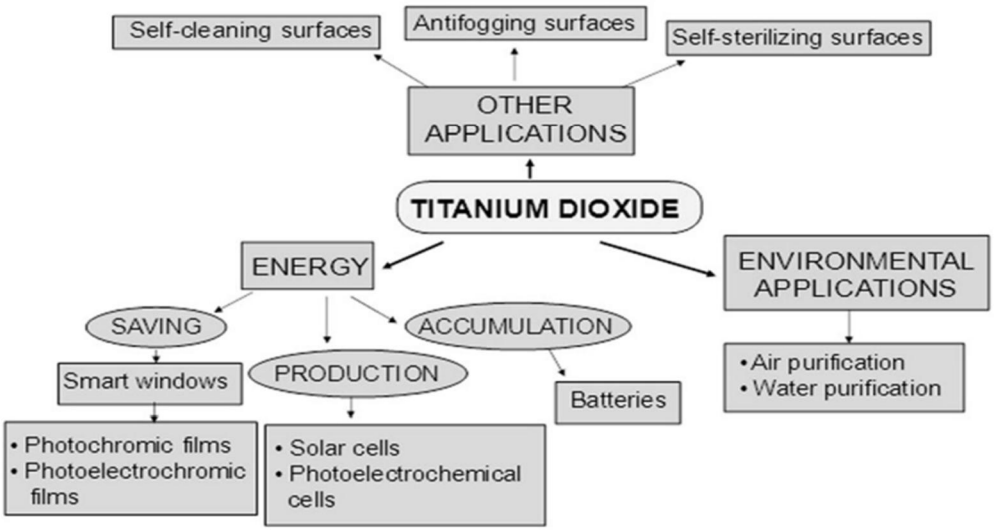

Figure 7: Applications of Titania related to catalysis adopted from Kominami *et al*. [48]

It mostly exists in two tetragonal forms, rutile and anatase. Brookite a rhombic form, that is extremely difficult to synthesize in the laboratory but both anatase and rutile can be readily prepared. These two forms of TiO_2 are frequently used in the most photocatalytic studies. Anatase appears to be more active among the two phases. This is probably due to differences in the extent and nature of the surface hydroxyl groups present at low temperature. [54] P-25 contains 70% anatase and 30% rutile whereas brookite is photocatalytically inactive. [55]

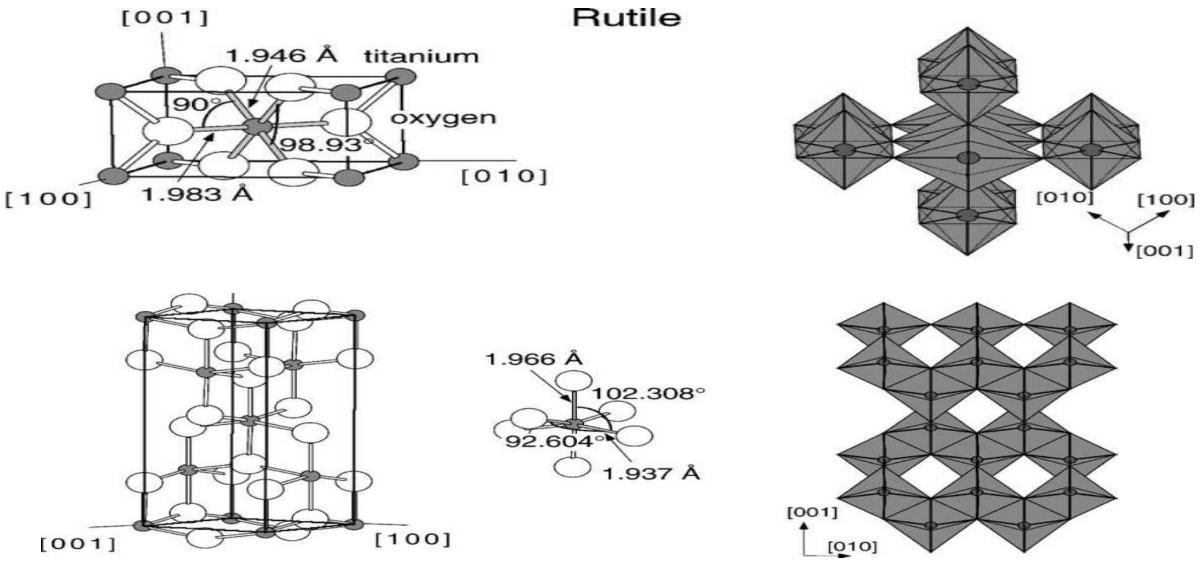

Figure 8: Bulk Structure of Rutile and Anatase TiO_2 (Image was taken from Diebold © 2002 Elsevier Science). [41]

Rutile is the most stable thermodynamically phase at elevated temperature.[56,57,58] Its structure can even be intact at temperature between 672-1072 K.[59] The surface reaction of the three crystal structures of TiO_2 are also different due to the surface enthalpies. On heating, anatase and brookite are convert to form rutile, but it also cause to alter energetics as a function of particle size.

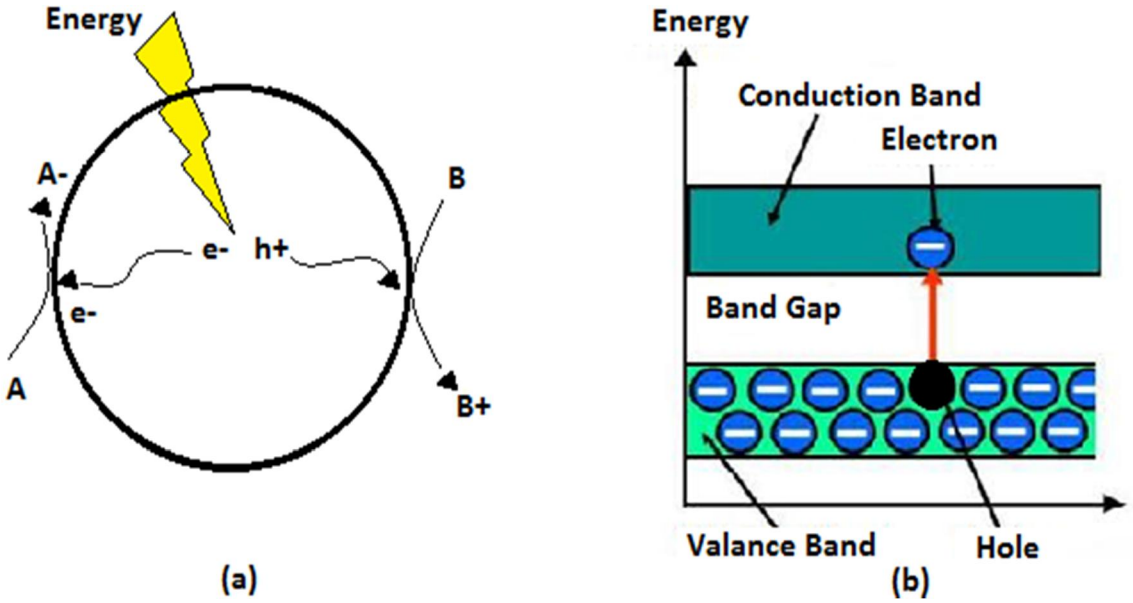

Figure 9: (a) Mechanism of Photo-catalysis for semiconductor materials with a hole and electron generation ($A^{-\ reduced}$ $B^{+\ oxidised}$ products). (b) Semiconductor with Conduction Band and Valance Band separated by Band Gap energy.

As a semiconductor, TiO_2 has a fully occupied valence band electrons but entirely empty conduction band, these bands are separated by a forbidden region called as "narrow band gap" of energies.[60,61] The absorption of a photon with an energy equivalent to or greater than its band gap difference (>3.0 eV) can promote an electron from the fully filled valence band into the empty conduction band, creating a polarization with an excited electron in the conduction band and hole in the valence band. However, one of two possible mechanisms may occur due to this opposite charge pair separation. [62]

(1) Reaction can occur on theses charge pair i.e. reaction of an electron donor at hole or acceptor at conduction band.

(2) Recombination of the photogenerated electron-hole pair, either radiatively or non radiatively.

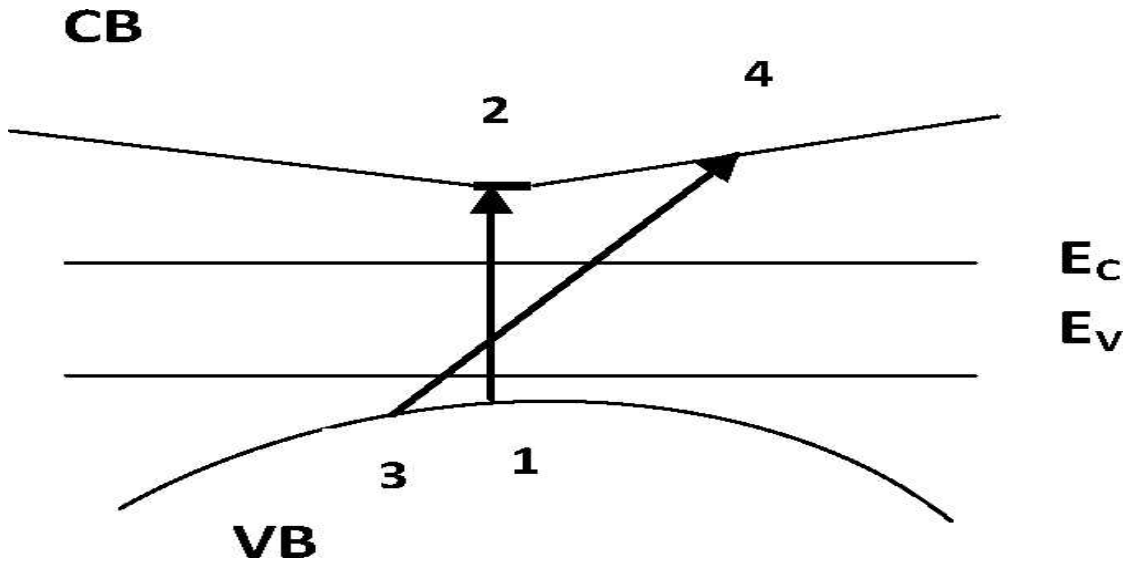

Figure 10: Schematic band structure of crystalline TiO_2 adopted from Barginsky *et al.* [63]

[E_v and E_c are the interface levels. The arrow indicates two ways that light absorption takes place: direct electron transition (1 to 2) and indirect (3 to 4) that occurs at the interface.]

In order to achieve a desirable photocatalytic activity, it is important for a semiconductor to be efficient and entrap energy from ambient light. TiO_2 is considered as an indirect semiconductor, and this mechanism of light absorption is through the interband electron transitions, but it is not so much effective as it is restrained by the symmetry of the crystal in case.[60,62] When the absorption of photon occurs momentum of the electron obtained from the electromagnetic energy is not conserved at the surface of a crystal, or at the interface between two crystals.[64]

Thus, it is far more effective for the TiO_2 crystal to engage light through indirect electron transitions mechanism. In small nanocrystals, porous and microcrystalline of TiO_2 semiconductors, a large dipole matrix element and high electron density in the valence band results in a large share of the interface atoms which allows for such indirect transitions (see Figure 10).[63] For crystallites with dimensions smaller than 20 nm, absorption of light on the crystal interface is the most important mechanism of absorption.

The band gap of bulk TiO_2 is narrower than that of nanomaterials TiO_2 because the former has a large overall dimension structure.[60] Hence, it can be observed that the size

and surface area of a TiO_2 particle are important in governing its chemical and physical properties and, as a result, in its overall function as a photocatalyst.

1.2.2 Deposition of Titanium Dioxide

There are some drawback properties of TiO_2 that hinder its effectiveness as a photocatalyst. The main practical barrier hindering titania and its marketing on an industrial scale is the bulk TiO_2 has wide intrinsic band gap - 3.0 eV for rutile and 3.2 eV for anatase. This can't allow its utilization of the major solar energy spectrum reaching earth surface, as these energy band gaps related to the energy of near-UV light (which is only 8% of the total energy radiated from the sun when reaches earth).[60] Over 30 years ago a TiO_2 based electrode produced hydrogen from water without decomposition under UV illumination. Insights have been recently achieved into the photochemistry of several important molecules involved in photocatalytic reactions, such as O_2, CO, methanol, H_2O and H_2 only under UV spectrum on TiO_2 surface. [42,43] But for large-scale applications, catalysts are desired that work efficiently with solar radiation containing about one half of visible light alongside a small contribution of UV light, both of which can be converted into chemical energy. [65]

Secondly, TiO_2 photocatalytic efficiency can be lowered by the un-excitation of the photoexcited electrons (recombination).[66] This limiting factor of TiO_2 of fast recombination, lowering the efficiency of the photo-catalytic process. [67] As shown by Figure 9, photoexcitation creates a region of positive charge density called as hole caused by the promotion of an electron from a site. Holes are positively charged nuclei and they hold a definite position in the crystalline lattice. Electrons from another source near the surface or from another site in the crystal can fill the hole, subsequently from an external cation, or from the drop of the original electron back into its original molecular orbital (recombination). Latter is highly undesired in photocatalysis. These defect sites in the lattice structure generate a lower quantum yield which can result in recombination centres and consequently, a poor efficiency for photocatalytic reactions.[68,69] The phenomenon can be illustrated by the scheme presented in Figure 11. Photoexcited electrons of the valence band can be captured either in the conduction band crossing whole barrier (a), or in a defect site close to the conduction band (shallow traps) (b)[57]

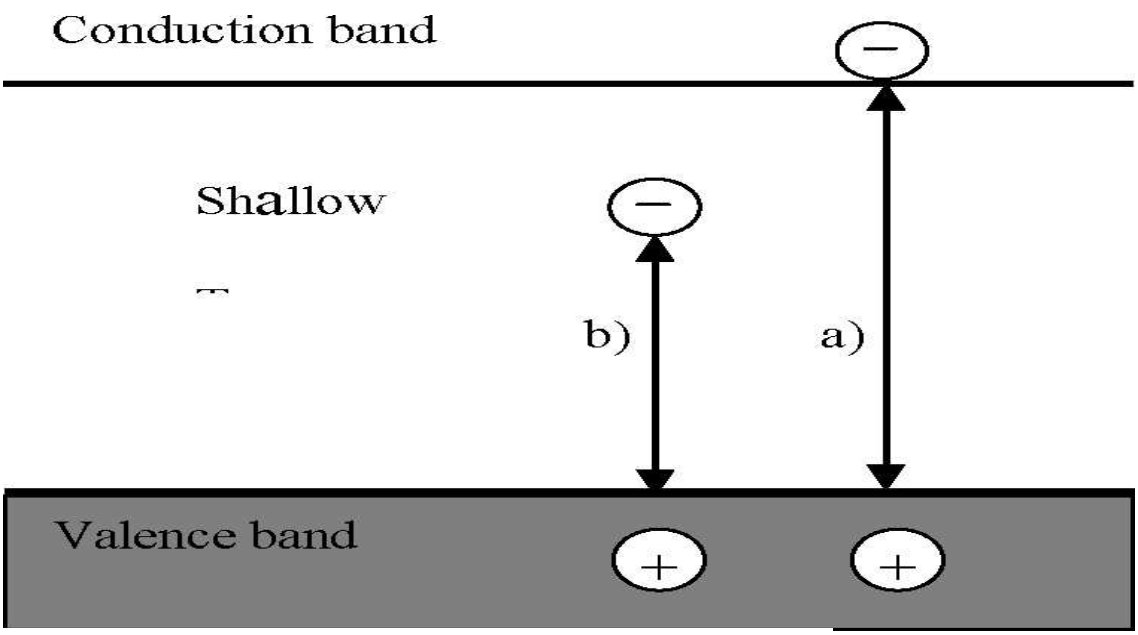

Figure 11: Scheme of UV-Induced Charge Separation in TiO_2 adopted from Sclafani *et al.* [57]

The studies also reported by different authors demonstrate that TiO_2 particles thickness inversely effects the both rutile and anatase phase of tutania catalysis, as it decreases the quantified charge diffusion. [68] Titania is only active in UV region due to its bandgap, so it is also important to introduce visible photo-response through inert noble metals to overlap the absorption with solar spectrum. [65]

In order to overcome these hurdles, recent researches are directed toward the catalysts in the form of immobilization of noble metals on the surface of titania to make the package as heterogeneous catalyst. Therefore it has been great interest in modifying TiO_2, either to shift the band gap into the visible light region and/or to prevent the direct recombination of photogenerated electron/hole pairs.[14,20,60,69] There are two major methods that have been proposed to modify the optical properties of TiO2:

(1) surface chemical modification (sensitization)

(2) bulk chemical modification (doping)

Sensitization is a method to treat the TiO_2 for production of photocurrent. This sensitizer may be any metallic, inorganic, or organic material. A variety of inorganic and organic dyes have been reported as sensitizers for TiO_2, particularly in the water splitting through dye sensitized solar cells (DSSCs).[71,72] In a DSSC, the sensitizer produces higher energy electrons than available in TiO_2 normally.[73,74]

The other commonly used process is doping used to narrow the band gap and change the electronic properties of titania. Titania is doped by other components, like organic or inorganic, into the bulk material, altering its optical activity. Chemically TiO_2 can be modified by substituting either the cations (Ti^{4+}) with other transition element or the anions (O^{2-}) with other anions like Cl^-. These changes finally affect the material's electronic properties and thermal stability.[44]

Non-metals raise the valence band to maximum energy level after doping with, normally non-metallic dopants are less electronegative than bonded oxygen atoms of TiO_2. While metallic elements doping lower the conduction band to minimum energy level, as most metals used in doping are more electronegative than Ti. Noble metal dopants (nanoparticle or nanocluster) may also act as sinks for the photogenerated charge carriers, and can support interfacial charge-transfer processes with inhibiting electron-hole recombination.[57,69,75]

In this thesis the catalysts consist of gold nanoclusters immobilized on the surface of P-25 (Au/TiO_2). This approach is related to metal doping, but the properties of TiO_2 after modification are conceptually different. In the vicinity of the noble metal (i.e. gold nanoclusters) titania (P-25) does not change the solid framework - instead, simply contact interfacial with the gold clusters. Here, the hypothesis is the gold nanoclusters on the P-25 surface will donate the photoexcited electrons to conduction band (e_{CB}~) under visible light (blue light LED ~>420) for reduction reaction and trap electron under UV light from conduction band so help to prevent the recombination of electron-hole pairs.

Among the different metals, gold nanoparticles/clusters have been widely used to enhance the efficiency of TiO_2, due to the excellent catalytic activity and selectivity of as heterogeneous catalysts. This activity mainly determined by their characteristics like shape, size, Au–titania interface, and Au–titania charge transfer.[67,76,77] The immobilization process further depends on the deposition methods and conditions, crystallographic phases, crystal surfaces, and surface defects and pores. The practical applications of supported Au-titania catalysts would be greatly enhanced if the morphology and size of deposited gold nanoclusters can be well assured during the deposition. [78]

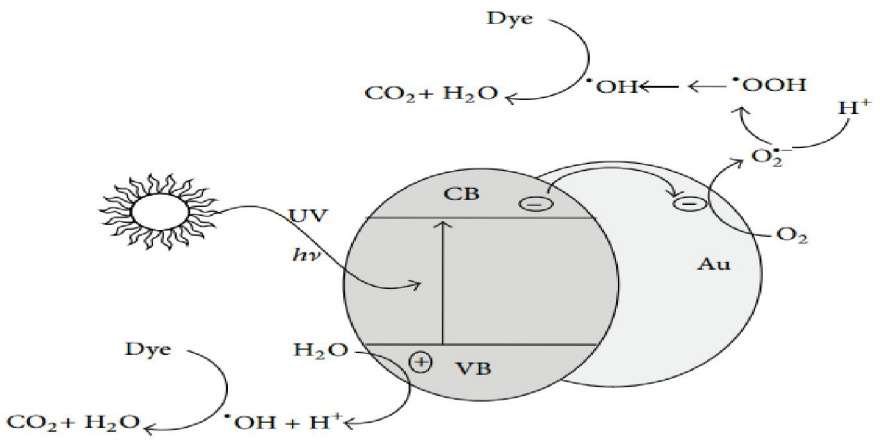

Figure 12: Mechanism of Photo-degradation under UV light through Au/TiO_2 adopted from Padikkaparambil *et al.*[79]

Recently, the integration of gold nanoparticles into semiconductors TiO_2, has emerged as a promising entrance to visible-light-active photocatalysts for many applications, such as decomposition of organic pollutants and selective oxidation and reduction reactions of organic compounds as well as for hydrogen generation from aqueous alcoholic solutions. [80]

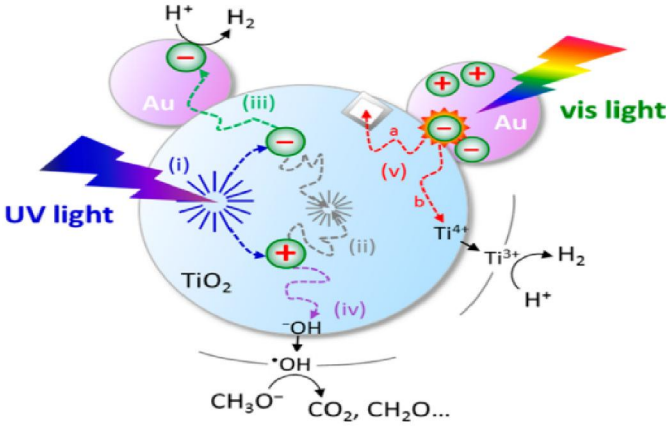

Figure 13: Photo-response of AuTiO_2 in a H_2O/MeOH Mixture adopted from Li *et al.* [80]

Chemically-synthesised and atomically precise ligand protected Au_9 clusters deposition on pristine and activated titania by sulfuric acid for degradation of industrial dyes have never been reported. Gold particles with a small size under 5 nm are known to be catalytically active. It is demonstrated that the catalytic activity of gold occurs with the loss of metallic characters of Au nanoparticles at around < 1 nm where each particle can be considered as a nanocluster. Such heterogeneous Titania based catalysts can be

activated by washing with solvents, $KMnO_4$ treatment, calcination and solvent extraction to remove all ligands. Removal of ligands can also be done under different environments i.e. under vacuum, O_2, O_2 followed by H_2 and ozone.[81,82] However, in some cases catalytic activity is associated with the ligands attached to clusters on the support. [80]

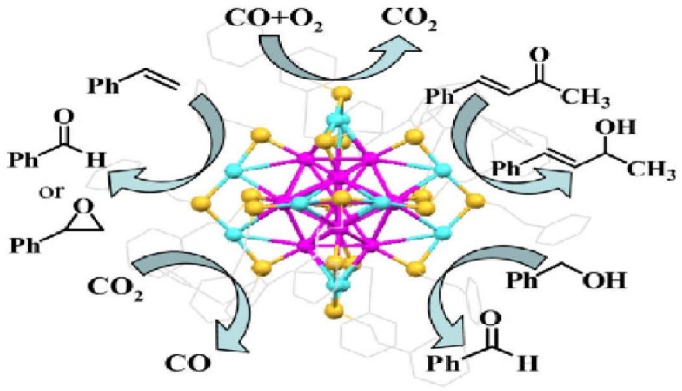

Figure 14: Catalytic activities of Gold nanoclusters adopted from Li *et al*. [80]

Detailed studies of pre-treated H_2SO_4 washed P-25 and post treatment of deposition with different loadings of gold nanoclusters $Au_9(PPh_3)_8(NO_3)_3$ on P-25 as heterogeneous photocatalysts under UV and blue light are the main focus in this research. Acid washed Titania has been showed vivid results with and without Au nanoclustes for different photo-catalytic experiments. [80,81]It is reported earlier that the clusters deposited on H_2SO_4 pre-treated P-25 show remarkable resistance to aggregation.[83] The effect of the interfacial TiO_2 with Au has been studied for degradation of dyes but the Au_9 with titania under visible light has not been explored.

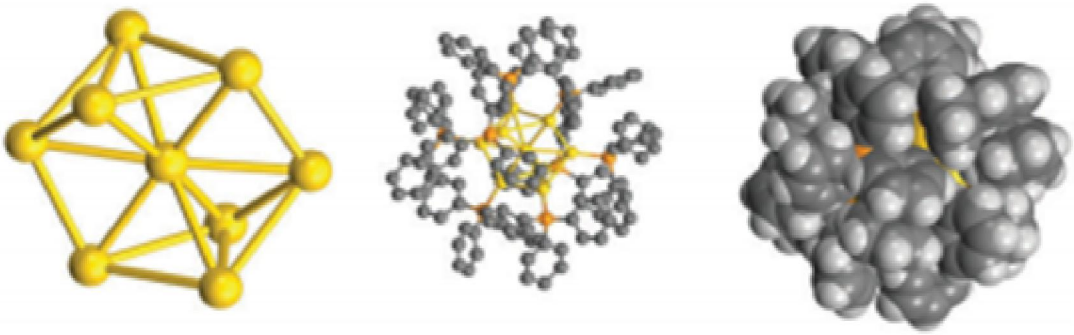

Figure 15: Ball and stick model, geometries of the metal cores model and space-filled models adopted from Anderson *et al*.[81]

1.2.3 Photocatalytic Degradation of Textile Dyes by TiO_2

TiO_2-mediated photocatalytic degradation of organic dye molecules via oxidation have been reported. TiO_2 significantly increases the rate of photodegradation of a wide range of organic dyes under mild operating conditions, and is able to mineralise a wide spectrum of organic contaminants.[48] The degradation of industrial dyes attracts significantly because effluent containing a complex mixture of coloured and potentially toxic compounds. To minimize the hazardous environmental impact of dyes, the amount of residual dyes must be degraded. Thus, the development of efficient post-dyeing wastewater treatment methods capable of removing coloured products from the water is of predominant importance. The industrial dyes are harmful when in large concentration and not only they disturb eco-system but also cause many diseases i.e. skin disorders, cancer and asthma to humans. [25,37]

During photogenerated electron-hole pairs may produce oxidant radical species such as superoxide, hydroxyl, or peroxide from redox reactions. These are actually initiate and capable of heterogeneous photodegradation of organic substrates including dyes near TiO_2 surface. It has been reported that these radicals will readily oxidize most azo dyes. [84,85,86] Reactions relevant to the photodegradation of organic dyes on the surface of TiO_2 are described in Scheme 2.

Scheme 1: Photo response at the surface of TiO_2[31]

$TiO_2 + h\nu \rightarrow e^- + h^+$ (Eq. 1)

$e^- + Ti(IV)O\text{-}H \rightarrow Ti(IV)O\text{-}H^-$ (Eq. 2)

$h^+ + Ti(IV)O\text{-}H \rightarrow Ti(IV)O^{\cdot}\text{-}H$ (Eq. 3)

$h^+ + \frac{1}{2}\, O^{2-}_{(lattice)} \rightarrow \frac{1}{4}\, O_2\,(g) + vacancy$ (Eq. 4)

$e^- + O_{2\,(surface)} \rightarrow O_2^{-}{}_{(surface)}$ (Eq. 5)

$O_2^{-}{}_{(surface)} + H^+ \rightarrow HOO$ (Eq. 6)

$h^+ + Ti(III)O\text{-}H^- \rightarrow Ti(IV)O\text{-}H$ (Eq. 7)

$e^- + Ti(IV)O^{\cdot}\text{-}H \rightarrow Ti(IV)O\text{-}H$ (Eq. 8)

$O_2^{-}{}_{(surface)} + Ti(IV)O\text{-}H \rightarrow O_{2\,(surface)} + Ti(IV)O\text{-}H$ (Eq. 9)

Scheme 2: Degradation of dye at the surface of TiO_2 [31]

$TiO_2 (h_{vB}^+) + H_2O \rightarrow TiO_2 + H^+ + OH\cdot$ (Eq. 10)

$TiO_2 (h_{vB}^+) + OH^- \rightarrow TiO_2 + OH\cdot$ (Eq. 11)

$TiO_2 (e_{CB}^-) + O_2 \rightarrow O_2^{-\cdot} + TiO_2$ (Eq. 12)

$O_{2\ (surface)}^{-\cdot} + H^+ \rightarrow HOO\cdot$ (Eq. 13)

Dye + $OH\cdot \rightarrow$ degraded products (Eq. 14)

Dye + $h_{vB}^+ \rightarrow$ oxidation product (Eq. 15)

Dye + $e_{CB}^- \rightarrow$ reduction products (Eq. 16)

Hydroxyl radical is a very strong oxidizing agent and the most reactive specie in case of degradation of azo dyes (Eq. 14).Those dyes which don't react with the hydroxyl radical can follow either reduction or oxidation pathways as shown by Eqs. 15 & 16, but these are overall less effective routes.[31]

Scheme 3: Excitation process in Au/TiO_2. [12]

$Au - TiO_2 (h\nu) \rightarrow Au - TiO_2 (h_{vB}^+) + Au - TiO_2 (e_{CB}^-)$ (Eq. 17)

$Au - TiO_2$ + Dye $\rightarrow$ products (Eq. 18)

$Au + (e_{CB}^-) \rightarrow Au (e^-)$ (Eq. 19)

$Au(e) + O_2 \rightarrow O_2^{-\cdot}$ (Eq. 20)

In the presence of gold nanoparticles on the surface of TiO_2, it is hypothesized[18] that the accumulation of e_{CB}^- in the gold sites producing Au(e–) (Eq. 19) can prevent the electron-hole pairs recombination. The lifetime of the charge separation is thought to be longer, thus, increasing the photocatalytic activity on the surface of TiO_2 (as shown in *Scheme* 1 and 2). In this case, the presence of oxygen and the superoxide anions, which are important species for photooxidation, can be formed (Eq. 20).

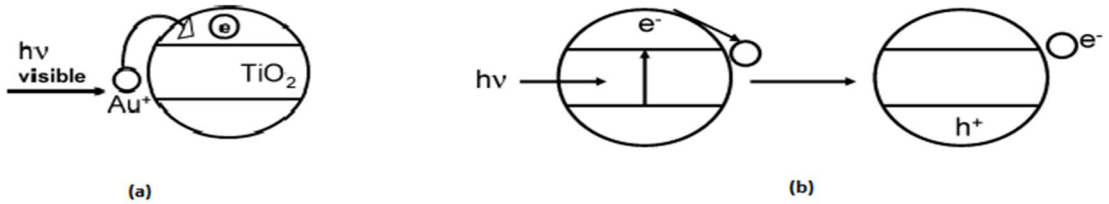

Figure 16: Photo response of $AuTiO_2$ a) visible b) UV adopted from Primo *et al.* [87]

In this thesis the catalysts consists of gold nanoclusters immobilized on the surface of P-25 (Au/TiO_2). This approach is related to metal doping, but the properties of TiO_2 after modification are conceptually different. In the vicinity of the noble metal (i.e. gold nanoclusters) titania (P-25) does not change the solid framework - instead, simply contact interfacial with the semiconducting P-25. Here, our hypothesis is that gold nanoclusters on the P-25 surface will donate the photoexcited electrons to conduction band (e_{CB}~) under visible light (blue light LED) for reduction reaction and trap electron under UV light from conduction band so help to prevent the recombination of electron-hole pairs.

1.3 Aims of Study

The main target of the project is to formulate an eco-friendly wastewater treatment photocatalyt for use in the textile industry, using a TiO2-based catalyst under solar irradiation. The present study may be divided into the following sections:

Systematic study of photocatalytic dye degradation of CI RB-19 an industrial dye, using different loadings of $Au_9(PPh_3)_8(NO_3)_3$ deposited on acid washed and pristine TiO_2 as catalysts. The effect of altering parameter such as different loading of $Au_9(PPh_3)_8(NO_3)_3$, change of irradiation type (UV or blue).

The $Au_9(PPh_3)_8(NO_3)_3$ have been synthesized earlier by Julie and Rahol, Ph.D. students in the Golovko group. The photocatalytic chambers were used available in lab designed and constructed by the Electrical and Mechanical Workshop at the Department of Chemistry of the University of Canterbury. Kinetics analysis of some important results is studied. Reaction progress was monitored by UV-Vis spectroscopy (Cary 100 Bio UV-Visible spectrophotometer "VARIAN").

Chapter 2 - Catalysts Used in this Study and their Characterisation

This chapter presents the fabrication method, general properties and characterisation of all the catalysts prepared and used for dye photodegradation, as listed in Table 4. All gold-containing catalysts were made using $Au_9(PPh_3)_8(NO_3)_3$ as a starting material which was deposited either onto pristine P-25 TiO_2 or sulfuric acid pre-washed P-25 TiO_2. The samples in this work will be referred to by their codenames. Typically Au containing catalyst will be denoted as follows (Au loading)-(support)-(post-treatment). For example, 0.17-AW-AM corresponds to the materials which contains 0.17 wt% of Au_9 (by gold) deposited on the sulfuric acid pre-washed P-25 TiO_2 without any activation post-treatment ("as made"), while codename 0.50-P-C corresponds to the material which contains 0.50 wt% of Au_9 (by gold) deposited on the pristine (hence, "P") P-25 TiO_2 which was activated by calcination (typically at 200 °C for 2 hours under vacuum) post-treatment.

Table 4: List of catalysts used in the study.

No.	Catalyst codename	Brief summary of fabrication approach
1.	P	Commercial Evonik (formerly Degussa) P-25 TiO_2 used for benchmarking
2.	AW	Stirred commercial P-25 TiO_2 treated with 1M solution of H_2SO_4 for 5 h. Dried at 100 °C after washing with MilliQ water and methanol.
3.	0.17-P-AM	11.7 mg of $Au_9(PPh_3)_8(NO_3)_3$ deposited on 3.000 g of P-25 TiO_2 and dried under vacuum (Schlenk line).
4.	0.17-AW-AM	11.7 mg of $Au_9(PPh_3)_8(NO_3)_3$ deposited on 3.000 g acid washed P-25 TiO_2 and dried under vacuum (Schlenk line).
5.	0.17-P-C	0.17 wt% $Au_9(PPh_3)_8(NO_3)_3$ P-25 TiO_2 catalyst calcined at 200 °C for 2 hours.
6.	0.17-AW-C	0.17 wt% $Au_9(PPh_3)_8(NO_3)_3$ on acid washed P-25 TiO_2 calcined at 200 °C for 2 hours..
7.	0.34-P-AM	23.5 mg of $Au_9(PPh_3)_8(NO_3)_3$ deposited on 3.000 g of commercial P-25 TiO_2 and dried under vacuum (Schlenk line).
8.	0.34-AW-AM	23.5 mg of $Au_9(PPh_3)_8(NO_3)_3$ deposited on 3.000 g of acid washed P-25 TiO_2 and dried under vacuum (Schlenk line).

9.	0.34-P-C	0.34 wt% $Au_9(PPh_3)_8(NO_3)_3$ P-25 TiO_2 catalyst calcined at 200 °C for 2 hours.
10.	0.34-AW-C	0.34 wt% $Au_9(PPh_3)_8(NO_3)_3$ on acid washed P-25 TiO_2 catalyst calcined at 200° C for 2 hours.
11.	0.5-P-AM	34.7 mg of $Au_9(PPh_3)_8(NO_3)_3$ deposited on 3.000 g of commercial P-25 TiO_2 and dried under vacuum (Schlenk line).
12.	0.5-AW-AM	34.7 mg of $Au_9(PPh_3)_8(NO_3)_3$ deposited on 3.000 g of acid washed P-25 TiO_2 and dried under vacuum (Schlenk line).
13.	0.5-P-C	0.5 wt% $Au_9(PPh_3)_8(NO_3)_3$ P-25 TiO_2 catalyst calcined at 200° C for 2 hours.
14.	0.5-AW-C	0.5 wt% $Au_9(PPh_3)_8(NO_3)_3$ on acid washed P-25 TiO_2 catalyst calcined at 200° C for 2 hours.

2.1 Titanium Dioxide Degussa P-25 TiO_2 - Industry Standard

The P-25 TiO_2 powder with the trade name "Aeroxide" produced by Evonik Degussa GmbH used in this study was purchased from Chemicals NZ Limited. The P-25 TiO_2 was selected as a reference catalyst because it is widely used as a support for various metal nanoparticles.[1] Importantly, Golovko research group performed numerous XPS studies of gold clusters on P-25 TiO_2 (as obtained and pretreated using various surface modification treatments which was often followed by catalyst activation using selected range of post-treatment methods) as well as used gold clusters deposited and activated on P-25 TiO_2 as heterogeneous (photo)catalysts.[1,81,82,101] P-25 TiO_2 is a well-established photocatalyst - despite its relatively low surface area (up to 50 m^2/g) it shows high photocatalytic activity under UV light.[1] The physical and the chemical properties of Aeroxide P-25 TiO_2 as provided by the manufacturer are summarized in Table 5.

Table 5: Physical and chemical properties of "Aeroxide" P-25 TiO_2.

Properties	Units	Typical values
Specific surface area (BET)	m^2/g	50 ± 15
Average primary particle size	nm	20
Density (20 °C)	g/cm^3	3.8

Tamped density acc. To DIN EN ISO 787/11, Apr. 1983	g/L	~ 130
Moisture content after 2 hours at 105 °C	wt%	< 1.5
Ignition loss 2 hours at 1000 °C based on material dried for 2 hours at 105 °C	wt%	< 2.0
Titanium dioxide	wt%	> 99.50
Al_2O_3 – content	wt%	< 0.300
SiO_2 – content	wt%	< 0.200
Fe_2O_3 – content	wt%	< 0.010
HCl	wt%	< 0.300
Sieve residue (by mocker, 45 pm) acc. To DIN EN ISO 787/18, Apr. 1984	wt%	< 0.050

P-25 TiO_2 is synthesized by the hydrolysis of $TiCl_4$ in the atmosphere of hydrogen flame (100 °C), resulting in a crystalline nanoparticulate product mixture consisting of both anatase and rutile phases, with anatase content varying between 60 and 80% by mass. Figure 17 shows the TEM (Transmission Electron Microscopy) image of the fumed P-25 TiO_2.[109] The arrows shown in the figure highlight observed lattice fringes in the single crystals of TiO_2.[90,109]

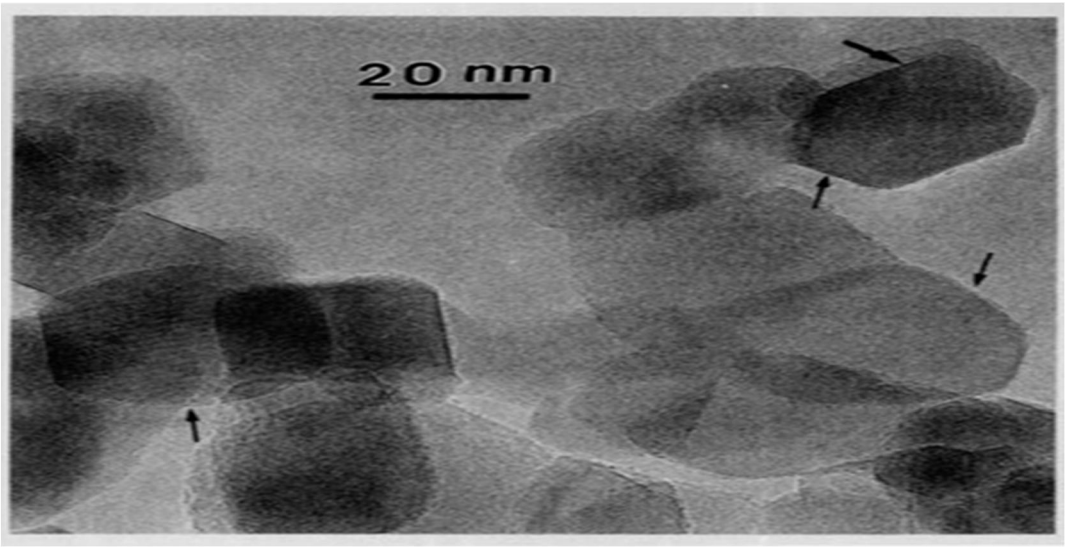

Figure 17: TEM image of fumed TiO_2. Adapted from Datye *et al.*[109]

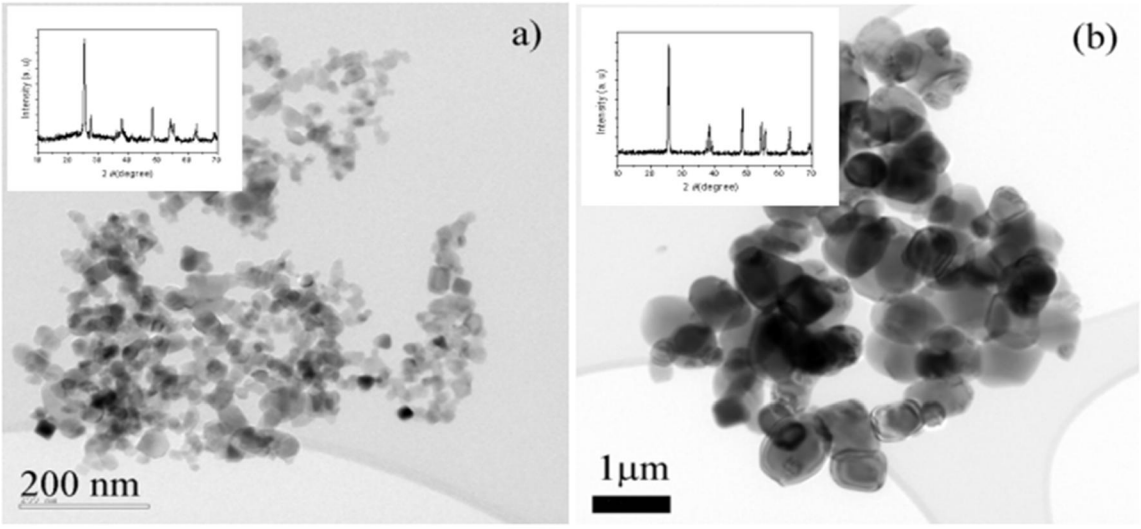

Figure 18: a) TEM image and X-ray diffractogram of P-25 TiO_2 **b)** typical TEM image of bulk TiO_2 with X-ray diffractogram. Adopted from Deng *et al.*[110]

Ohno *et al.*[88] reported that the enhanced photocatalytic activity of P-25 TiO_2 is due to the synergistic effect of the mixture of anatase and rutile phases. According to the author, the anatase and rutile particles exist independently in the P-25 TiO_2 powder. However, under the practical photocatalytic reactions, the two phases agglomerate, and the anatase particles and rutile particles are in contact. This mixed structure is important for the high activity of the P-25 TiO_2 as it leads to reduced recombination of photoexcited electrons with holes enabled by the migration of electrons from rutile to anatase phase.[88] The mechanism of photodegradation is shown in Figures 12 and 13 (Chapter 1, Introduction, p 20). Hurum *et al.*provided further evidence that the rutile phase is necessary for better photocatalytic activity, observing improved charge separation and reduced e/h recombination in the case of mixed-phase P-25 TiO_2 using EPR (Electron Paramagnetic Resonance) spectroscopy.[89]

2.2 Acid Treatment of P-25 TiO_2

In order to achieve better, controlled deposition of Au clusters on titania different pre- and post-treatment methods can be applied that could result in Au stabilization.[105,106] The reproducibility of catalyst preparation highly depends on the optimization of the

parameters of such treatments. Immobilization of Au clusters on P-25 TiO_2 could NOT be easily achieved by ultra-high vacuum (UHV) techniques, which is in stark contrast to easy deposition of chemically made clusters from solution. In the case of UHV techniques, metal nanoparticles are typically fabricated/landed on smooth and flat supports either *via* gas phase transportation of size-selected clusters or support-assisted deposition by self-assembly.[81,82] It is reported that pre-treatment of P-25 TiO_2 using sulfuric acid helps to prevent agglomeration of Au clusters on this substrate (according to the XPS data) with no appreciable change in the TiO_2 surface morphology. The field-emission transmission electron microscopy study of the Au_9 clusters on titania pre-treated by sulfuric acid showed diminished aggregation compared to the case of Au_9 on pristine P-25 TiO_2 support.[83] However, only metal-free sulfuric acid-washed P-25 TiO_2, *e.g.* without any noble metal nanoparticles, was tested as a catalyst for degradation of Rhodamine B under visible and UV light.[92] The authors demonstrated negligible degradation of the dye under visible light using acid-treated P-25 TiO_2 compared with the dye degradation by pristine P-25 TiO_2 under UV. According to Hidalgo *et al.* the BET surface areas for nonsulfated materials exhibited of around 70 m^2/g while sulphated materials around 30 m^2/g, irrespective of the gold deposition onto both cases supports. The lower surface areas observed for the sulfated materials was likely result from the higher calcination temperature (700 °C) used in the preparation of TiO_2 by hydrolysis of titanium tetraisopropoxide. Sulfate also prevented to change in phase at 700 °C from anatase to rutile having 12-13 nm and 25-27 nm anatase size for sulphated and non-sulphated respectively. The much higher improvement in the activity of sulfated samples compared to the TiO_2 was ascribed to the stronger bonding and superior electronic junction by XPS between the gold particles and the TiO_2 surface on the highly defective surfaces of the sulfated materials analysed by TEM.[113] It is also reported by Adnan *et al.* that the sulfate pre-treatment did not influence the average size of the gold particles and helped to avoid agglomeration in the "as made" samples based on TEM and UV-vis DRS data.[101] Ruzicka *et al.* compelled that H_2SO_4 pre-treatment also inhibits cluster aggregation upon calcination: this can be seen in the low-wavelength Surface Plasmon Resonance peak by DRS figure 31 and the presence of a high-intensity Au HBP and Phosphorus XPS ligand peak which was indication of discrete, ligand with protected Au clusters.[83]

Experimental details

Commercially available P-25 TiO_2 (30.000 g) was washed with 300 mL 1M sulfuric acid prepared in MilliQ using AR grade H_2SO_4 (Sigma-Aldrich, 37 wt%). Stirring was continued at 600 rpm for 5 hours. The excess of unreacted acid was removed in the following manner: the mixture was centrifugated at 5000 rpm for 10 minutes, the supernatant was removed using Pasteur pipette and the titania was redispersed in 150 mL of MilliQ water using vortex agitator (2 minutes), followed by centrifugation at 5000 rpm for 10 minutes to recover the solid. This procedure was repeated 3 times with MilliQ water and 3 times with methanol (AR grade, Sigma-Aldrich). The acid washed titania containing residual amounts of methanol was dried under vacuum of rotary vane pump using Schlenk line at 100 °C for 5 hours.[81]

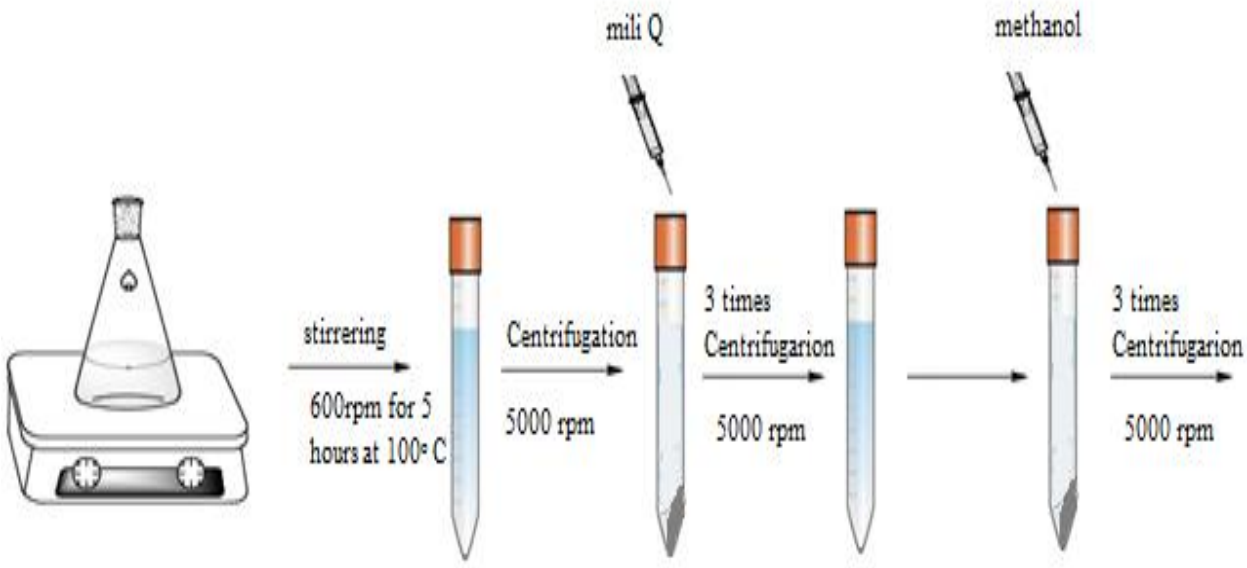

Figure 19: Schematic diagram of acid washing of P-25 TiO_2.

2.2.1 Thermogravimetric Analysis

It was important for the purpose of this research project to investigate the thermal stability of the SO_4^{2-} groups on the P-25 TiO_2. Thermogravimetric analysis (TGA) is the quantitative technique for measuring the weight loss (and sometimes the weight gain) of a material as a function of temperature and time, typically under a controlled environment

- in an inert atmosphere (*e.g.* nitrogen flow).[95] The principle of the method is based on the fact that when materials are heated, they normally lose mass by simple processes such as drying, release of structural water/solvent, structural decomposition (*e.g.* loss of functional groups such as SO_4^{2-}) or gas evolution.[101] To understand the thermal stability of the material, it is necessary to obtain knowledge of the magnitude (in wt%) and temperature range in which these processes and reactions take place. Typically, weight loss of the specimen is plotted against temperature and time to give a thermograph. The thermal behaviour of modified TiO_2 was studied by TGA using a SDT Q6000 Thermogravimetric Analyser with following parameters: a heating up rate of 10 °C/min up to 1000 °C, nitrogen gas flow rate of 100 cm^3/min, cooling down rate of 10 °C/min (Figure 20). Approximately 5 mg of the acid washed sample of P-25 TiO_2 was used for analysis with quasi-isothermal and isobaric programme of the heating furnace.

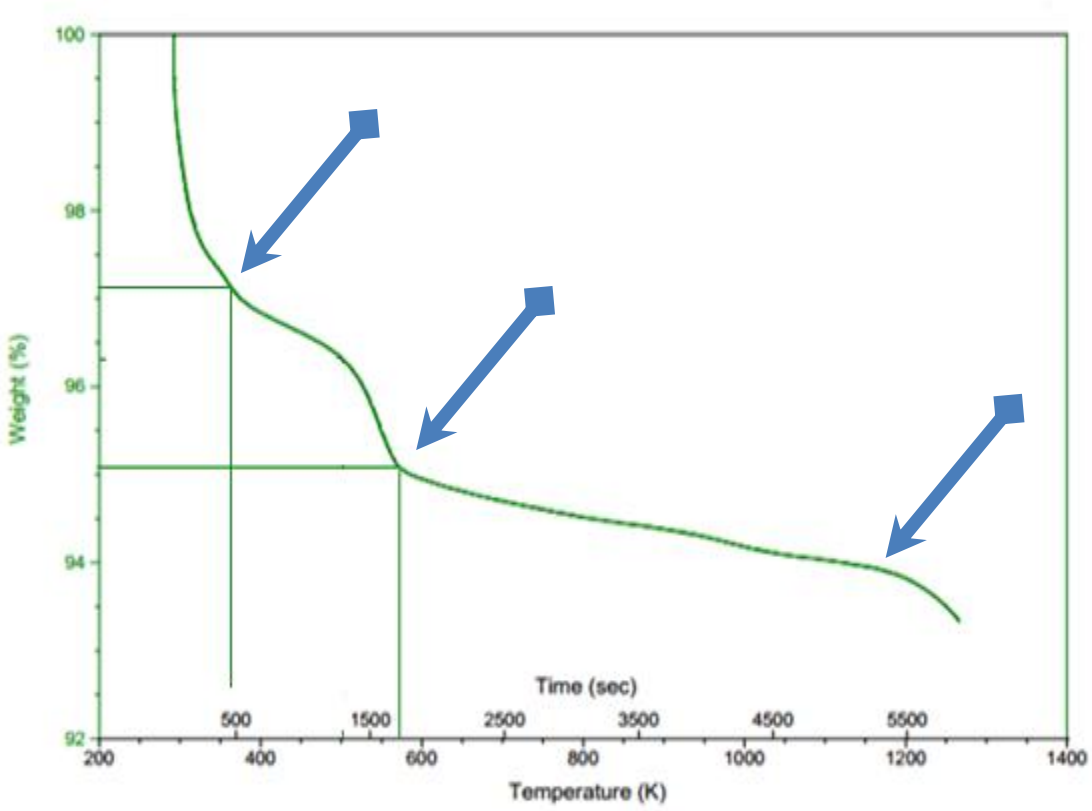

Figure 20: Thermogravimetric Analysis (TGA) graph of acid washed P-25 TiO_2.

To the best of my knowledge there are no previous studies reporting TGA of sulfuric acid washed P-25 TiO_2 (*e.g.* case when TiO_2 material was synthesised first and then treated with sulfuric acid). However, there are several reports of synthetic methods of titania

which involve media containing sulfuric acid; some of these reports also provide TGA data.[95,107,108] According to Colón*et al.* TiO_2/SO_4^{2-} synthesized using titanium tetraisopropoxide (TIP) as precursor that was hydrolysed in sulfuric acid has lost 15 wt% above 400 °C and negligible below 400 °C (Figure 21). The surface of sulphated TiO_2 was 98 while for non-sulphated was 90 at 400 °C.[107]

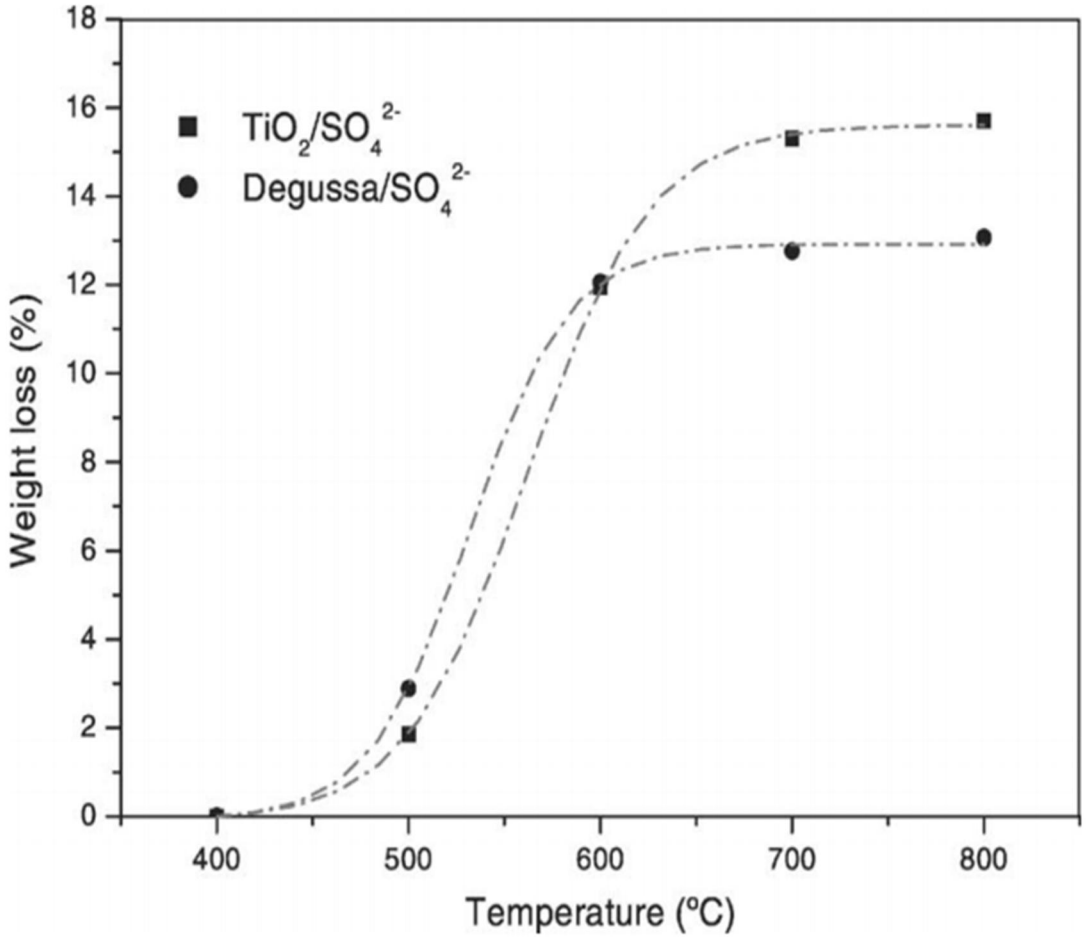

Figure 21: Loss of mass of sulfate adopted by Colón *et al*.[107]

Previously reported by Tabrizain *et al.* thermogravimetric analysis of nano TiO_2-$NHSO_3H$ (synthesized by hydrolysis of $TiCl_4$, with product later converted into nano-TiO_2-NH_2 and then modified using chlorosulfonic acid to synthesized nano TiO_2-$NHSO_3H$. TGA graph of nano TiO_2-$NHSO_3H$ showed (figure 22 left) that (*ca*. 1 wt%) between 100 °C and 225 °C, which was ascribed to the de-hydroxylation of the nano TiO_2 surface. In the same study the thermograph depicts three major stages with the first region was below 100 °C which was attributed to the loss of trapped water. The second

weight loss (11%) in the region between 225 and 308 °C. The third step (T> 314 °C up to 800 °C) was attributed to decomposition of $NHSO_3H$ on the n-TiO_2 having $NHSO_3H$.[95]

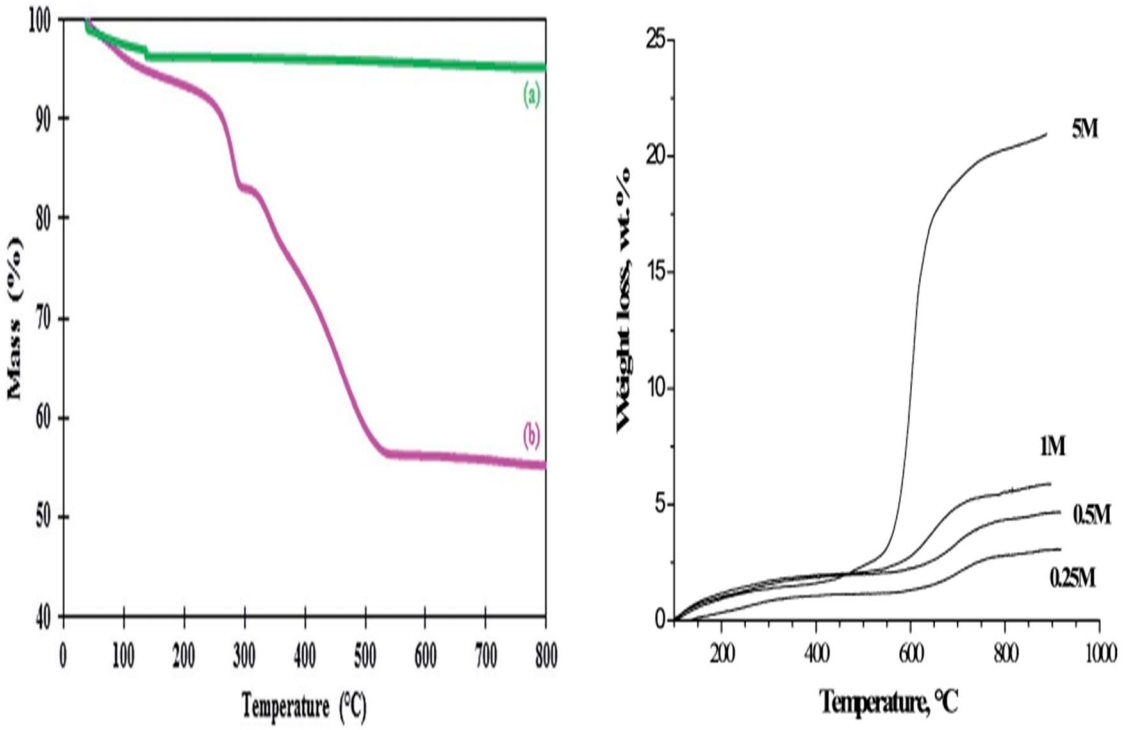

Figure: 22: **Left a)** TGA graph of nano-TiO_2 **b)** nano-TiO_2-$NHSO_3$ adopted from Tabrizain *et al.*[95] **Right** TGA analysis for SO_4^{2-}—TiO_2 synthesised by $Ti(OH)_4$ at different molarities of sulfuric acid adopted from Barraud *et al.*[108]

Barraud and co-authors[108] studied sulfated TiO_2 synthesized starting from $Ti(OH)_4$ hydroxide, yielding material that had a total surface area of 116 m^2/g (0.25 M H_2SO_4) and contained 14 nm anatase size but with 1 M the surface area was 60 m^2/g (Figure 21) suggests that there is no considerable loss of weight (only 2.5 wt%) in temperature range from the room temperature to 500 °C for 1 M sulfuric acid. This finding is very much in agreement with the findings of the presented here study.

nano-TiO_2-NH_2 and n-TiO2-$NHSO_3H$ showed in particles diameter sizes to about 50–80 nm and 90–140 nm respectively with aggregation of nano-TiO_2. According to author, the position and relative intensities of all peaks in the XRD pattern of nano-TiO2-NH_2 and nano-TiO_2-$NHSO_3H$ confirmed well with XRD pattern of nano-TiO2, indicating

retention of the anatase crystallite phase structure during functionalization of nano-TiO_2.[95] The TGA data reported by two different authors are shown in figure 21.

In our study, acid washed P-25 TiO_2 started to lose its weight (*ca*. 3 wt%) rapidly from 25 °C (298 K) to 77 °C (350 K), which may be attributed to the presence of the residual methanol which was used as a solvent in the final washings of acid washed P-25 TiO_2 and was not completely removed despite prolonged final drying stage (100 °C, vacuum, 5 h). There is pronounced feature in the TGA (highlighted by the two blue arrows on the left in Figure 20) which corresponds to a relatively small mass loss (2 wt%) in the temperature range between 350 K (~77 °C) and 573 K (~300 °C). Interpret/assign this mass loss – how this correlates with the literature? Figure 20 clearly illustrates that the change in mass occurring after 500 K is minute, suggesting acid washed P-25 TiO_2 doesn't lose considerable mass up to *ca*. 1200 K.

2.3 Synthesis of $Au_9(PPh_3)_8(NO_3)_3$

$Au_9(PPh_3)_8(NO_3)_3$ was synthesized by the former Golovko group member, Mr. Julien Aupoil, following protocol described by Anderson *at el*.[81] A solution of $NaBH_4$ (0.072 g, 1.92 mmol) in absolute ethanol (92 mL) was added to the magnetically stirred solution of $AuPPh_3(NO_3)$ (4.0 g, 7.6 mmol) in ethanol (160 mL). The solution became deep red within two hours, after which point the solution was filtered to remove insoluble impurities and solvent was removed *in vacuo*. The obtained solid was dissolved in 20 mL CH_2Cl_2 and filtered through sintered glass filter funnel (porosity 3). Removal of solvent on rotary evaporator yield product as black precipitate, which was washed with 50 mL of Tetrahydrofuran THF. Upon washing, the solid becomes dark-green. The solid was further washed with THF (3 x 50 mL) and hexane (3 x 50 mL). The precipitate was crystallized from a methanol solution by slow diffusion of diethyl ether at 4° C. Dark green crystals formed within 5 days. Yield 1.24 g, 36 %.[31] P NMR (chloroform, 25 °C); δ 56.8 ppm referenced to H_3PO_4. Mass spectrometry (MS) was performed using Bruker maXis UHR-TOF MS with an electrospray ionization (ESI) source and positive-ion polarity, with obtained and calculated spectra shown in figure 23 and 24 respectively and Table 6 presenting a summary of MS data. Crystal structure is shown in the figure 15 (Introduction, p 21). [81,82]

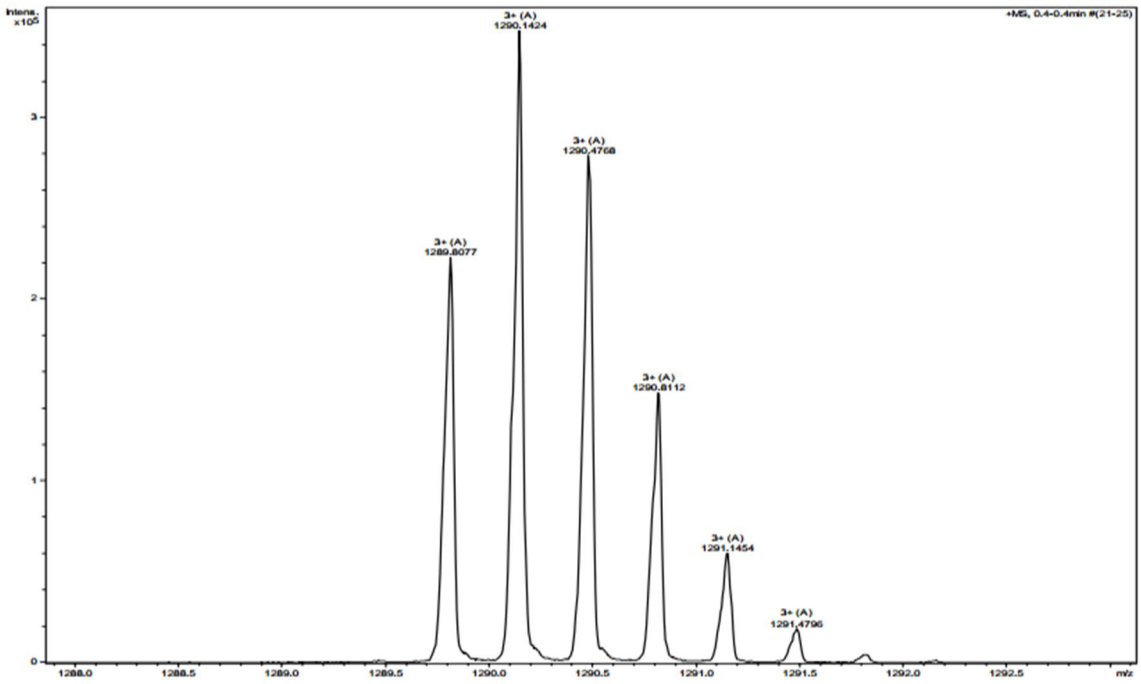

Figure 23: Molecular ion peak for the $[Au_9(PPh_3)_8]^{3+}$. Adopted from Anderson *at el.* [81]

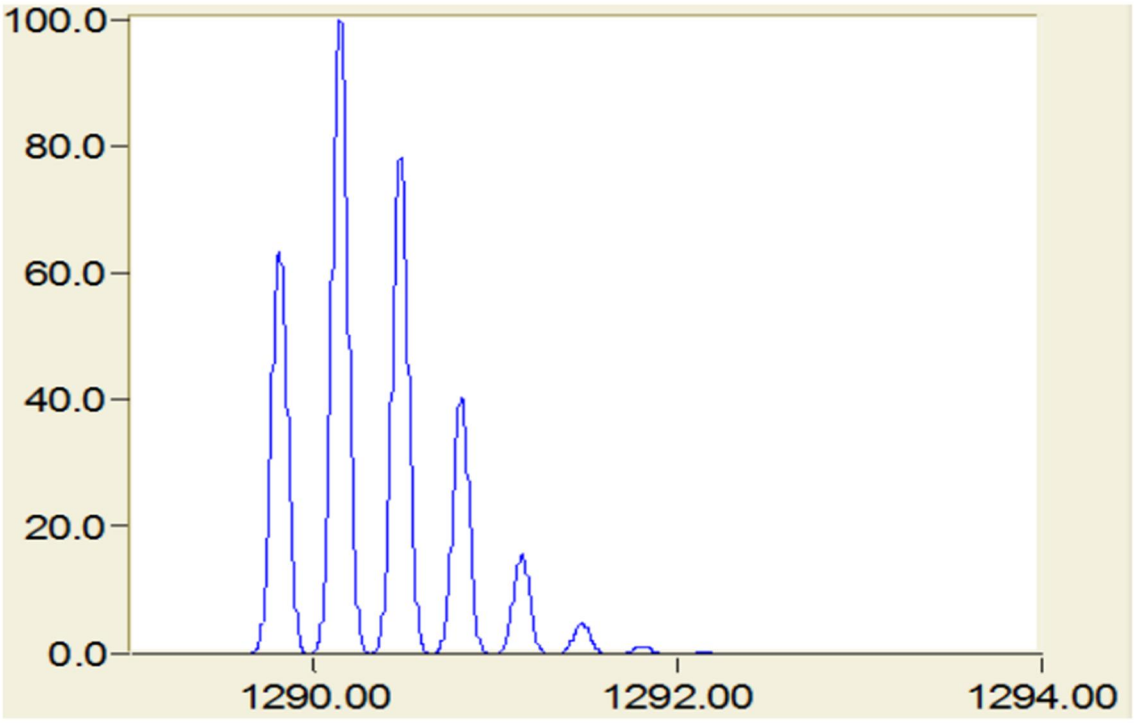

Figure 24: The isotopic distribution and simulated spectra pattern for the molecular ion. Adopted from Anderson *at el.*[81]

Table 6: Values of m/z, fraction and intensity for the simulated high resolution MS for Au_9. Adopted from Anderson *at el*.[81]

Mass/Charge	Fraction	Intensity
1289.80877	0.2087423	63.49
1290.1421	0.3287728	100
1290.47543	0.257153	78.22
1290.80877	0.1331733	40.51
1291.1421	0.0513696	15.62
1291.47543	0.0157422	4.79
1291.80877	0.0039922	1.21
1292.1421	0.0008617	0.26
1292.47543	0.0001616	0.05
1292.80877	0.0000267	0.01
1293.1421	0.0000075	0

2.4 Deposition of $Au_9(PPh_3)_8(NO_3)_3$ on Titania

Modification of P-25 TiO_2 to enable the visible light photocatalysis is important because pristine TiO_2 can only be activated by the UV light which comprises only 8 % of the irradiation reaching Earth.[60] Catalysts with 3 different cluster loadings (0.17, 0.34 and 0.5 wt%) on both acid washed and pristine TiO_2 were fabricated and activated *in vacuo*. For this purpose, 11.7, 23.5 and 34.7 mg of $Au_9(PPh_3)_8(NO_3)_3$ clusters were dissolved in 20, 25 and 30 mL of methanol respectively and added to a suspension of 3.000 g of P-25 TiO_2 (pristine and acid washed) dispersed with sonication in 50 mL of methanol in a Schlenk tube. The mixture was continuously stirred (1000 rpm) at room temperature under nitrogen atmosphere in a Schlenk tube covered with aluminium foil for 12 hours. After the solvent was removed under vacuum on a Schlenk line at room temperature during 5 hours of continuous stirring/agitation. Six different 'as made' samples of $Au_9(PPh_3)_8(NO_3)_3$ deposited on titania were obtained by the above procedure.[83] Six more catalysts were obtained by taking half of the amount of the 'as made' catalysts from each batch described above and calcining these samples at 200 °C under vacuum on a Schlenk line for 2 hours (Table 4). The Schlenk tubes containing

catalysts were covered with aluminium foil at all stages of catalyst fabrication and activation to minimize light-induced cluster aggregation.[83]

2.5 Atomic Absorption Spectroscopy Analysis (AAS): Gold content

Atomic absorption spectrometry (AAS) is commonly used for the analysis of the metal concentration in solutions with the advantage of lower price compared with other analytical techniques.[79] This analytical technique measures the concentrations of elements by the wavelengths of light specifically absorbed by an element. Atoms of elements correspond to the energies needed to promote electrons from one energy level to another, higher, energy level.[80] Gold in the form of ionic species, typically $AuCl_4^-$, homogeneously dissolved in water-based media can be reliably detected within a wide range of concentrations (µg/kg to mg/kg) depending on the atomizer used. Hence, for analysis by this technique, the metals present in the solid sample in the form of metal particles must be extracted and converted into species suitable for analysis. This sample preparation step is achieved by means of decomposition. For gold, a highly effective method of extraction uses concentrated *aqua regia* as the digester, prepared from pure analytical grade acids. *Aqua regia* (1:3 HNO_3:HCl) liberates oxidizing compounds such as molecular chlorine and nitrosyl chloride (NOCl) while chlorine ions available in solution facilitate formation of stable complex ions $[AuCl_4]^-$. This reagent is very potent for gold dissolution.[111]

Experimental

The gold content in the catalysts used in this study was determined quantitatively by atomic absorption spectroscopy (AAS) using a Varian SpectrAA 220FS instrument. A calibration curve was obtained *via* the analysis of calibration solutions, which were prepared by dilution of commercially available standard solution of $HAuCl_4$ (1 mg/mL in 0.5 M HCl) to 10, 20, 30, 40 and 50 mg/L. For the digestion of gold, 30 mg each catalyst sample were treated with a freshly prepared mixture of hydrochloric (37 %) and nitric acids (65 %) (volume ratio 3:1, total volume 10 mL) at 80 ºC overnight. The resulting mixture of dissolved gold and solid support was separated by centrifugation, solids were washed with 5 % solution of *aqua regia* in MilliQ water and both the liquid obtained after the removal of solid catalyst and the washings were collected and combined. The

volume of combined liquid was reduced to 6-7 mL under heating at 115 ºC and the volume were made up to 10 ml in 0.5 v % solution of *aqua regia* in MilliQ. [111]

Table 7: AAS results of deposited Au_9 catalyst.

%age loadings codes	Expected values (mg/L)	AAS analysis mean values (mg/L)
0.17-AW-AM	5.15	5.26 ± 0.5
0.17-P-AM	5.15	5.28 ± 0.5
0.17-AW-C	5.15	5.17 ± 0.5
0.17-P-C	5.15	5.11 ± 0.5
0.34-AW-AM	10.29	11.22 ± 0.5
0.34-P-AM	10.29	10.93 ± 0.5
0.34-AW-C	10.29	10.28 ± 0.5
0.34-P-C	10.29	10.93 ± 0.5
0.5-AW-AM	15.27	14.54 ± 0.5
0.5-P-AM	15.27	14.6 ± 0.5
0.5-AW-C	15.27	16.86 ± 0.5
0.5-P-C	15.27	16.3 ± 0.5

The results of AAS imply that the gold loadings are reasonably close to the expected target values and there is no major loss of gold during catalyst fabrication process. The values for 0.5 wt % might due to the error in weighing.

2.6 Transmission Electron spectroscopy (TEM)

In order to enhance the photocatalytic activity and dragging P-25 towards visible light region, $Au_9(PPh_3)_8](NO_3)_3$ clusters have been immobilized on the TiO_2 surface. The Au_9 clusters were synthesized by Glovoko's group prior to study this. To study proper distribution of clusters different loadings of 0.17, 0.34 and 0.5 wt% of as made and calcined Au_9 on both acid washed P-25 and pristine P-25 were made. TEM images were taken for surface analysis.

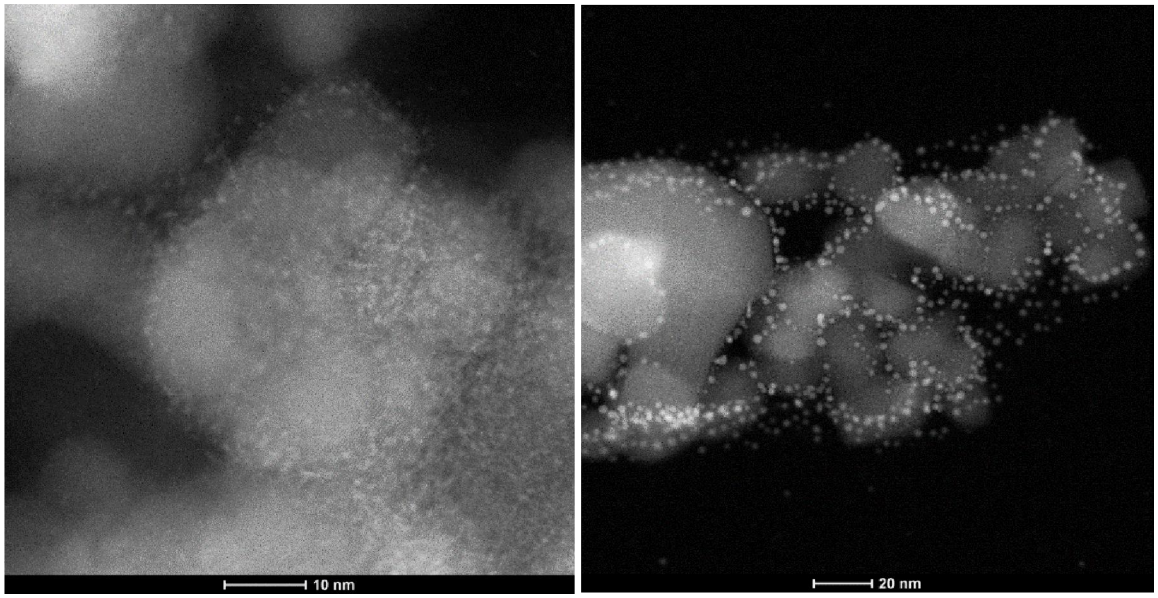

Figure 25: 0.17% Au_9/acid-washed P-25, as made taken on carbon film in the background. (Left image is zoom in while right is zoom out image).

The Au_9 clusters appear to agglomerate around the edges of the P-25, perhaps near the periphery of the P-25 on the carbon support (see figure 24). Pristine P-25 does not resist to agglomerate the clusters on titania surface.[83] The TEM images of these catalysts show the deposition of phosphine protected ligands containing Au_9 deposition which are more obvious in case of acid washed P-25 in figure 23 compared to pristine P-25. The better clusters attachment can decrease the recombination rate between electron-hole pairs and consequently increase the radicals produced in the medium and enhance the efficiency of the photodegradation and adsorption processes.[81,82] The colour change from white to light yellow of as made catalysts indicates the presence of gold cluster in the catalyst matrix. Gold clusters may act as electron traps, accumulating photoexcited electrons, preventing electron-hole recombination, and improving photocatalytic activity of the TiO_2 catalyst.[81] Au_9 clusters are appeared to be evenly distributed in TEM analysis when they were deposited on acid washed P-25.

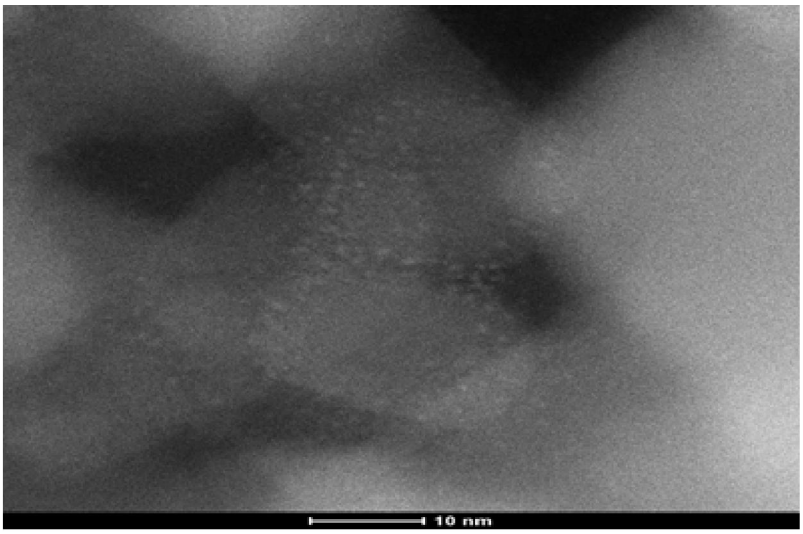

Figure 26: 0.17% Au_9 on pristine P-25, as made.

Immobilization of phosphine protected Au_9 on Acid washed and pristine P-25 were subjected to calcination at 200° C to remove the ligands smoothly. To investigate the light trapping ability of these calcined Au_9 deposited clusters experiments were performed for photo degradation of RB-19. The TEM images of calcined Au_9 deposited on the surface of titania show that the clusters are less prominent on the surface rather on the edges of Titania. On the other hand, the distribution of clusters in case of calcined catalysts on acid washed P-25 seems to be bigger, uneven and rough shown in figure 25.

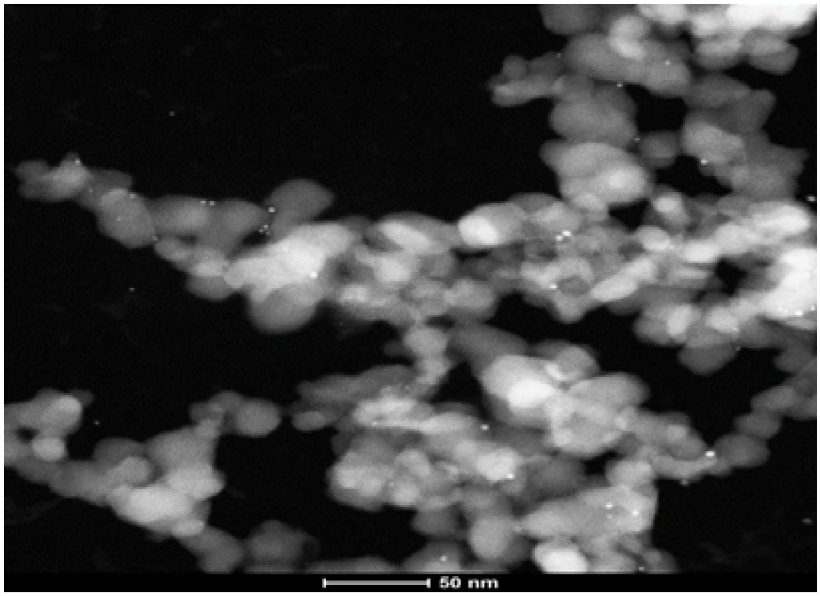

Figure 27: 0.17% Au_9/acid-washed P-25, Calcined at 200˚ C under Vacuum.

2.7 X-ray Photoelectron Spectroscopy (XPS) Analysis

XPS (X-ray photoelectron spectroscopy) is a potent surface analysis technique which can be used to determine chemical composition of the surface layer (*via* integration and normalization of the element-specific peaks in the spectra) and can provide information on the oxidation states and/or particle sizes, which can be inferred from the values of the electron binding energies. In the case of gold, binding energy of the electrons in the $4f_{7/2}$ orbital is commonly used to understand oxidation state or particle size of the gold species.[81] The oxidation state is one of the key factors determining the peak position (or electron binding energy). For example, the case of bulk gold with zero (*i.e.* Au^0) oxidation state the $4f_{7/2}$ peak appears at 84.0 eV with a 3.67 eV separation to the $4f_{5/2}$ peak which appears at 85.0 eV. Upon complete oxidation of Au^0 to Au_2O_3, the $4f_{7/2}$ peak shifts to 85.8 – 86.2 eV.[81,96,97] The effect of the oxidation state on the observed binding energy is often referred to as effect of the initial state. However, the peak position depends not only on the initial state but also on the final states effect, the latter defined by the relaxation of the photogenerated hole which often depends on the cluster/particle size and their interaction with the support.[81,98] The metal nanoclusters can stay in a charged state after excitation for a defined period of time, which is often longer than in the case of the bulk metal, affecting observed binding energy of the photoelectron.[81] Weak and broad Auger peaks (the energy release due to the electron ejection can also be transferred to another electron, which is ejected from the atom) overlapping with peaks due to photoelectrons in the experimental spectra could make it difficult to analyse XPS spectra. A Shirley background (inelastic scattering of electrons, the Shirley background can be explained by assuming a special form of the inelastic energy loss cross-section) was applied to remove the electron-scattering background and maintain the intrinsic line shape from the raw data.[81,98,99] Hence, the shifts in $4f_{7/2}$ peak positions in XP spectra of Au_9 clusters towards bulk gold can indicate aggregation of clusters into large metallic in nature particles. Such aggregation could be accompanied because of decrease in the relative gold content at the surface as observed by XPS. This is due to the fact of limitation electron mean free of larger gold.

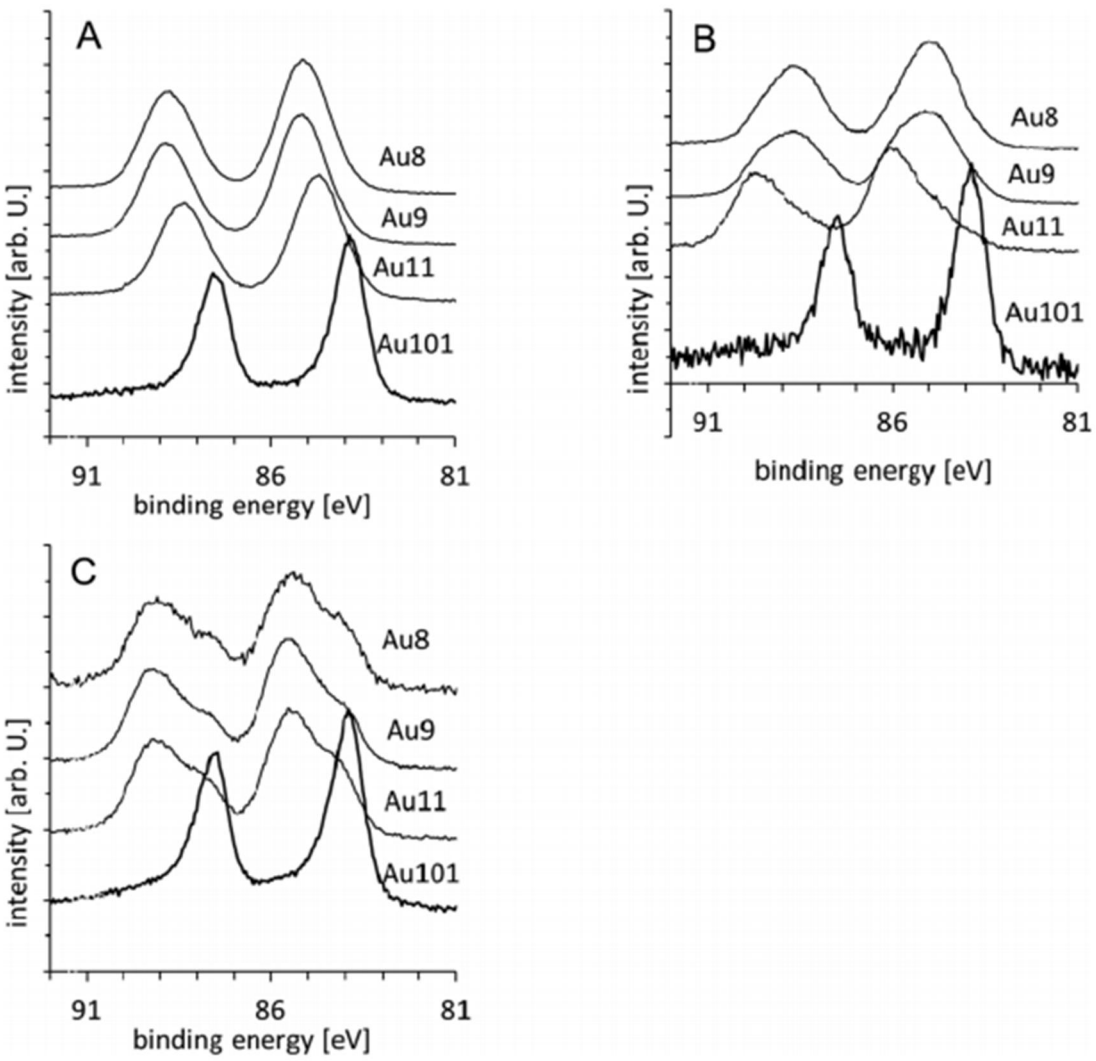

Figure 28: 0.17 % Au XPS spectra of Au samples: (A) untreated, (B) washed and (C) calcined clusters adopted by Anderson *et al*.[81]

According to Anderson *et al.,* the 4f electrons of the Au_9 deposited onto acid washed titania have higher binding energy, gold doublet with the Au-LB *i.e.* Low binding energy (84.8 ± 0.1 eV) peak positions relative to bulk Au $4f_{7/2}$ are +0.8 eV only a minutely different to those of the untreated samples. The author observed FWHMs (full width of half maximum) were the same within the error as those for the Au-LB energy peak in the untreated P-25 TiO_2 samples. The Au-HB *i.e.* High binding energy peak (85.9 ± 0.1) was +1.9 eV to Au_9 LBP. This binding energy was very close to that of fully oxidized Au_2O_3 thin films which shows a shift in binding energy of 1.8 to 2.1 eV.[81,82]

According to Anderson *et al*. the Au 4f XP spectra of the calcined samples (0.17 wt% Au_9 on acid washed P-25 calcined at 200 C under vacuum for 2 h) required use of two doublets to fit the experimental spectrum. The Au $4f_{7/2}$ peak of the doublet corresponding to aggregated particles (Au-LBP) was found shifted by only + 0.2 eV relative to the bulk Au, which is only a marginal difference taking errors (+/-0.1eV) into account.[81,82]

Importantly, follow-up studies by the Golovko group demonstrated that when Au_9 clusters are deposited onto pristine titania support cluster aggregation during deposition and calcination is more pronounced according to the XP and UV-vis DR spectroscopic evidence. Specifically, XP spectrum of the 0.17 wt% Au9 as deposited on the anatase was fitted with two doublets.[81] Later, comprehensive study by Jan-Yves Ruzicka *et al*. of the effects of various titania pre-treatments on the XPS signatures of Au_9 clusters deposited and activated using calcination and ozonolysis with same LBP 83.7 ± 0.1 but without HBP signal. The authors confirmed earlier findings for the case of acid washed P-25. While in the case of pristine P-25 TiO_2 they observed 83.7 ± 0.1 and 85.3 ± 0.2 eV LBP and HBP respectively.[82]

Experimental

In the reported here study the XPS spectra were obtained by Mr. Rohan Hudson, MSc student of Prof. Greg Metha, University of Adelaide, in the laboratory of Prof. Gunther Andersson, Flinders University, in order to characterize the surface composition of these catalysts and elucidate aggregation state of the gold clusters. All samples listed in the Table 4 were analysed asap as received from University of Canterbury (samples were stored in the freezer prior to analysis). Sample preparation for the XPS study involved making a suspension of a specific specimen in methanol (AR grade) followed by drop-casting a thin film of this material onto *ca*. 1 x 1 cm Si wafer and allowing it to dry in air at room temperature.

Peaks in the XP spectra were fitted for following elements:

- Titanium 2p (456-470 eV)
- Oxygen 1s (516-539 eV)
- Carbon 1s (272-295 eV)
- Gold 4f (80-95 eV)

- Phosphorous 2p (125-137 eV)
- Nitrogen 1s (394-404 eV)
- Sulfur 2p (166-176 eV)
- Silicon 2p (95-110 eV)

Methodology

- XPS spectra taken of samples before and after *in-situ* heating to 200 °C in UHV chamber, in an attempt to remove advantageous carbon.
- Spectra were fit using the *CasaXPS* Software Package, with a Shirley Background applied to all regions of interest.[81,82]
- Elemental percentages of all elements of interest were calculated as per Equation 1:

$$\text{Elemental } \% = \frac{c_i A_i}{\sum_i c_i A_i}$$

  Where c_i is the known calibration factor corresponding to element *i*, and A_i is the total area under a peak corresponding to the element *i*.
- For samples which were duplicated or triplicated, all intensities, binding energies and relative elemental percentages listed below are taken as the average of the multiple scans.

2.7.1 XP Spectra of Au_9 on acid washed P-25 TiO_2

According to Golovko group Andersson *et al.* reported the binding energy (BE) of the Au $4f_{7/2}$ electrons for untreated Au_9 clusters (0.17 wt%) on sulfuric acid washed P-25 titania to be 85.1 ± 0.1 eV. For the equivalent sample prepared in reported here study, the BE was found to lie at 85.1 eV, which agrees well with previous observations. Similar $4f_{7/2}$ peak positions of 85.1 - 85.3 eV for the 0.34 and 0.5 wt% loaded samples indicate that the Au_9 clusters remain intact upon deposition on acid-washed P-25 even as the metal loading increases significantly.

After vacuum-calcination, however, the peak positions and normalized intensities of the Au signals change dramatically. Figure 23 shows the relative peak positions (for $4f_{7/2}$ peak only, as referenced to the main carbon peak at 285 eV) and normalized intensities (indicated by bar height in a.u.) of the Au $4f_{7/2}$ peaks observed for all acid-washed P-25

samples. Two types of peaks are evident in these spectra, and are hereafter referred to as the low binding energy peak (LBP) and high binding energy peak (HBP) respectively.

The LBP of each vacuum-calcined sample appears at 84.0 ± 0.2 eV, and corresponds well to the known binding energy of the bulk gold. This perhaps indicates some degree of aggregation of the clusters to larger gold nanoparticles.

The position of the HBP, however, is dependent upon the weight loading of the cluster on titania, with the binding energy shifting from 86.2 eV to 85.6 eV with increase in the weight loading. Andersson *et al.* observed this HBP for 0.17-P- AM at 85.5 ± 0.1 eV, and ascribed shift to higher binding energy compared to the as made sample to partially-oxidised gold clusters forming Au-O bonds with the titania surface. Such an interpretation may be appropriate for the samples studied here, with the overall degree of cluster oxidation and hence the chemical shift of the HBP more pronounced for lower surface loading of cluster. Important difference between reported here XPS study and earlier studies reported by Golovko group is that the calcination was performed in situ under UHV and XP spectra were collected immediately after cooling to room temperature. Such procedure completely excludes oxidation due to oxygen from the atmosphere while ligand removal under UHV at the elevated temperature should be very efficient (since earlier study mentioned phosphine removal under UHV even at room temperature). [83]

It should be noted that a HBP position at ≈ 86 eV for 0.17-AW-C is very similar to that of the oxidised bulk gold 85.8 – 86.2 eV.[81,96,97] However, heat-treatment under UHV and the fact that gold oxide decomposes at 160 °C,[114] rules out formation of the bulk gold oxide particles *i.e*. gold nanoparticles formed *via* cluster aggregation, which have subsequently been completely oxidised. The HBP position very close to that of the bulk Au_2O_3 observed here for 0.17-AW-C may be interpreted by establishment of even closer direct contact of the flake-like Au_9 core with the oxide support which could have been facilitated by more efficient ligand removal under used here conditions (*cf*. earlier non-UHV studies).[81] The progressive shift of the HBP position to lower binding energies with increase in the gold loading could be interpreted by formation of cluster oligomers (e.g. clusters which just started aggregating) which are nevertheless still ultra-small and non-metallic in nature and are in excellent contact with oxide support. The increase in metal

loading would result in the formation of slightly larger oligomers/aggregates in intimate contact with support which would be in line with observed trend in HBP positions.

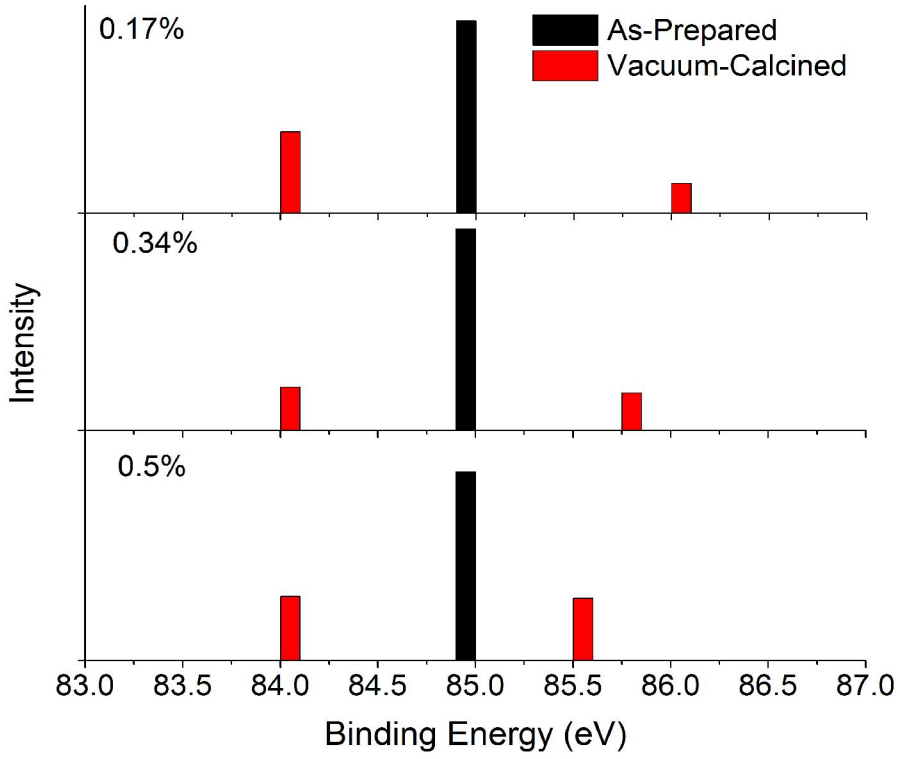

Figure 29: Binding energies and relative intensities of Au $4f_{7/2}$ XPS signals observed for Au_9 clusters deposited upon acid-washed P-25 titania. Note that intensities are given relative to those of the untreated cluster peak for each weight loading.

When comparing the Au 4f XPS spectra of the as-prepared and vacuum-calcined samples, a loss of overall intensity is observed after calcination. This is unlikely to be due to loss of clusters to larger gold particles from the surface or loss via gas phase, as the calcination is undertaken in a static UHV environment.[81,114] Hence, this intensity loss is likely to be due to the formation of larger gold nanoparticles; as the particle size increases, fewer photoelectrons will be detected, as these are limited by the electron mean free path.

A plot of elemental percentage of gold in samples deposited on acid-washed P-25 relative to the anticipated percentage of gold from the given weight loadings of $Au_9(PPh_3)_8(NO_3)_3$ is shown in. While the overall proportion of gold in the samples does increase with nominal weight loading, the two do not agree well. For both as-prepared and vacuum-

calcined samples, the overall percentage of gold in the sample in fact decreases from 0.17 wt% to 0.34 wt% nominal loading.

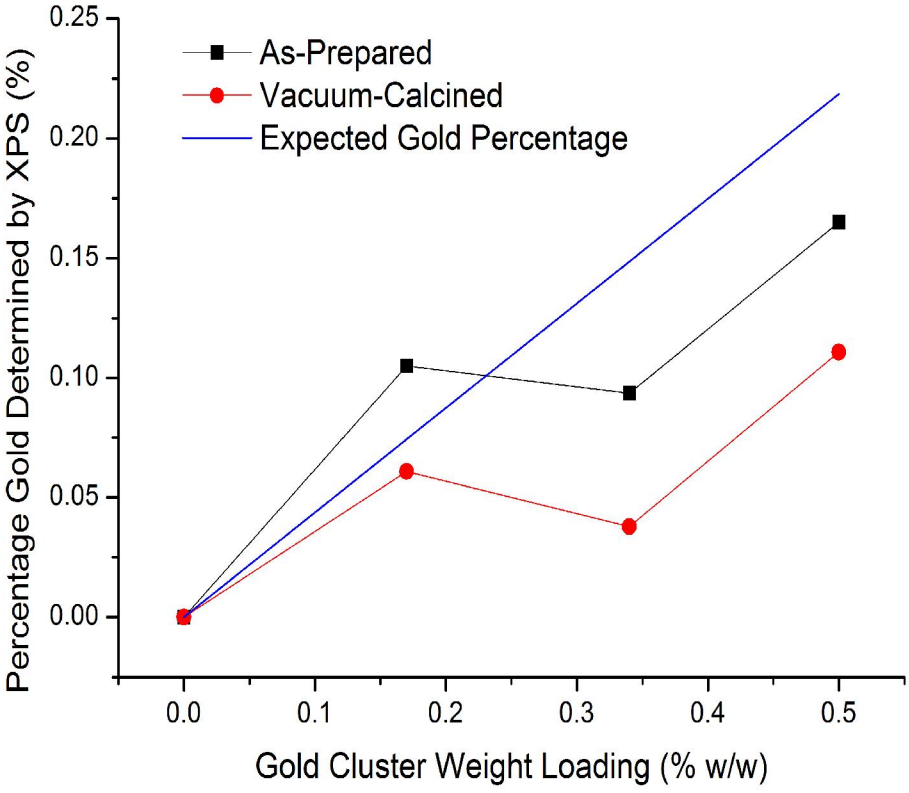

Figure 30: Atomic percentages of gold present in samples of Au_9 deposited upon acid-washed P-25 determined from XPS spectra. 'Expected gold percentages' were calculated from nominal cluster weight loadings of $Au_9(PPh_3)_8(NO_3)_3$.

As discussed above, only Au 4f peaks due to the unaggregated clusters are observed for the as-prepared samples, and so this decrease in gold content cannot be explained by cluster agglomeration and subsequent XPS signal attenuation as all gold atoms in pristine clusters should be visible by XPS. Hence, the logical explanation is that fewer clusters were successfully deposited onto titania for the 0.34 wt% loaded samples than expected. As expected, the percentage of gold in each sample decreased on calcination in vacuum, due to the aforementioned limited mean-free-path of photoelectrons from large, bulk-like aggregated gold nanoparticles. Thus, overall trend for "as made" *vs*. calcined samples is as expected.

2.7.2 Sulfur XP Spectra

In all samples of Au_9 clusters deposited on acid-washed P-25, sulfur signals were observed in XPS spectra which corresponded to 1 - 3% of the samples' total makeup. The high variability of sulfur percentage between samples may be due to inhomogeneous binding of sulfate groups to the titania surface. Due to this variability, comparing total sulfur content between as-prepared and vacuum-calcined samples is very difficult. However, by examining the fraction of sulfur lost during *in situ* UHV heating, inferences may be made about the relative stability of the sulfate groups on the titania surface (figure 31).

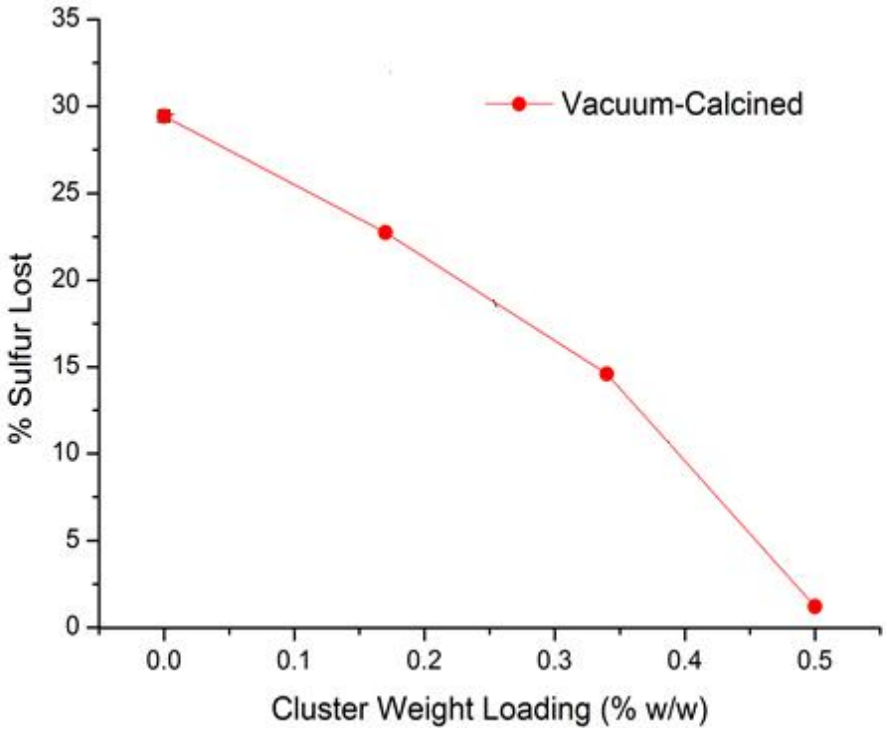

Figure 31: Proportion of sulfur XPS signals lost during *in situ* heating of samples in UHV chamber. "0%" cluster weight loading corresponds to a control experiment of acid-washed titania with no clusters deposited.

As can clearly be seen, while the proportion of sulfur lost from calcined samples under UHV heating shows appreciable correlation to the nominal cluster weight loading, an inverse proportionality. This could potentially be due to any sulfate groups the titania not bound to gold species having been lost during the calcination process. If binding of the sulfate residues on the titania surface to ultra-small gold clusters does stabilize them the

trend for sulfur content in calcined samples observed in figure 31 will correlate well with the trend of gradually increasing intensity of the Au XP peak at high binding energy observed in figure 29. An analysis of the sulfate group stability on the titania surface through techniques such as thermogravimetric analysis (TGA) could shed more light upon this phenomenon (figure 20).

2.7.3 Gold XP Spectra of Au_9 deposited and activated on pristine P-25 TiO_2

Peak positions and relative intensities of Au $4f_{7/2}$ peaks observed by XPS for Au_9 clusters deposited upon pristine P-25 are shown in figure 32. In addition, the gold signal intensities observed for these samples were much lower compared to the case of samples containing Au_9 on acid-washed P-25 TiO_2, and as such the signal-to-noise ratio was very poor.

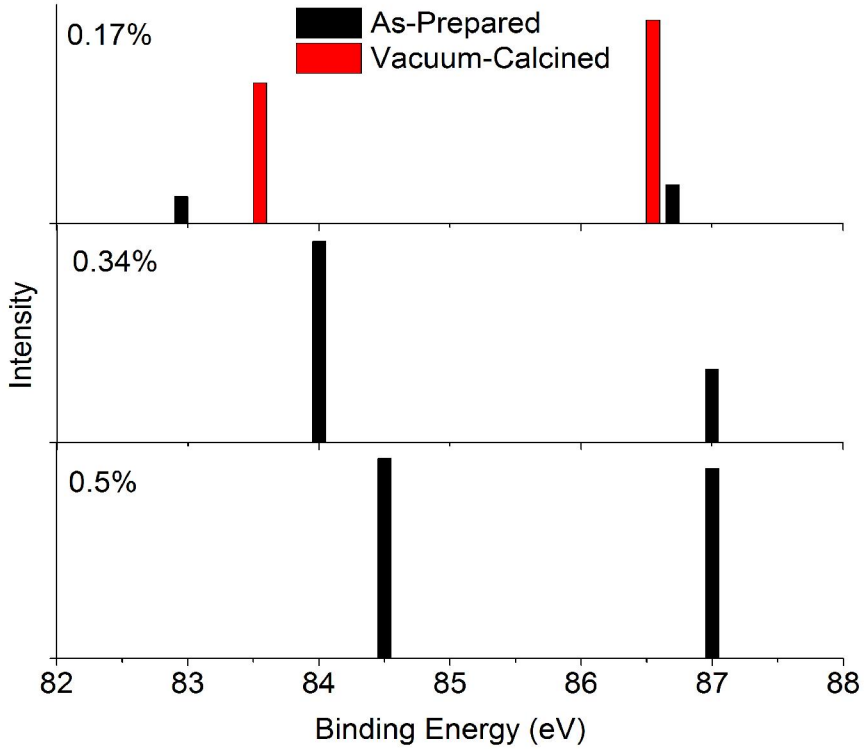

Figure 32: Binding energies and relative intensities of Au $4f_{7/2}$ XPS signals observed for Au_9 clusters deposited upon pristine P-25 titania. Note that intensities are given relative to those of the untreated cluster peak for each weight loading. Full width half maxima are excluded for clarity, but are summarized in Appendix.

In the case of the as-prepared samples, the HBP has shifted to even greater binding energies than observed on acid-washed titania. Binding energies of 87 eV or higher are

highly indicative of fully oxidised gold particles. The LBP's of all samples are consistent with bulk gold, however the range of binding energies has widened considerably, with BE's ranging from 83 to 84.5 eV. The shift of LBP in the case of 0.17 wt% sample to higher binding energies upon calcination seem strange; perhaps, fragmentation of large aggregates or more probably a better contact with oxide support (similar to partial oxidation) could explain such unexpected shift. Small shift of the HBP for this sample is likely to be insignificant (within experimental error). As sulfuric acid-washing titania has been previously established to assist in 'anchoring' gold clusters to titania, then it should not be surprising that compared to the acid-washed samples, those deposited onto pristine titania may move around more easily and hence agglomerate more easily.

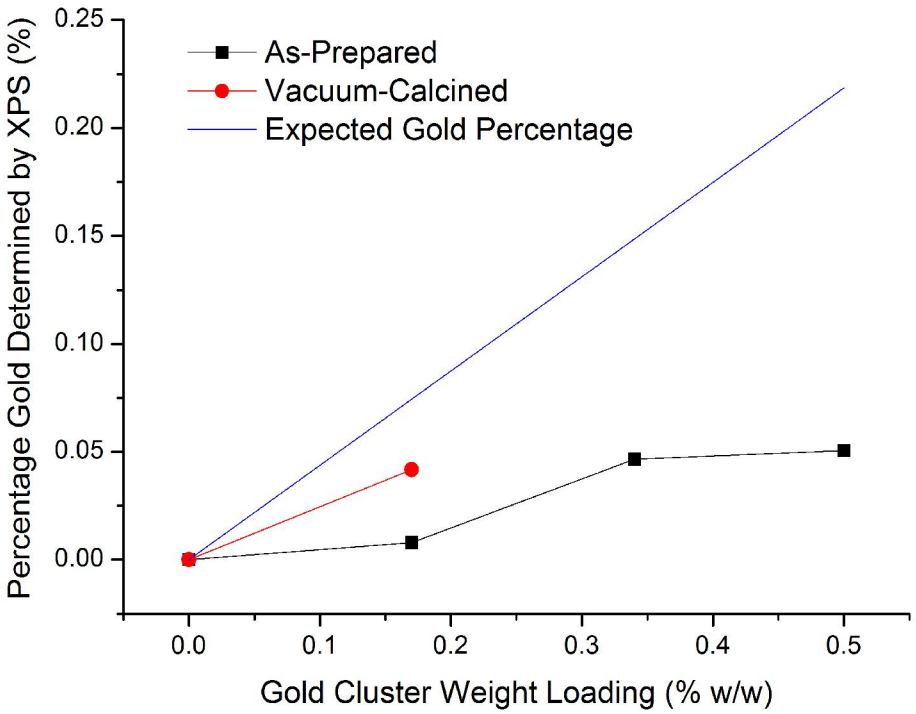

Figure 33: Atomic percentages of gold present in samples of Au_9 deposited upon bare P-25 TiO_2 determined from XPS spectra. 'Expected gold percentages' were calculated from nominal cluster weight loadings of $Au_9(PPh_3)_8(NO_3)_3$.

For the vacuum-calcined sample investigated, the results are quite unusual when compared to the equivalent as-prepared sample. As can be seen in figure 32, calcination in vacuum of the 0.17 wt% loaded sample appears to dramatically increase the Au 4f signal intensities. The binding energies of both the LBP and HBP are relatively similar to

that of the as-prepared sample, indicating somewhat similar chemical states of the gold, however the intensities show that there is almost 5x as much gold present after calcination than before (see figure 33). This finding suggests that cluster agglomeration is the only reason of lower gold content on titania surface according to the surface-sensitive XPS, as one can generally only detect those photoelectrons which have enough energy to escape the surface from 0 to 10 nm while limited mean free path of the photoelectrons in gold means that some of the gold atoms in large particles will be undetected.[99]When considering the elemental percentages of gold detected by XPS for the as-prepared samples on bare titania, an overall increase is observed with increase in nominal/target weight loading; again, however, it does not match the expected weight loadings of each sample. In this case, the discrepancy between expected gold percentage and observed is far greater than that for the acid-washed titania series. Two possible reasons for this exist. Agglomeration of the clusters to nanoparticles (as evidenced by the LBP in observed in the "as made" samples) would decrease the gold XPS signal due to the limited electron mean free path. In addition, without pre-treatment with sulfuric acid, it is reasonable to assume that the clusters would not bind as effectively to pristine titania as they would with sulfate groups present. Hence, during the deposition process, fewer clusters may be successfully binding to the titania, and so may be more easily dislodged and lost during drying/transfer/preparation processes.

Other Important Observations

- No phosphorous or nitrogen signals (corresponding to the ligand and counter ion of the Au_9 core respectively) were observed in any of the investigated samples. This is likely to be due to the low concentration of these elements being so low that any signal was indistinguishable from noise.
- For many samples, satellites of the silicon 2p peak at 100 eV were convoluted with the gold signals at 84-88 eV. These are labelled 'Silicon Satellites' in the XPS fits in the appendices.
- Upon *in situ* heating in the UHV chamber, significant aggregation of clusters (inferred by Au $4f_{7/2}$ shifts from 85 to 84 eV) often resulted from such treatment.

As such, all subsequent analysis of the gold signals is taken from spectra before *in situ* heating (i.e. "as made" samples), to afford a more accurate representation of the chemical state of gold species.

2.8 UV-vis diffuse reflectance spectroscopy study

The gold loadings of 0.17, 0.34 and 0.5 wt% on P-25 TiO_2 were selected with an aim to establish an optimal loading allowing large enough Au content and yet minimise the aggregation of gold clusters. UV-vis diffuse reflectance spectroscopy (UV-vis DRS) is a technique used for solid materials since light cannot penetrate into deep opaque samples, it is reflected on the surface of the samples. Metallic gold nanoparticles in the size range from *ca*. 2-3 nm to *ca*. 100 nm show localized surface plasmon resonance while in gold clusters due to their smaller size LSPR bands are absent in the cases of as made gold clusters catalysts confirming that the Au particle size is below 2 nm (e.g. clusters retained their non-metallic state).[101] The appearance of an LSPR band in the UV-vis DR spectra of Au_9 supported on the P-25 TiO_2 after calcination was also observed in the work of Adnan *et al.* (data is shown in figure 28),[101,102] indicating formation of plasmonic gold nanoparticles due to increase in particle size above 2 nm threshold.[102-104] It was previously reported that the position of the LSPR band undergoes the red shift as the size of gold particles increases, although sometimes this trend changes due to the effect of the dielectric constant of the immediate chemical environment.[101]

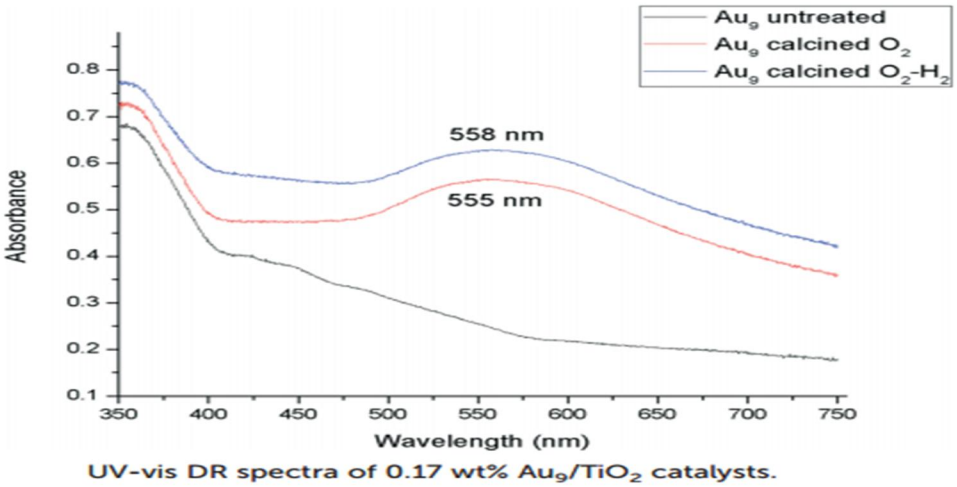

Figure 34: UV-vis DRS of 0.17 wt% Au_9 on pristine P-25 TiO_2 adopted from Adnan *et al.*[101]

Experimental

UV-vis DR spectra were recorded at University of Canterbury and University of Adelaide by Mr. Rohan …. Pellets of the freshly-made and calcined samples were pressed into samples holders using spatula and ensuring uniformly smooth surface. The spectrum were taken thrice for each catalyst and mean value was obtained.

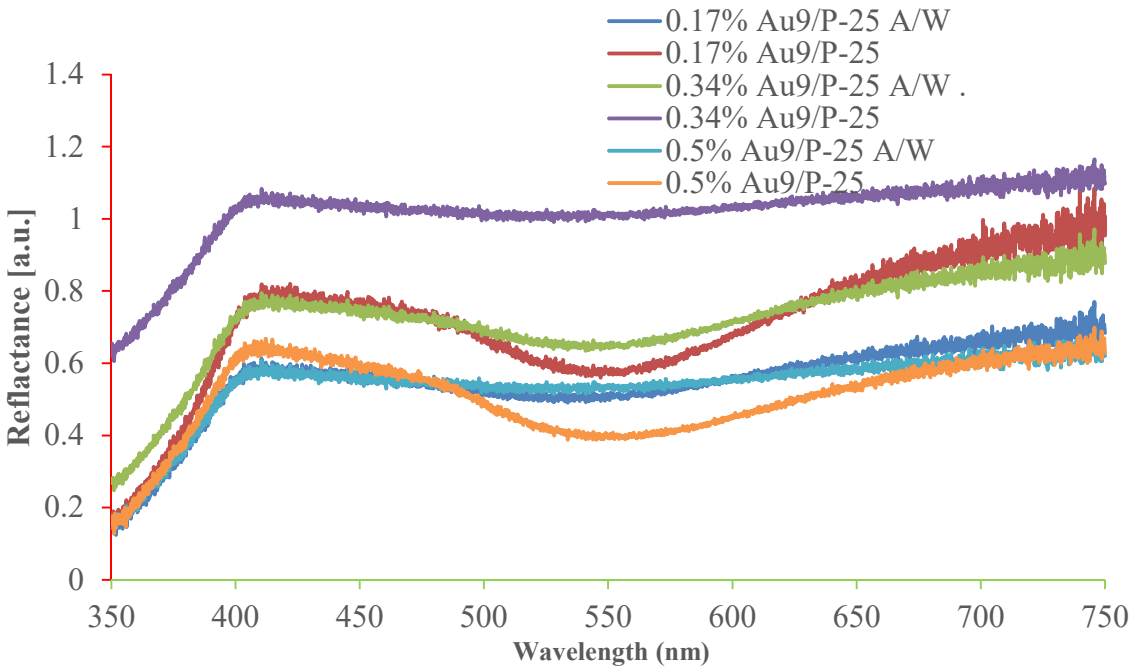

Figure 35: UV-vis DR spectra of "as made" Au_9 catalysts (showing Au_9 SPR signature).

The results of DRS suggests that there are clusters which show their absorbance between 400 - 450 nm in a good agreement with literature.[101] The sample 0.34 wt% Au_9 on pristine P-25 TiO_2 showed maximum absorbance compared to others. Acid washed as made catalysts were showing their signatures in the region while non-acid washed catalyst the results were not quite obvious. This may infers that acid washed support of P-25 TiO_2 is more resistant to cluster aggregation.

On the other hand, post treated support with acid washed and pristine P-25 TiO_2 show more agglomeration with lager particles signs at higher wavelength than 450 nm. The process of calcination is somewhat too harsh to remove only the ligands smoothly but it also causes to aggregate the gold clusters into larger nanoparticles. The clusters with

loading 0.34 wt% as made on P-25 TiO_2 does not show its shoulder at 550 nm and the absorbance of clusters are much higher than their respective calcined catalysts. [101]

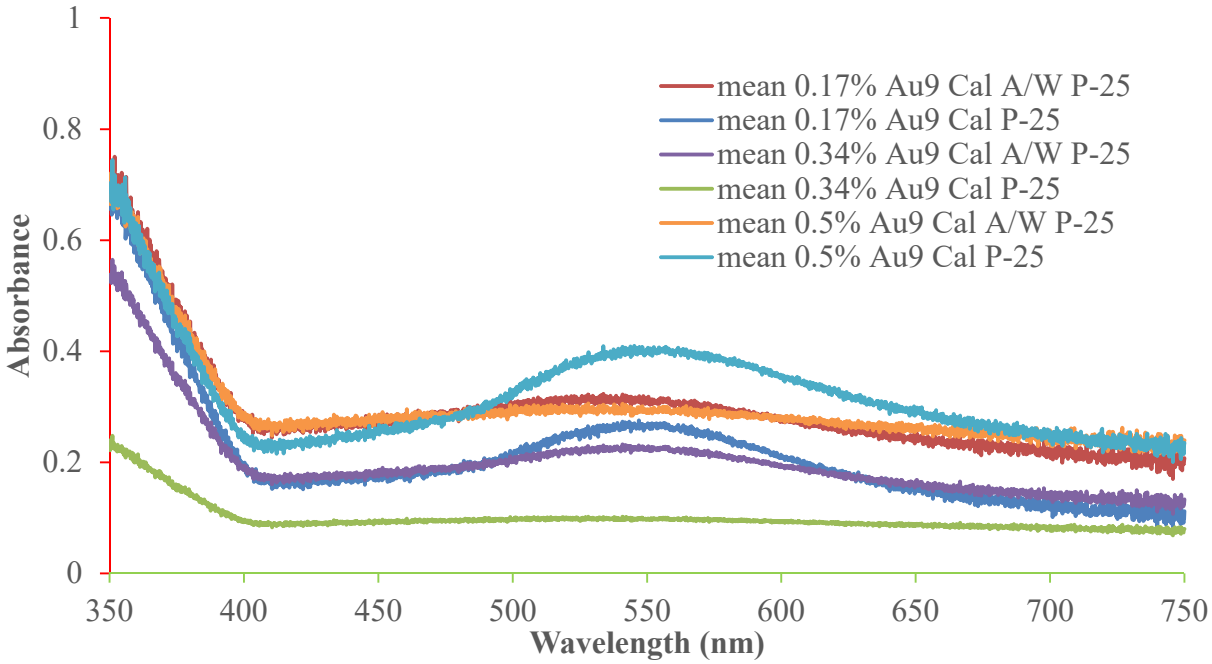

Figure 36: UV-vis DR spectra of calcined Au_9 d catalysts.

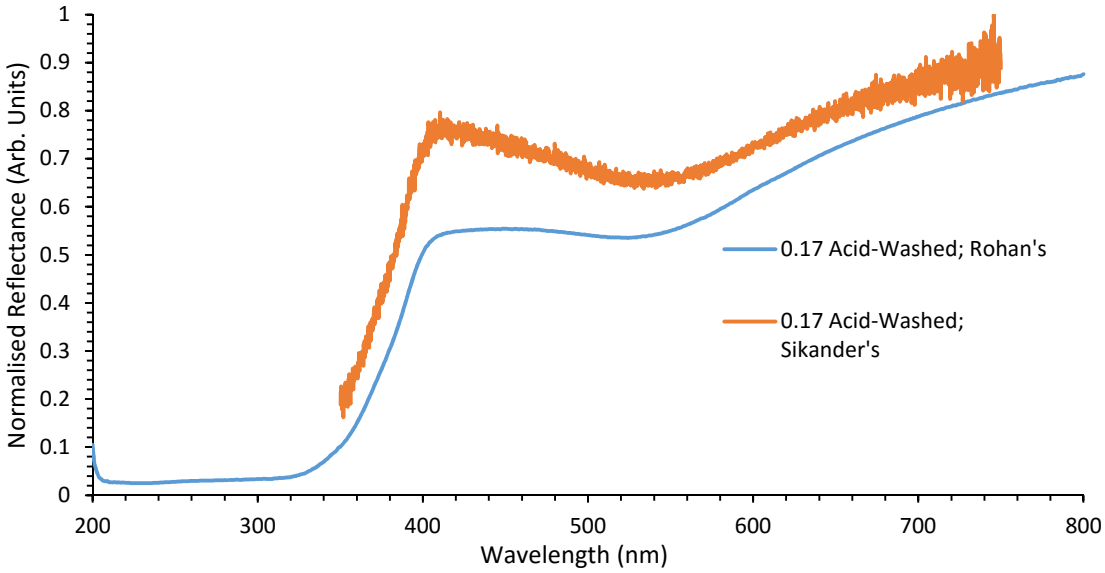

Figure 37: Comparison of DRS Data for 0.17-AW-C.

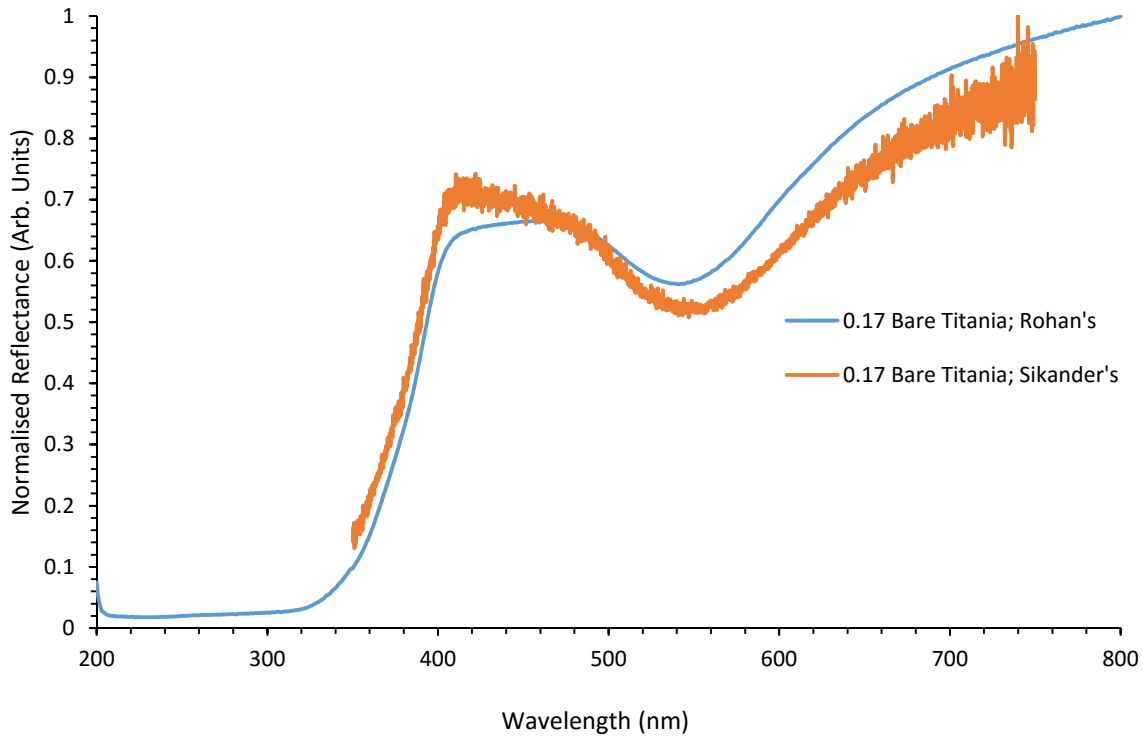

Figure 38: Comparison of DRS Data for 0.17-P-C.

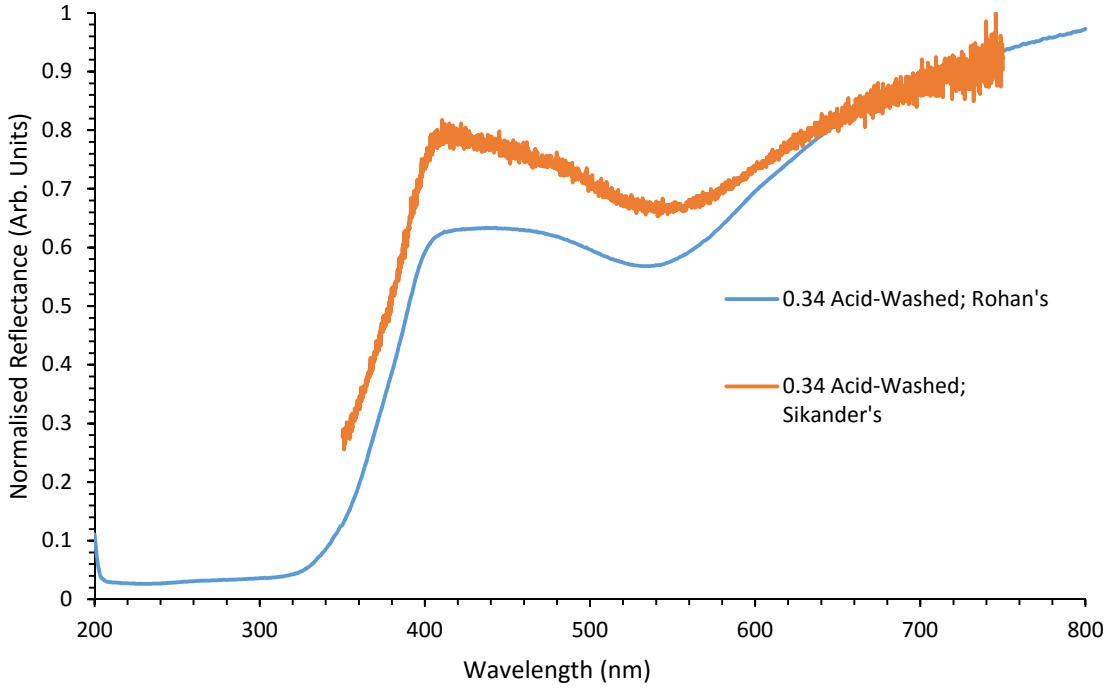

Figure 39: Comparison of DRS Data for 0.34-AW-C.

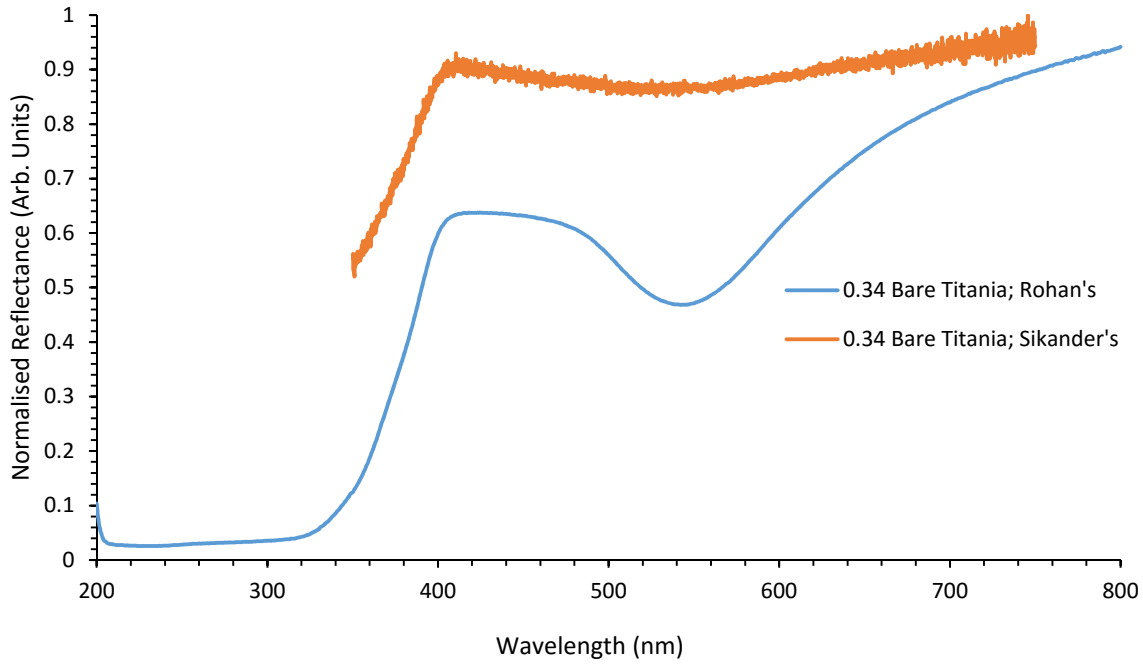

Figure 40: Comparison of DRS Data for 0.34-P-C.

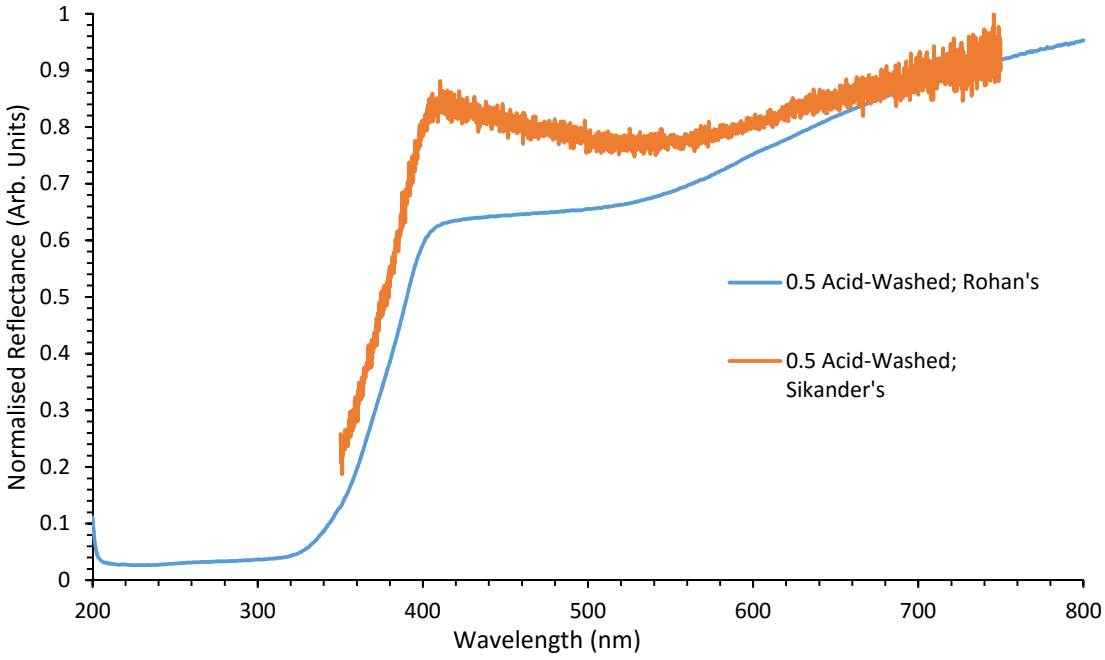

Figure 41: Comparison of DRS Data for 0.5-AW-C.

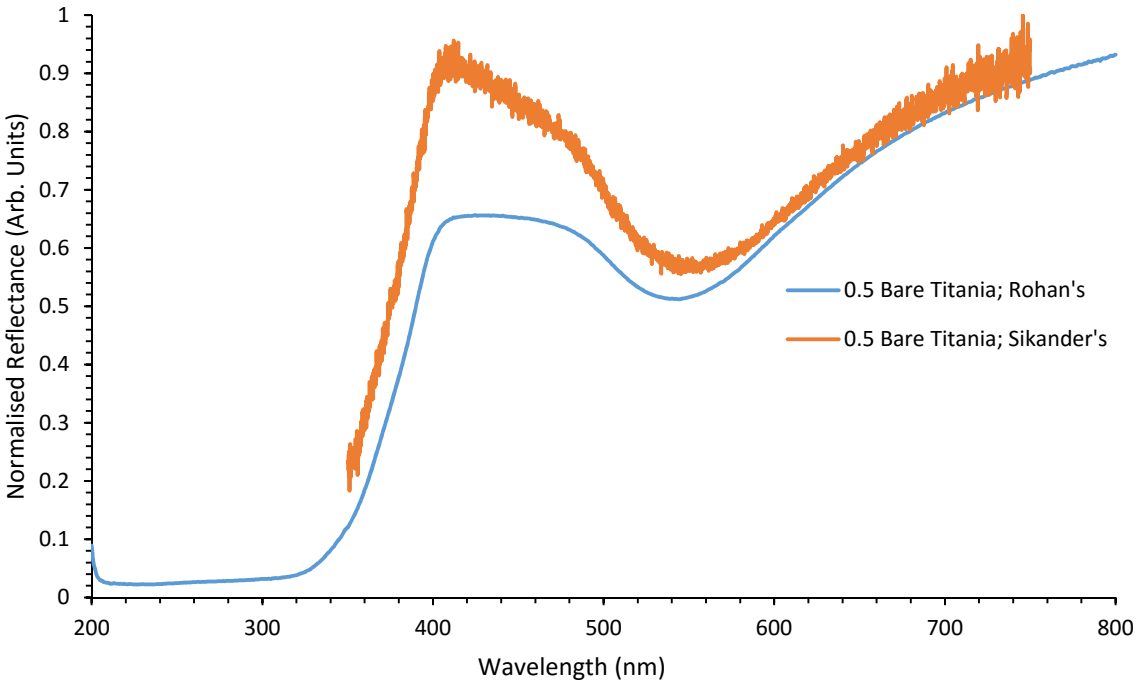

Figure 42: Comparison of DRS Data for 0.5-P-C.

Chapter 3 – Photocatalytic degradation of Reactive Blue 19 dye

This chapter presents the results of a study on photocatalytic degradation of Reactive Blue 19 (RB-19), an industrial dye,[1] using various TiO_2-based catalysts listed in Table 4 (Chapter 2, p25). Some experiments reported in this chapter were designed to establish standardized techniques for reliable analysis of degradation to compare with Au_9 deposited P-25 TiO_2 catalysts. In particular, the experiments focused on:

Characterisation of dye solutions by UV-Vis spectroscopy: estimates of non photocatalytic degradation,[1] errors in measurements, baseline correction, the effect of temperature under various conditions (exposure to light *i.e*. UV and blue 50 W two LEDs for each set of wavelength *vs.* experiments in the dark), reproducibility and catalyst recycling.

All experiments were carried out in triplicate, and standard error was calculated by dividing standard deviation to root square of number of replicates (3), allowing use of the error bars in the graphs for better comparison between the experiments. All catalytic reactions carried out in the preliminary study used commercial "Aeroxide" TiO_2 Degussa P-25 as catalyst. Acid washed P-25 TiO_2 was used to compare the results for the catalysts of Au_9 deposited on acid washed P-25 TiO_2.[1,81,82]

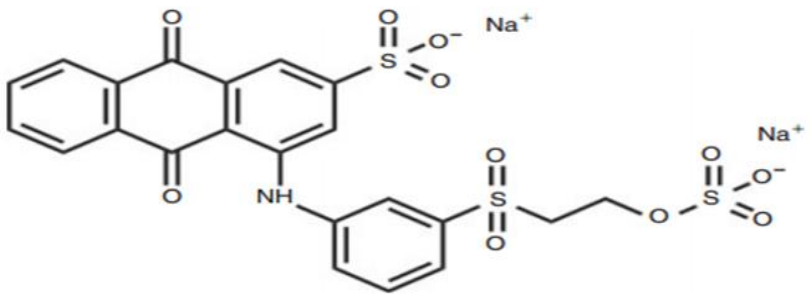

Figure 43: Chemical structure of Reactive Blue 19 (RB-19) (FW=626.54 g/mole) adopted from Abu Bakar *et al*.[1]

Reactive Blue 19 (RB-19) dye was selected for photocatalytic degradation as representative and popular industrial dye. The chemical structure of RB-19 (figure 43) shows that the dye is an anthraquinone derivative; it is a commercially valuable bright blue reactive dye.[25] The dye RB-19 is mainly used to colour the materials made up of

cellulosic fibres. It is readily soluble in water and has excellent adherence to materials because of the strong covalent bonds that it forms with the fibres.[1] Repeated measurements of the RB-19 solution (five times) by UV-Vis spectroscopy indicated that the average maximum absorption wavelength of the dye falls at 594.00 ± 1.26 nm with molar absorption coefficient of η = 7270 L/(mol·cm).[26] In all experiments absorbance did not exceed 0.7. An example absorption spectrum is presented in figure 44.

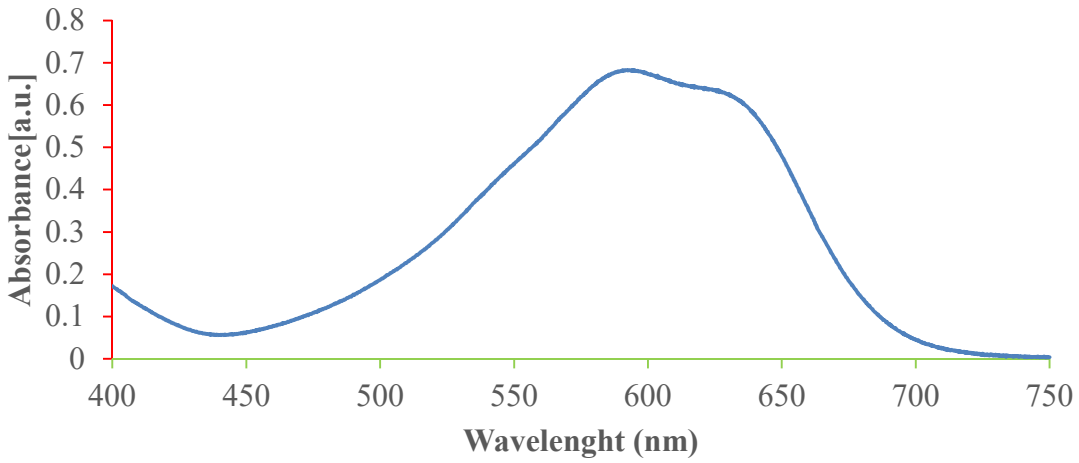

Figure 44: The UV–visible absorption spectrum of RB-19 dye in water. The absorption maximum of the dye occurs at λ = 594.00 ± 1.22 nm.

3.1 Characterisation of dye solutions using UV-Visible spectrophotometry

In visible light spectrum, the interaction between dye and electromagnetic radiation shows itself as colour. Therefore UV-Visible spectroscopy allows the study of dyes and dye degradation very properly. The Bouguer-Lambert-Beer Law is the relationship between light absorbance and dye concentration is given in *Scheme 4*.[26]

The Bouguer-Lambert-Beer Law

$$\boldsymbol{Log}\left(\frac{\boldsymbol{I^{\circ}}}{\boldsymbol{I}}\right)\breve{\upsilon} = \boldsymbol{Log}\left(\frac{\mathbf{100}}{\mathbf{T(\%)}}\right)\breve{\upsilon} \quad \equiv \quad \mathbf{A}\breve{\upsilon} = \boldsymbol{\varepsilon}\breve{\upsilon}.\mathbf{c}.\mathbf{d}$$

Where's $\mathbf{A}\breve{\upsilon} = \boldsymbol{Log}\left(\frac{I^{\circ}}{I}\right)\breve{\upsilon}$ is *absorbance,* $\mathbf{T}\breve{\upsilon} = \frac{I^{\circ}}{I}.\mathbf{100}$ in %, is *transmittance*, and $\breve{\upsilon}$ is *molar* decadic extinction coefficient.

I° and I are the intensities of the monochromatic wavelengths of light entering the

sample and emerging out from the sample respectively; *c* is the concentration of the light-absorbing dye and *d* is the optical pathlength through the sample (in cm) present in the cell. The functional correlation between radiation intensity and wave number *v* is called the "absorption spectrum of a compound".[46]

3.1.1 Dye Concentration, Stability and Reproducibility for Measurement

The Bouguer-Lambert-Beer Law has, however, one limitation - that it only applies to solutions of low concentrations (absorbance should not exceed 1).[26] In such cases, the extinction coefficient ε is independent of the concentration of a dye at the given wave number υ (wavelength λ) while in a concentrated solutions, ε changes depending on the refractive index of the solution. Due to the limitation imposed by this law, preliminary UV-Vis spectroscopy experiments were performed using solutions with concentrations used previously reported by Golovko's group.[1] Specifically, 0.08 g/L ($1.3x10^{-4}$ mol/L) of RB-19 was selected according to comply with the Bouguer-Lambert-Beer Law. At this concentration the initial absorbance is just less than 0.9: low enough that ε should remain constant as the dye degraded, but high enough that accurate results could be obtained from dye degradation studies as pronounced drops in absorbance can be easily detected.[1]

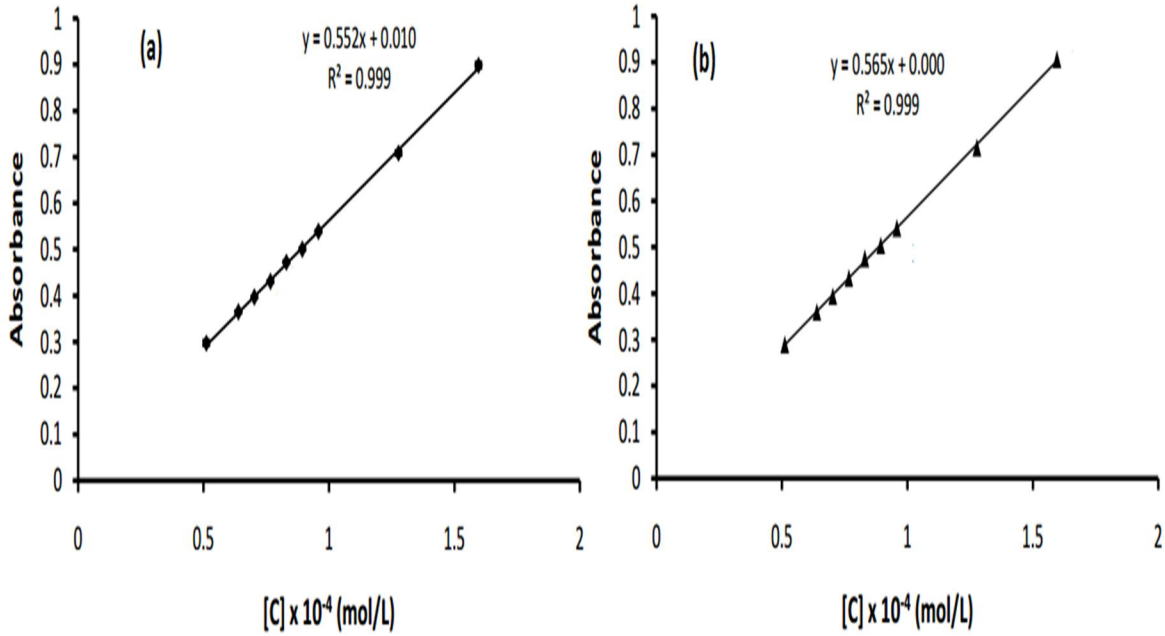

Figure 45: Calibration plots (concentration vs. absorbance) for RB-19 Dye. (a) First

measurement (b) second measurement (after 5 hours).

The graphs suggest that the 5 hours delay between measurements does not significantly affect the results with the fact that linear regression $R^2 = 0.99$ is very fine, but the slope is slightly different (0.552 *vs*. 0.565, *ca*. 2 % increase). This observation indicates that the dye is relatively stable in water.

3.2 Non-Photocatalytic degradation

In this section the performance of TiO_2-based catalysis in the dye photocatalytic degradation reactions under various conditions was investigated, including the effect of temperature (in the dark, exposure to blue light and UV irradiation) without catalysts *vs.* experiments in the dark in the presence of a catalyst. For the sake of proper understanding "dye adsorption" headings will refer to any experiments performed in the dark, while all reactions under blue and UV irradiation will be referred to as "photocatalytic reactions" in the presence of catalysts. Reactions in the dark had been carried out to elucidate potential for removal of dyes by different catalysts listed in table 4 in absence of light. It is assumed that dye adsorption at the surface of titania is the major driving force for dye removal from solution in these experiments. Hence, it was important to perform such study to set a baseline needed to gauge efficiency of true photocatalytic effect in dye degradation. In order to find a set of standard conditions at which to fix key test parameters, a series of preliminary experiments were carried out.

3.2.1 Dye adsorption study

Before commencing the photocatalytic reactions, which require a special equipment *i.e.* chamber with two 50 W LEDs to provide blue or UV irradiation, experiments were performed in the dark. Initial reaction conditions were set up based on the conditions of catalytic oxidation used in the literature for heterogeneous catalysts and developed by our group earlier for photocatalytic degradation of dyes.[1]

All dye adsorption studies were carried out at 40 °C because that was the final temperature recorded after 2 hours under both UV and blue light irradiation (temperature raise due to heat generated by two 50 W LEDs within enclosed reaction chamber).

Experimental

All the dye adsorption experiments were performed in a three-neck glass tube covered in the aluminium foil under continuous stirring (1000 rpm) at 40 °C using preheated stirred water bath on a hot plate with temperature control to 1 °C *via* thermocouple feedback loop.

1. All reagents (dye solution and TiO_2 based catalysts) were mixed together at the beginning of reaction.

2. "*Step-by-step*": dye solution and TiO_2 powder were mixed first until the adsorption equilibrium was reached.

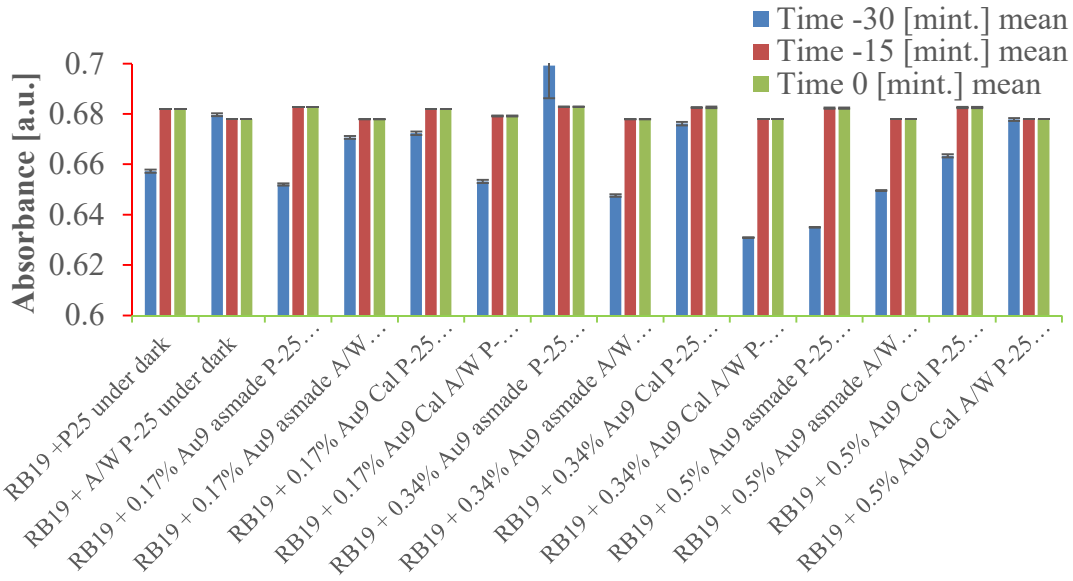

Figure 46: The absorbance of the dye solution on the surface of catalysts (Time -30 to 0 minutes).

To examine the adsorption of RB-19 on the surface of the catalysts, a series of experiments were carried out by mixing each catalyst with RB-19 solution with the same concentration (0.08 g/L) as was used for photocatalytic degradation prevuoisly[1]. The experiments were repeated 3 times to obtain the average values. Firstly, samples were taken at -30 minutes (*i.e.* upon initial quick mixing prior to sonication), then after sonication (denoted as time -15 minutes) and finally at time 0 minutes before commencing the experiment under dark conditions or before raising the temperature from

room temperature to 40 °C. In the case of adsorption study the vessel was wrapped with aluminium foil and suspensions of catalyst with dye were constantly stirred under dark conditions for 120 minutes. Samples were taken at time intervals 15, 30, 40, 60, 90 and 120 minutes and measured the absorbance each time with UV/visible spectrophotometer after centrifugation 3 times and removing the catalysts.

The above graph shows the decrease in absorbance due to adsorption dye onto the surface of catalysts, with maximum value 6.84%, $(1 - \frac{Abs.of\ dye\ with\ catalyst}{Abs.\ of\ pure\ dye}) \times 100$ for case of 0.34 wt% loading Au_9 Cal A/W P-25. While minimum 0.01% was recorded for 0.34 wt% loading of Au_9 as made P-25 at given time after catalysts introduced to the dye solution. At time -15 minutes irrespective to the initial values the percentage values were observed around 1.65 to 2.14% for each catalyst under study. Table 8 represents all these values of percentage absorbance decreased, calculated by the above formula, arbitrary named as percentage adsorption. It is mentionable that there is no further change in absorbance for each catalyst, between -15 minutes and up to time 0 minutes. For non-washed pristine P-25 the values of absorbance were relatively less as compare to acid washed P-25. The narrow difference in absorbance was observed within time -30 to 0 minutes. However, the dye adsorbed slightly more on acid washed P-25 at time -30 minute, as compare to non-treated P-25 but sooner the sonication was did dye released from acid washed catalysts and absorbance got back to equilibrium with almost same position just like pristine P-25 at 15 minutes in agreement with Abu Bakar *et al.*[1] All the values are given in the table 8 for each catalyst in percentage adsorption with respect to dye absorbance.

Table 8: Percentage decrease in absorbance of RB-19 on surface of the catalysts by physical adsorption.

Catalysts	%age adsorption at time -30 [mint.]	%age adsorption at time -15 [mint.]	%age adsorption at time 0 [mint.]
RB-19 +P25 under dark	4.21	1.74	1.74
RB-19 + AW P-25 under dark	1.97	2.14	2.14
RB-19 + 0.17-P-AM under dark	4.74	1.65	1.65
RB-19 + 0.17-AW-AM under dark	2.87	2.14	2.14
RB-19 + 0.17-P-C under dark	2.70	1.73	1.73
RB-19 + 0.17-AW-C under dark	4.62	2.02	2.02
RB-19 + 0.34-P-AM under dark	0.01	1.65	1.65

RB-19 + 0.34-AW-AM under dark	5.18	2.15	2.15
RB-19 + 0.34-P-C under dark	2.32	1.67	1.67
RB-19 + 0.34-AW-C under dark	6.84	2.14	2.14
RB-19 + 0.5-P-AM under dark	6.44	1.70	1.70
RB-19 + 0.5-AW-AM under dark	4.98	2.14	2.14
RB-19 + 0.5-P-C under dark	3.60	1.68	1.68
RB19 + 0.5-AW-C under dark	2.15	2.14	2.14

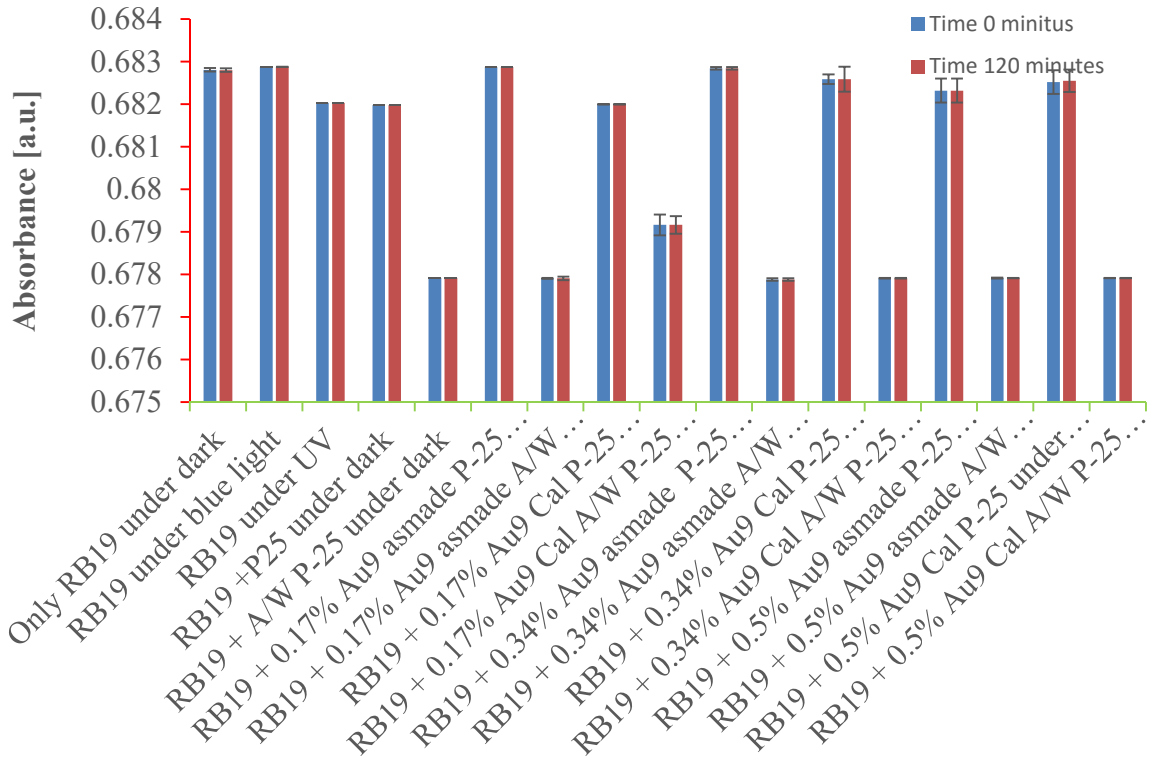

Figure 47: Study of non-photocatalytic degradation of dye under blue and UV in absence of catalyst or under dark in presence of catalysts at 40 °C.

There is no significance difference between at time -15 minutes and at time 0 minute absorbance indicating the physical adsorption is in an equilibrium before commencing the reactions. Moreover, from the Figure 47 it is demonstrated that under dark, dye did not change the equilibrium with the surface of catalysts till at end of the reaction time at 120 minutes.

Figure 48: The visual appearance of catalyst precipitate from RB-19 solution after centrifugation.

But it is quite obvious that acid washed catalysts have somewhat more adsorption compare to non-washed pristine P-25 based catalysts. To determine the self-degradation of dye under blue and UV light, same experiments were conducted in triplicate. There was no degradation of RB-19 under blue light for 120 minutes without catalyst while the mean value for UV compels a very minute degradation was occurred under UV which was negligible. Overall this suggests that no significant amount of dye adsorption on the surface of the TiO_2 based catalysts. The pellets after centrifugation for each catalyst were either white, yellowish or reddish in appearance for P-25 calcined Au_9 catalysts and yellowish for as made catalysts Au_9 respectively.

3.2.2 Background kinetics studies of P-25 and Acid washed P-25

In order to perform degradation of dye, even under the best conditions without exposure to light, requires a considerable amount of time (ca. 24 hours). Many reports have indicated that it is necessary to do the reaction at elevated temperatures and/or pressures (150-350 °C, 6-17 MPa) to obtain the same results without irradiation within a shorter reaction time.[91] Therefore, TiO_2-mediated photocatalytic dye degradation is believed to be a promising alternative due to its ability to remove the dye in a much shorter time frame and at ambient temperature. The breakdown of RB-19 on a heterogeneous catalyst surface is best modeled by Langmuir-Hinshelwood (L-H) kinetics.[91] For a surface-catalyzed unimolecular reaction the reactant adsorb on a solid surface and therefore the rate is given by:

$$r = \frac{kKC}{1 + KC} \equiv \text{k'C}$$

Where *k'* is pseudo rate coefficient, *k* is the rate coefficient of the reaction, C is the concentration of reactant solution and K is the equilibrium constant for the adsorption of the reactant onto the catalyst. Equation simplifies to either zero or first order kinetics in the limiting cases of either very high (C>>1) or very low C<<1) dye concentration, respectively. Thus, a number of studies of dye degradation model the rate as first order with respect to dye species. In order to study L-H rate of reaction and kinetics for photo-degradation of RB-19 on P-25 and acid washed P-25 were analyzed. In case of zero order or first order kinetics both plots of (A0-At) or ln(A0/At) versus time must be limner, with slope *k* but by plotting data for P-25 and acid washed P-25 the reaction does not fit in L-H model but somewhere in between (figure 49). If a reaction is zero first or second order kinetics than the line with function time (t) with absorbance, ln of absorbance and inverse of absorbance must be line respectively.

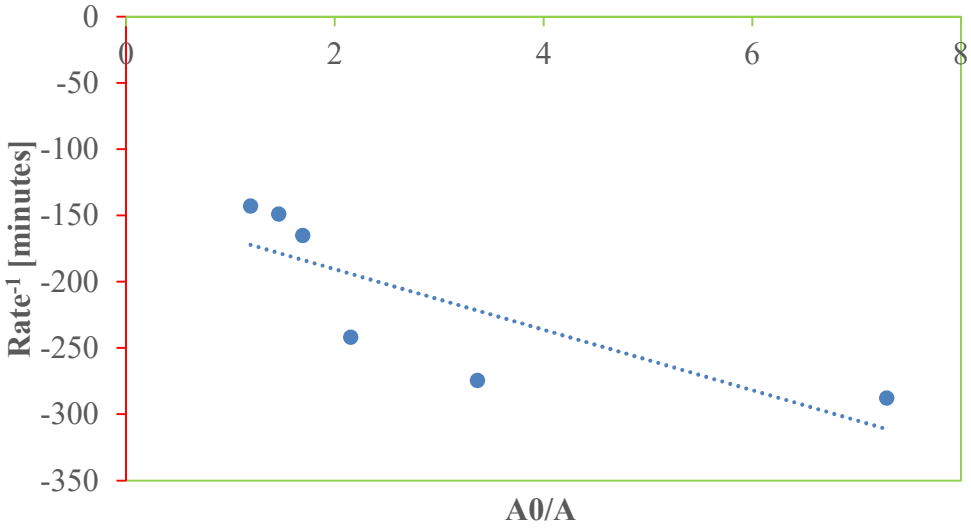

Figure 49: Attempted Langmir Hinschelwood fitting for the photodegradation of RB-19 on P-25 at natural pH.

More specifically, L-H equation for kinetics should obey if the plot of 1/r (inverse of rate) versus 1/C (inverse of concentration) if gives a straight line with slope 1/*k*K and intercept 1/*k*. The instantaneous rate of reaction was determined by the change in concentration over a given time. But the graph does not linear correlation between 1/r and 1/C suggesting this relation dose not obey the L-H model as demonstrated in figure 49. The possible reasons are by-products during photo-degradation may cause

interference with absorption profiles closely matching that of RB-19 or due to the existence of multiple degradation mechanisms. The pseudo first order does not reflect accurately the mechanism of degradation for RB-19 due to no adsorption. The scattered data points observed for L-H model while for a plot of [A]/[A_0]) vs. should time lead to follow first-order kinetics for pristine P-25 under UV (see figure 50).

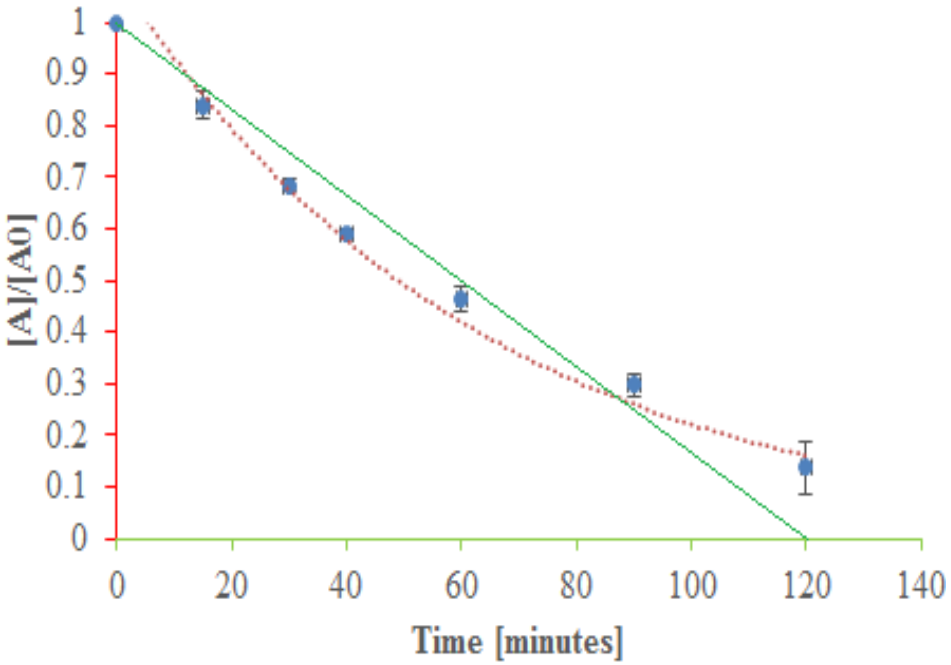

Figure 50: Zero and first order kinetics plots for the degradation of RB-19 on P-25. Dots indicate experimental data as 1st order. Performed at natural pH and dye under UV. Green line shows zero order.

The results for acid washed P-25 were somewhat follow the pseudo first order kinetics as it is shown in figure 52 and but it actually follows 2nd order (see figures 51, 58). It might be the presence of SO_4^{2-} ions present on the surface of P-25. The interaction of RB-19 with acid washed P-25 was also quite obvious in adsorption analysis when it was compare with pristine P-25. It seems that the presence of SO_4^{2-} ions on H_2SO_4-treated P-25, adsorption plays some role in photocatalytic process. However, the activity of the photo-catalyst during the UV irradiation mainly depended on their crystallinities rather than on their adsorption ability because they were more different in their crystallite sizes than in their specific surface area and there was no degradation of dye up to 120 minutes under dark experiments. Perhaps, acid washed TiO_2 behaves as an •OH scavenger (SO_4^{2-}

$+^{\bullet}OH \rightarrow SO_4^{\bullet -} + OH^-$) and further transfer of radical to the dye's negative charge SO_3^{2-} and subsequently the photodegradation of the dye.[92] These might be possible reasons for the photoactivity of the H_2SO_4-treated TiO_2. Hence, presence of SO_4^{2-} on the surface could change the photo-catalytic activity by changing the gap between valance and conduction bands when SO_4^{2-} doped on the surface P-25 which may change the mechanism of reaction altogether.[93]

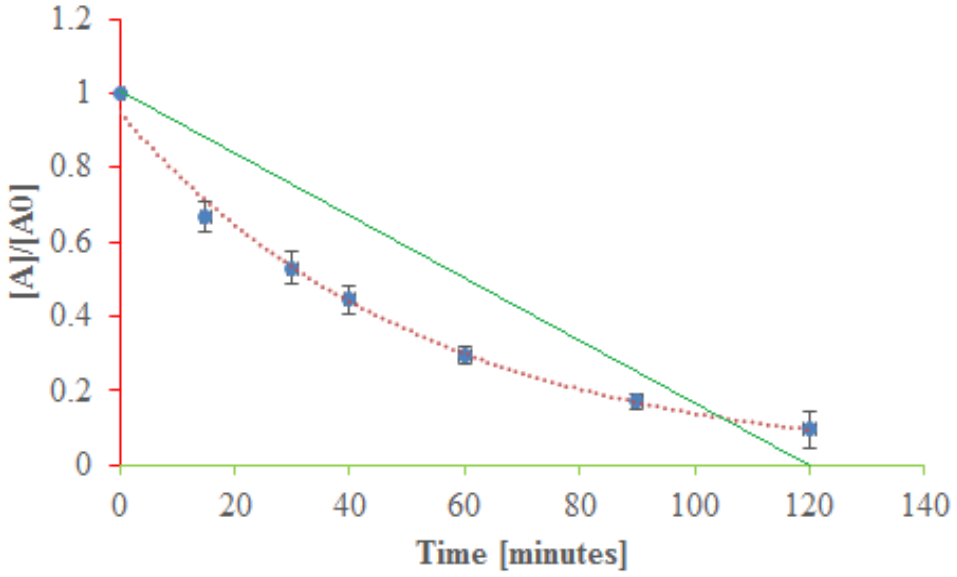

Figure 51: Zero and 2nd order kinetics plots for the degradation of RB-19 on A/W P-25. Dots indicate experimental data. Performed at natural pH and dye under UV.

Although the percentage degradation for both catalysts i.e. pristine P-25 and acid washed P-25 are same under UV but the mechanism may be different due to the presence of SO_4^{2-} ions.

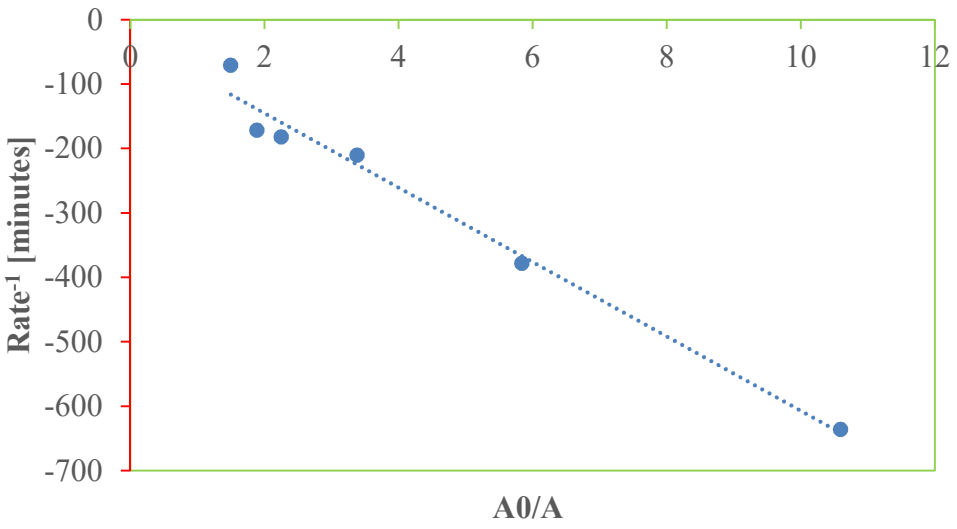

Figure 52: Langmir Hinschelwood fitting for the photodegradation of RB-19 on acid washed P-25 at natural pH under UV.

The degradation during the visible light irradiation depended on both the adsorption ability and visible absorption of the photocatalyst samples.

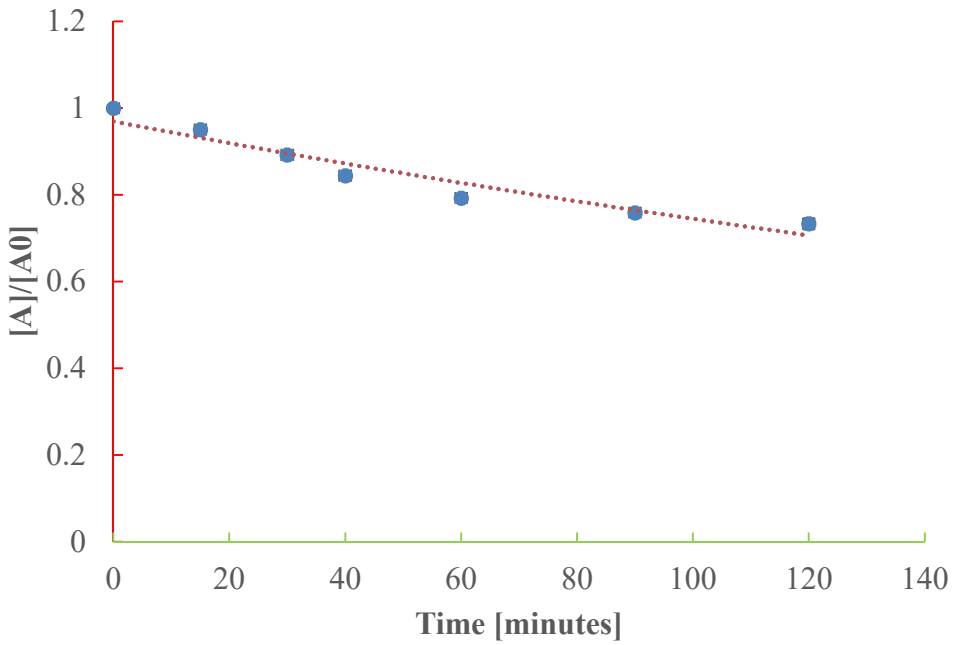

Figure 53: Pseudo-first order kinetics plots for the degradation of RB-19 on A/W P-25. Dots indicate experimental data. Performed at natural pH and dye under Blue light.

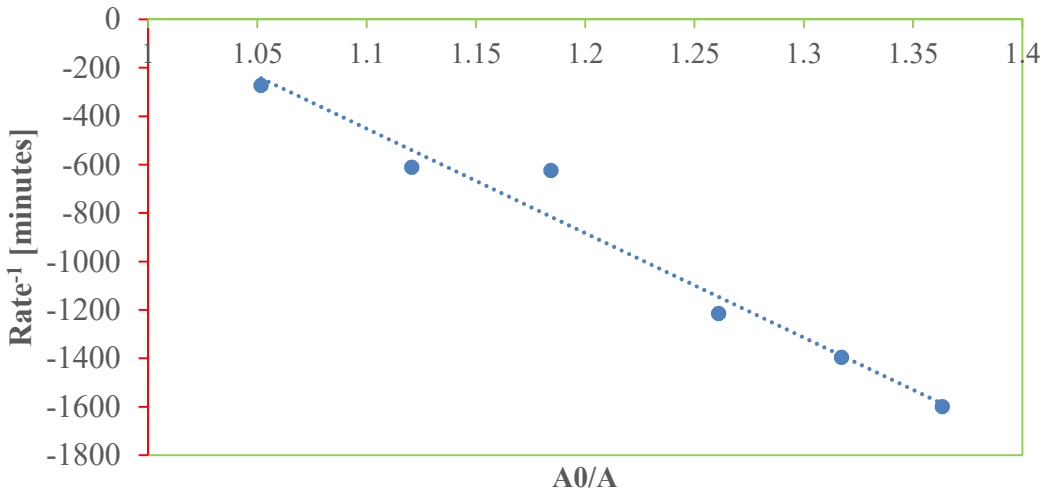

Figure 54: Langmir Hinschelwood fitting for the photodegradation of RB-19 on acid washed P-25 at natural pH under Blue light.

The activity of acid washed P-25 under blue light may be due to the narrowing band gap of TiO_2. Most importantly, the band gap of SO_4^{2-}/TiO2 can be shifted to the visible light region having sulfate species which are incorporated into the P-25 network. Due to replacing oxygen sites to form Ti-S bonds results the band gap is narrowed because mixing S 3p states with valence band (VB) contributes to the increased width of VB.[93]

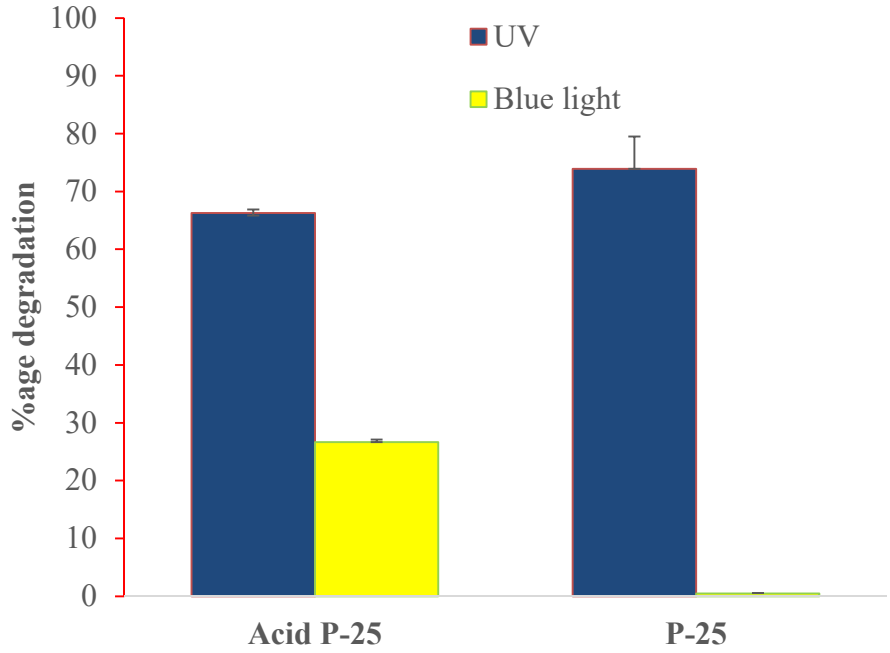

Figure 55: ((1-A)/A_0) x 100 % degradation after 120 min for A/W and pristine P-25.

The percentage photocatalytic degradation of RB-19 under UV and blue irradiation illustrates that pristine P-25 is totally inactive towards blue light but 26.7% degradation was observed in case of acid washed P-25. The percentage degradation was 73.9% and 66.3% under UV of pristine and acid washed titania for photo-catalysis. Decrease in degradation by using acid washed P-25 might be scavenger of $^{\bullet}OH$ by the SO_4^{2-} ions ($SO_4^{2-} + {}^{\bullet}OH \rightarrow SO_4^{\bullet-} + OH^-$) produce in case of UV irradiation. [92]

3.2.3 Effect Au_9 loading on RB-19 degradation

Effect of loading of Au were determined both under UV and blue light. Under UV, the percentage degradation of RB-19 was surprisingly decreased after deposition of different loadings of $Au_9(PPh_3)_8](NO_3)_3$ on P-25 surface with respect to only pristine P-25 when studied at 120 minutes. Figures 56 and 57 illustrate the effect of 0.17% $Au_9(PPh_3)_8](NO_3)_3$ present on P-25 (the maximum degradation was recorded for this particular loading under UV) in percentage photo degradation. That might be caused by the ligands with Au_9 that were hindering and interfering UV electromagnetic radiation to strike on the P-25 surface and finally not able to expel so much electrons from valance bands to conduction bands because of poorly entrapped energy. The reason with less photo catalytic activity may also be due to the poor attachment or agglomeration of Au_9 clusters on P-25.[81]

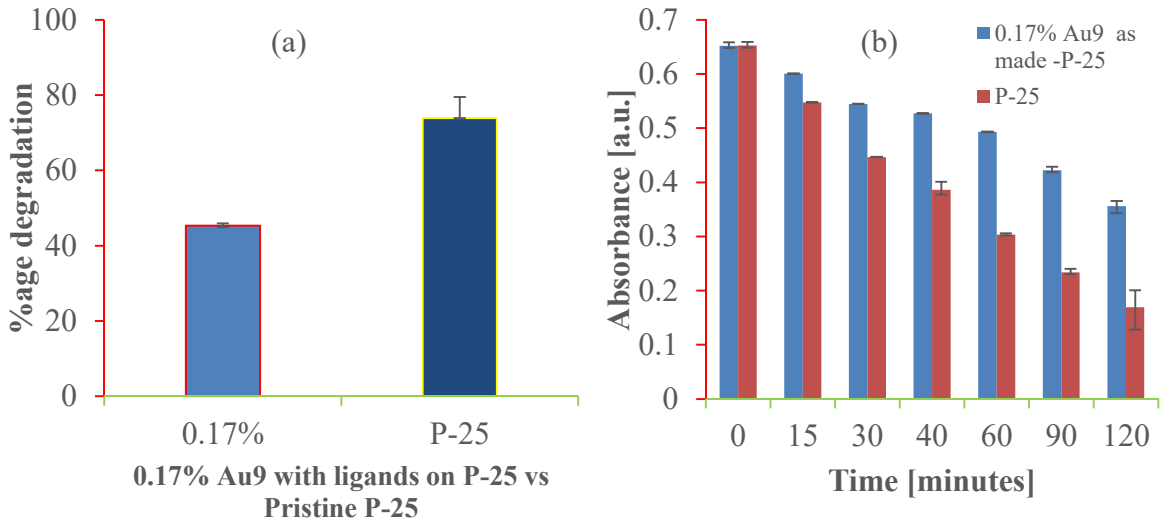

Figure 56: Effect of Au_9 as made on pristine P-25 surface for photo-degradation of RB-19 under UV. (a) Percentage degradation at 120 minutes (b) Decrease in absorbance as

function of time.

Under UV, deposited catalysts of 0.17 wt% as made $Au_9(PPh_3)_8(NO_3)_3$ P-25 showed percentage degradation of 45% which is in fact decreased down to 29% as compare to pristine P-25 degradation from 74% as shown in figure 56. However, 0.17 wt% Au_9 calcined on P-25 with degradation ability was 31%, even became more lessen down to 14% compare to as made Au_9 (45%). Without ligands although Au_9 clusters are more exposed to UV radiation but they are not playing any considerable part. Other loadings of Au_9 clusters also showed same results which illustrate that P-25 was saturated enough with clusters to give different results. Although it was observed a slight increase in degradation that can be negligible with gradual increase of loadings i.e. 0.17, 0.34 and 0.5 wt%.

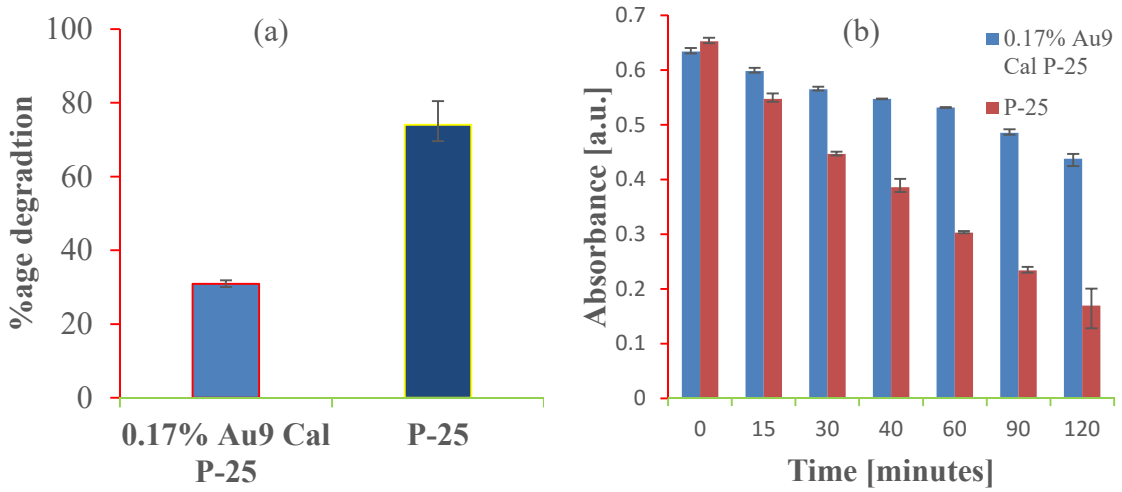

Figure 57: Effect of Au_9 calcined on pristine surface for photo-degradation of RB-19 under UV. (a) Percentage degradation at 120 minutes (b) Decrease in absorbance as function of time.

0.17 wt% was selected to compare the effect of gold on pristine P-25 because it showed the maximum degradation even compare to higher loadings 0.34 wt% and 0.5 wt% for both as made and calcined. The percentage degradation for 0.34 wt% as made and calcined were 44% and 32% while 0.5 wt% gave 43% and 30% respectively are shown in table 9.

In fact the results show that the gold clusters are not interacting with UV and it is only P-25 which showed the photocatalytic activity.

Table 9: Percentage degradation with rate coefficients of Au_9 clusters on pristine of P-25 under UV.

Percentage loadings wt%	Catalyst type Pristine P-25	Mean Percentage degradation	$k[\times 10^{-3}]$
0.17	As made	45.35 ± 1.17	4.86 ± 1.74
	Calcined	30.94 ± 2.54	2.93 ± 0.25
0.34	As made	44.80 ± 0.46	4.83 ± 2.32
	Calcined	33.52 ± 2.17	3.00 ± 1.12
0.50	As made	43.81 ± 1.93	4.54 ± 2.24
	Calcined	30.45 ± 1.27	2.79± 0.95

The kinetics of the reactions were analyzed for all experiments discussed in term of rate coefficients. It was observed that the kinetics of pristine P-25 with all loadings is first order $dC/dt = kC$, and therefore $Ct = C0\, e^{-kt}$ where Ct is concentration at time t (mol/L), C_0 is initial concentration (mol/L), and k is the rate constant (mol/L.s). However, for case of acid washed P-25 all loadings showed 2nd order kinetics. The representative graphs are shown in figure 58. The rate coefficient for acid treated P-25 with deposition of as made Au_9 were seen to be the highest but decreasing with higher loadings. Among the catalysts which are under observation calcined Au_9 deposited on pristine P-25 showed least coefficients of rate figure 59.

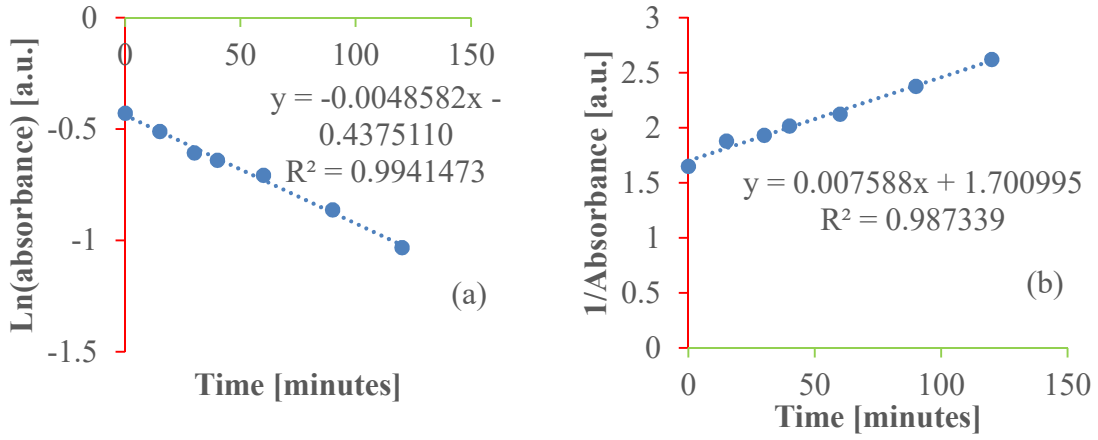

Figure 58: Representative kinetics graphs showing order of reaction under UV a) 0.17% Au_9 as made on P-25 surface (1st order kinetics) b) 0.17% Au_9 Cal. on A/W P-25 (2nd

order kinetics).

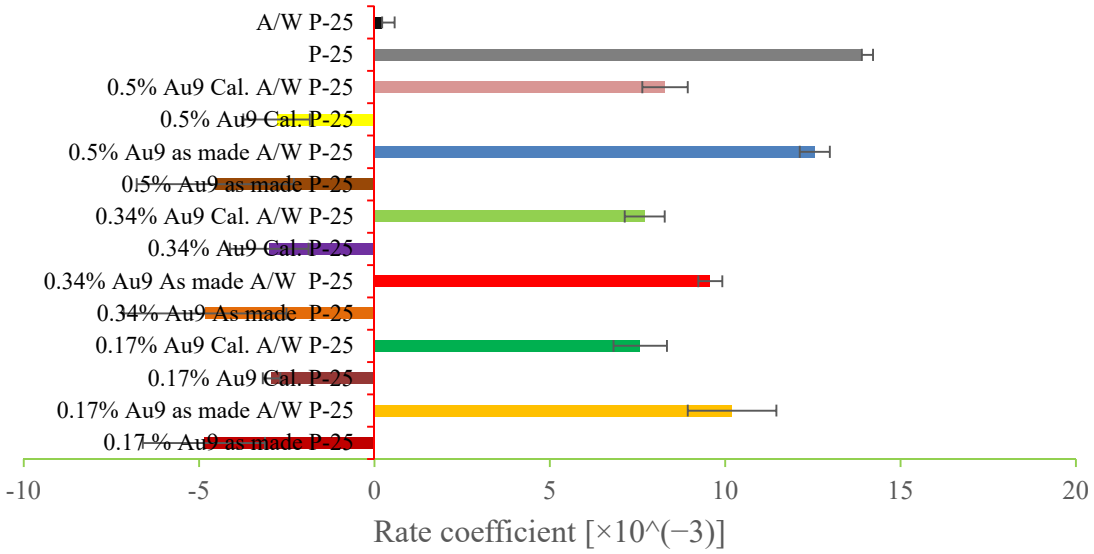

Figure 59: Rate coefficient for catalysts under UV. Positive number indicate pre-treatment improved the catalyst activity.

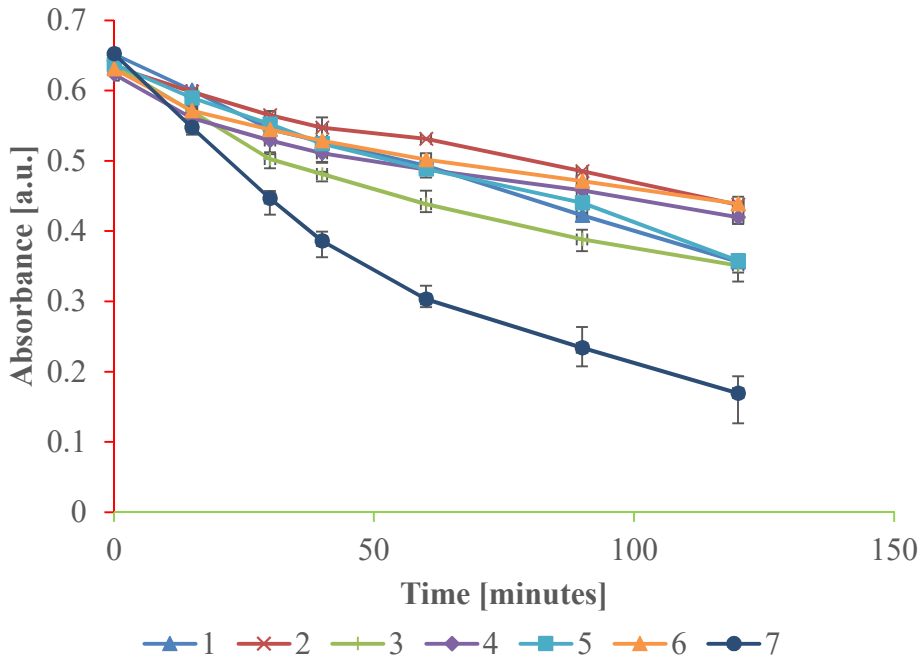

Figure 60: Decease in absorbance at time 15, 30, 40, 60, 90 and 120 minutes by the catalysts under UV. **1** (0.17% Au_9 as made P-25), **2** (0.17 wt% Au_9 calcined P-25), **3** (0.34 wt% Au_9 as made P-25), **4** (0.34 wt% Au_9 calcined P-25), **5** (0.5 wt% Au_9 as made P-25), **6** (0.5 wt% Au_9 calcined P-25) and **7** (pristine P-25).

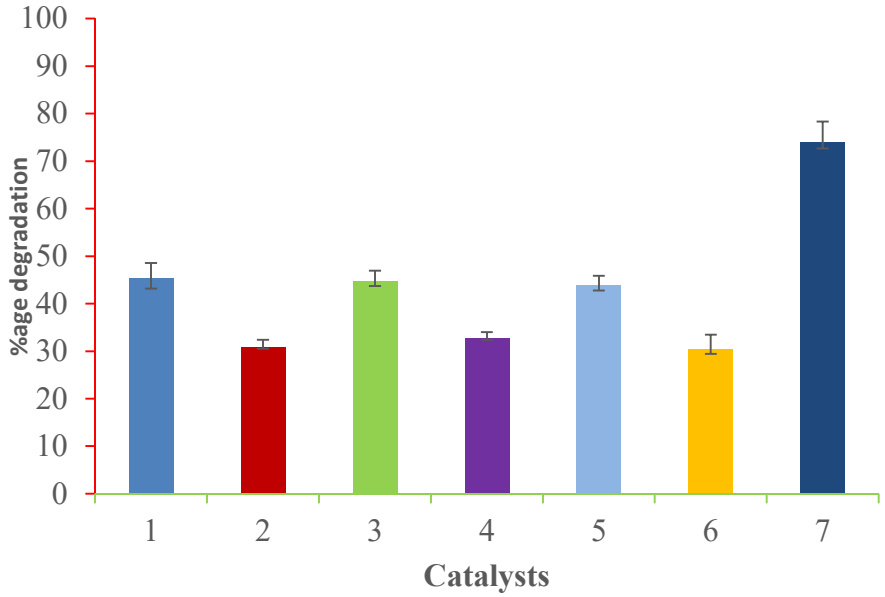

Figure 61: Percentage degradations of RB-19 by Au_9 deposited pristine P-25 catalysts at time 120 minutes under UV. **1** (0.17% Au_9 as made P-25), **2** (0.17% Au_9 calcined p-25), **3** (0.34% Au_9 as made P-25), **4** (0.34% Au_9 calcined P-25), **5** (0.5% Au_9 as made P-25), **6** (0.5% Au_9 calcined P-25) and **7** (pristine P-25).

In order to avoid agglomeration of Au_9 clusters, acid washed P-25 support is used. The deposition of Au_9 on acid washed P-25 gave results in less aggregation as shown in figure 57. Interestingly, the percentage photo-degradation under UV was similar for both pristine P-25 and acid washed P-25. While by comparison of pristine P-25 and acid treated P-25 there was a significance difference under blue. Acid washed P-25 is working alike pristine P-25 under UV but with more active under blue when compare to pristine P-25. This is an indication that SO_4^{2-} ions or doped Ti-S may not playing their role in the presence of gold clusters (figure 65) and in absence of gold clusters (figure 57) when irradiated with UV radiations. Surprisingly, the percentage degradation was decreased when acid washed support used in the presence of Au_9 clusters under UV with respect to only acid washed P-25.

The rate coefficients of pristine and acid treated support catalysts are given in table 9 and 10 respectively. The graphical representation of rate coefficients (see figures 59 and 64) also suggest the same trend with time degradation given in figures 60 and 62.

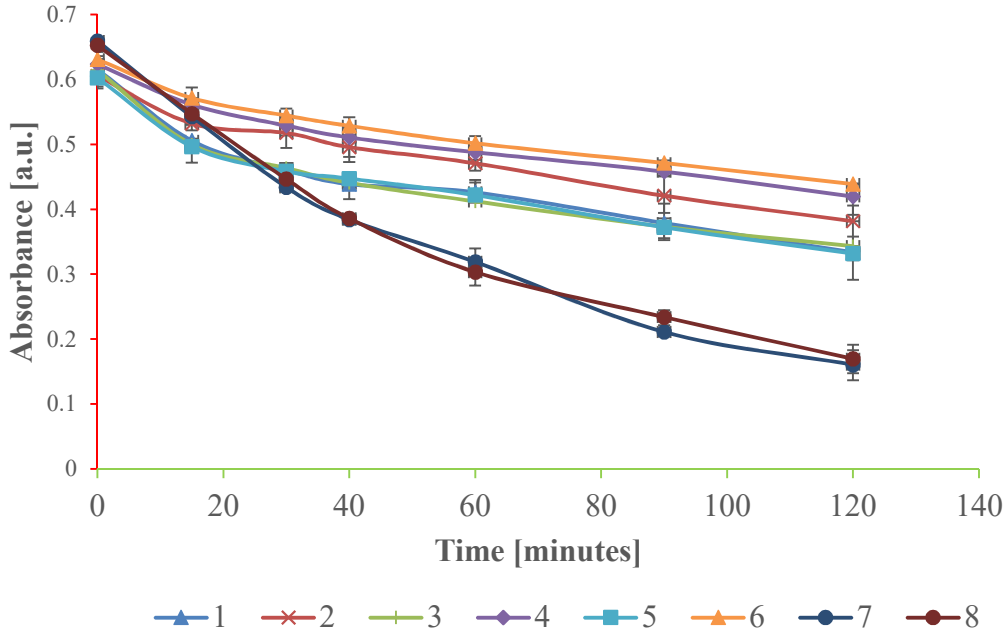

Figure 62: Decease in absorbance at time 15, 30, 40, 60, 90 and 120 minutes by the acid washed support catalysts under UV. **1** (0.17% Au_9 as made A/W P-25), **2** (0.17% Au_9 calcined A/W P-25), **3** (0.34% Au_9 as made A/W P-25), **4** (0.34% Au_9 calcined A/W P-25), **5** (0.5% Au_9 as made A/W P-25), **6** (0.5% Au_9 calcined A/W P-25), **7** (acid washed P-25) and **8** (pristine P-25).

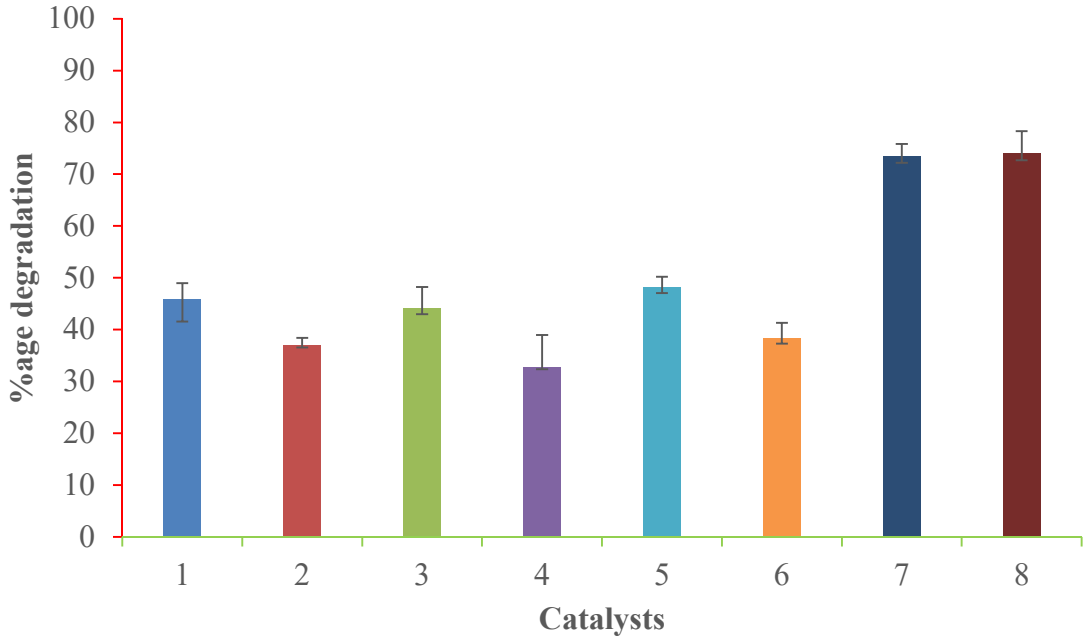

Figure 63: Percentage degradations of RB-19 by Au_9 deposited acid washed P-25

catalysts at time 120 minutes under UV. **1** (0.17% Au_9 A/W as made P-25), **2** (0.17% Au_9 calcined A/W P-25), **3** (0.34% Au_9 as made A/W P-25), **4** (0.34% Au_9 A/W calcined P-25), **5** (0.5% Au_9 as made A/W P-25), **6** (0.5% Au_9 calcined A/W P-25), **7** (acid washed P-25) and **8** (pristine P-25).

Table 10: Percentage degradation with rate coefficients of Au_9 clusters on acid washed surface of P-25 under UV (2^{nd} order).

Percentage loadings wt%	Catalyst type (Acid washed)	Mean % degradation by Acid washed P-25	$k[\times 10^{-3}]$ $mint^{-1}$
0.17	As made	45.77 ± 2.20	10.2 ± 1.26
	Calcined	36.97 ± 0.43	7.58 ± 0.76
0.34	As made	44.14 ± 2.13	9.58 ± 0.34
	Calcined	32.68 ± 3.31	7.71 ± 0.57
0.50	As made	48.15 ± 1.07	12.56 ± 0.43
	Calcined	38.34 ± 1.31	8.29 ± 0.65

The main idea of gold deposition on P-25 that it should be active under visible light, as UV constitute only a small fraction of the total photon flux from the sun reaching the earth surface. Visible light activity was done using 2 blue LEDs of 50W with wavelength ~>420nm. TiO_2 is inactive under visible light due to the band gab so the less energetic visible light can't promote electron from valance band to conduction band. However some activity, is even, sometimes observed on P-25, and this may be aid by sensitization

of the catalyst caused by adsorbed dye. But from figure 46 and 47 it is immediately apparent that there is no considerable adsorption before commencing the photocatalytic reaction up to end of the reaction. Almost all the catalysts were more active than P-25 under visible light. Surprisingly, some acid washed catalysts under visible light even showed better results than pristine P-25 under UV figure 65. It was previously observed that acid washed P-25 without Au_9 clusters also had some photo-degradation activity 26.7% which was shown in percentage degradation in figure 55. The photo degradation by 0.17, 0.34 and 0.5 wt% Au_9 deposited pristine P-25 with no pre and post treatment was done with catalysts, demonstrated 8%, 8.2% and 11% catalytic activity under blue light after 120 minutes. *As made* acid washed Au_9 clusters are seems to be interacting more than as made with pristine P-25 under blue light which only pristine P-25 can't do.

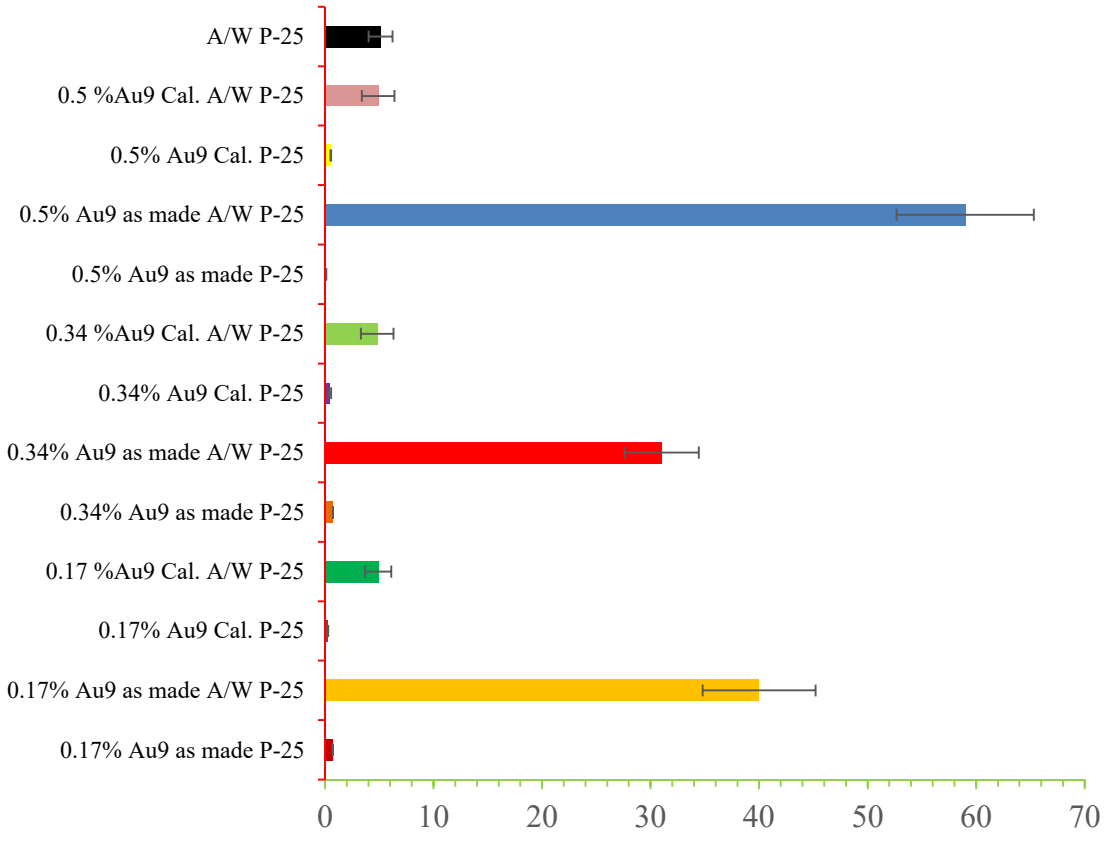

Figure 64: Rate coefficients for catalysts under blue.

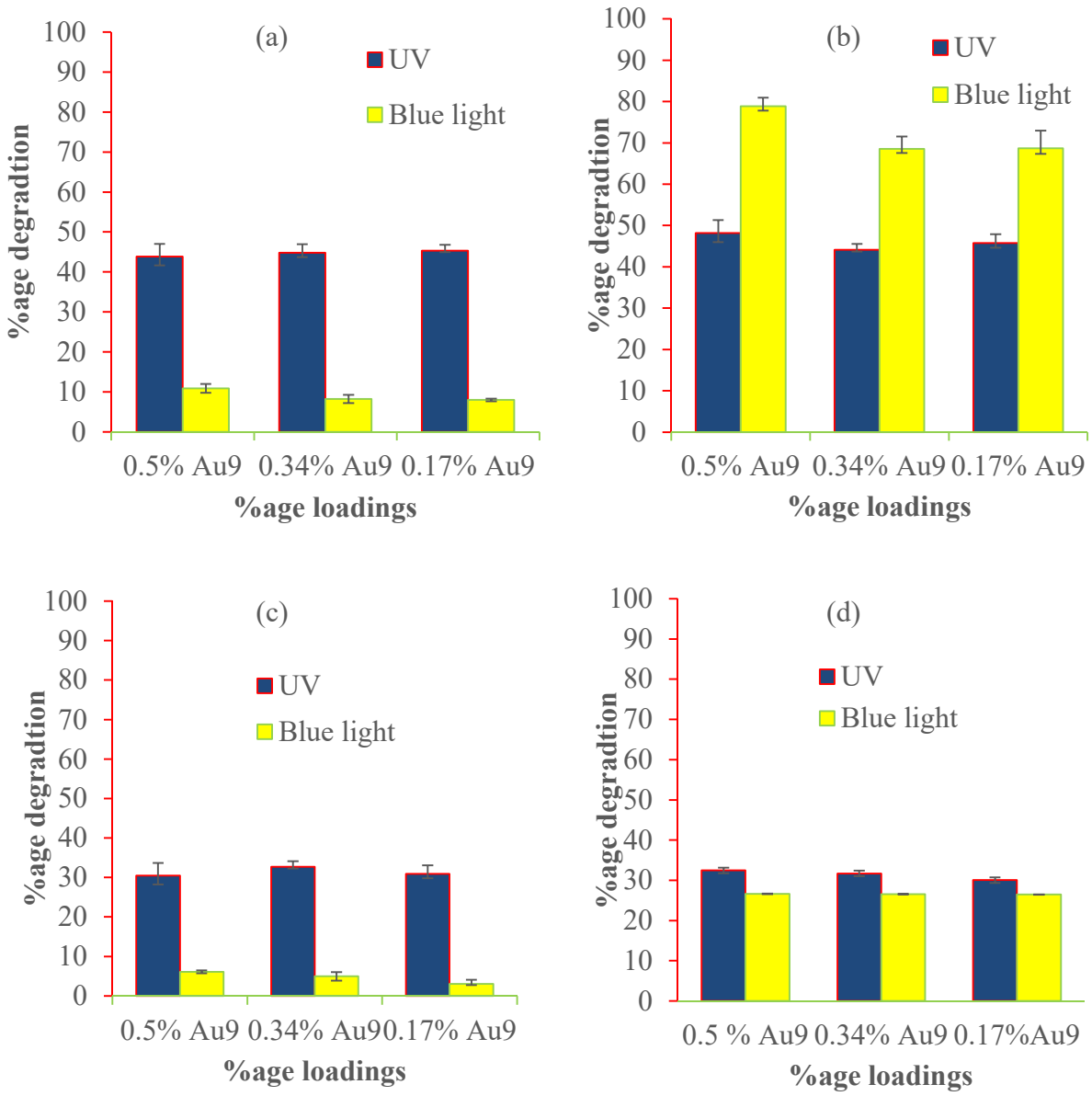

Figure 65: Comparison of percentage photo degradation of RB-19 under UV and blue light. a) $Au_9(PPh_3)_8(NO_3)_3$ P-25 b) $Au_9(PPh_3)_8(NO_3)_3$ A/W P-25 c) Au_9 Cal. P-25 d) Au_9 Cal. A/W P-25.

To further understand how post treatment of calcination or Au_9 clusters without ligands change the catalytic activity under blue light the experiments were conducted under blue are shown in above figure 65. The graph suggests that under blue irradiation photo catalytic activity was too small in case of pristine support either with as made or calcined Au_9. However acid washed P-25 gave remarkable results calcined Au_9. Even better results were obtained with as made Au_9 clusters on acid washed than pristine P-25 under UV.

This suggests that while pre-treatment i.e. washing with sulfuric acid SO_4^{2-} ions are incorporated which may lead to narrow the band gaps. It is even possible that sulfate present on the sulfate acting as co-catalyst to enhance photo catalytic activity. To probe this issue whether SO_4^{2-} ions are playing some part, TGA analysis was done shown in figure 20 in chapter 2. TGA graph illustrates that there is rapid loss occurred after 473 K (~200°C), suggesting acid washed P-25 doesn't lose its considerable mass. To peep into this matter recycling experiments were conducted are discussed at the end of this chapter.

Table 11: Percentage degradation and coefficient rates of different catalysts for RB-19 under blue light.

Percentage loadings wt%	Catalyst type on P-25	Mean Percentage degradation	$k[\times 10^{-3}]$
0.17	As made P-25	7.97 ± 0.32	0.714± 0.03
	As made A/W P25	68.66 ± 4.31	40 ± 5.21
	Calcined P-25	3.07 ± 0.31	0.248 ± 0.05
	Calcined A/W P-25	26.45 ± 2.13	4.9 ± 1.2
0.34	As made P-25	8.2 ± 1.0	0.71 ± 0.002
	As made A/W P25	68.55 ± 3.01	31 ± 3.43
	Calcined P-25	4.98 ± 1.1	0.43 ± 0.13
	Calcined A/W P-25	26.54 ± 1.43	4.8 ± 1.5
0.50	As made P-25	10.86 ± 1.07	0.1 ± 0.02
	As made A/W P25	78.89 ± 3.07	59 ± 6.32
	Calcined P-25	6.13 ± 0.31	0.53 ± 0.03
	Calcined A/W P-25	26.64 ± 3.2	4.9 ± 1.5
A/W P-25		26.66 ±	5.12 ± 1.1

3.3 Total Organic Carbon (TOC) Analysis

Reduction in Total organic carbon (TOC) analysis contents reflects the mineralization of organic compound. The reduction in total organic carbon is studied by Shimadzu, model TOC-V CSH. The instrument was operated at room temperature and 9 ml sample injection was poured in the TOC tube. Samples after treatment were filtered by Milli pore filter. Reduction in percentage total organic carbon content was measured using following equation.[112] TOC (%) = ($TOC_{initial}$–TOC_{final}/ $TOC_{initial}$) x 100

Table 12: Total Organic Carbon analysis.

Percentage loadings	%TOC reduction		UV (mg/100ml)			Blue (mg/100ml)		
	UV	Blue	TC	IC	TOC	TC	IC	TOC
0.17-P-AM	20.46	31.04	27.52	11.51	16.01	25.66	11.47	14.19
0.17-P-C	20.84	30.95	27.39	11.49	15.9	25.69	11.73	13.96
0.17-AW-AM	18.76	36.50	28.11	11.51	16.6	23.77	11.50	12.27
0.17-AW-C	27.2	33.47	25.19	11.60	13.59	24.82	11.44	13.38
0.34–P-AM	26.71	31.01	25.36	11.51	13.85	25.67	11.61	14.06
0.34–P-C	26.59	35.23	25.4	11.62	13.78	24.21	11.69	12.52
0.34-AW-AM	24.19	33.55	26.23	11.56	14.67	24.79	11.5	13.29
0.34–AW-C	32.75	31.88	23.27	11.61	11.6	25.37	11.42	1395
0.5-P-AM	25.98	35.40	25.61	11.7	13.91	24.15	11.51	12.64
0.5–P-C	20.78	31.56	27.41	11.59	15.82	25.48	11.63	13.85
0.5-AW-AM	22.63	31.88	26.77	11.55	15.22	25.37	11.49	13.88
0.5-AW-C	15.92	33.24	29.09	11.61	13.37	24.9	11.53	13.37
P-25	23.55		26.45	11.63	14.82	….	….	….
AW P-25	22.77	32.05	26.72	11.73	14.99	25.31	11.37	13.94

It is important to mention here that colour removal does not necessarily correspond to dye degradation. The analytical methods such as total organic content (TOC) was used to confirm dye degradation and it was observed from the results of TOC that all the catalysts have almost same TOC values (in a range of 13 to 16 mg/100 ml) along with considerable amount of inorganic (IC) content. Maria *et al.* studied photodegradation of RB-19 with TiO_2 under UV light. The author observed 10.18% TOC reduction at pH 4 having 100 mg/L of dye concentration with 30 mg of TiO_2 (anatase phase only) in 100 ml of dye.[112] The values may suggest that all of the catalysts were photocatalysing the dye into smaller organic constituents. The estimated value of total carbon content in 0.08 g/L RB-19 was 34 mg and the only dye stock solution showed that value (mean 34.6 mg ± 2.3) while in case of each catalyst the values were around 25mg. This may indicates some corban was released in the form gasses like CO_2 as reported earlier by Muggli *et al* in the degradation of dyes. [100]

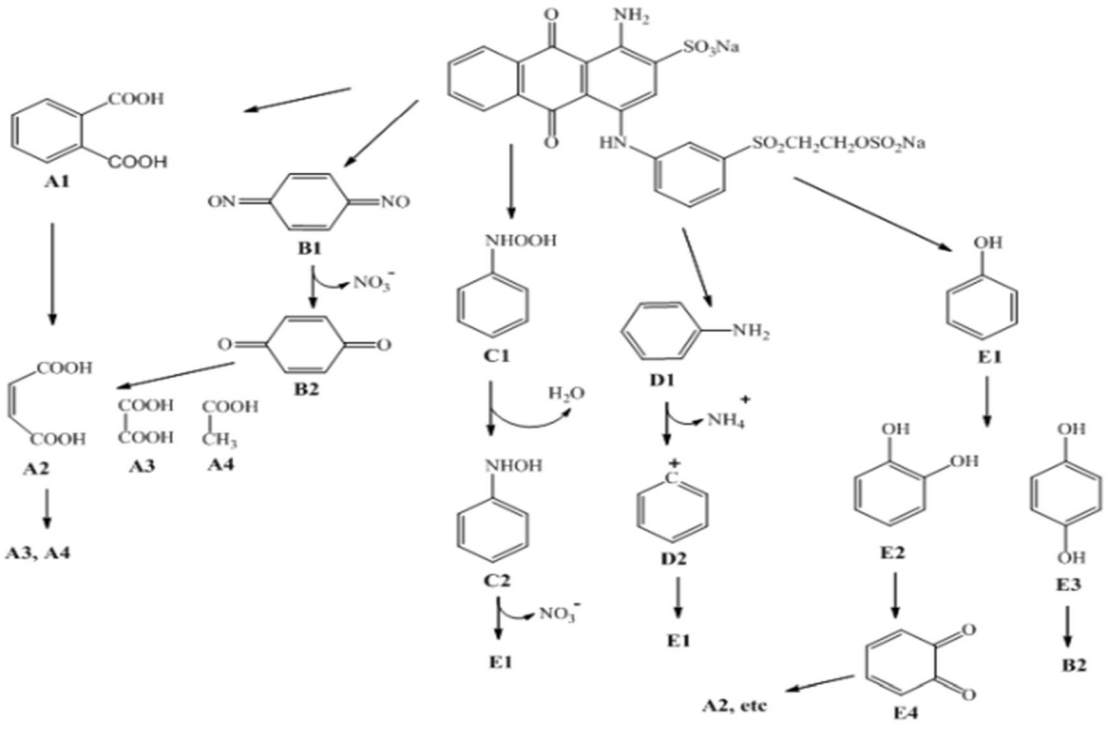

Figure 66: Possible photo-oxidation pathways of RB-19 by the hydroxyl radicals

resulting from photocatalysis[94]

Figure 66 shows all possible pathways of photo-oxidation of RB-19 by the hydroxyl radicals formed in photocatalysis as suggested by He *et al*.[94] It was reported that other than the desirable mineralization products (CO_2, etc.), the possible by-products of RB-19 by photodegradation include butenediacid, oxalic acid, acetic acid (A4), phenol (E1), and benzo-1,4-quinone (B2).

3.4 Recycling

Recycling experiments were conducted to investigate the catalytic ability of Au_9 based P-25 after one round of catalytic ability and to determine possible SO_4^{2-} present on acid washed P-25. 0.17% loadings was selected for this study and only one time that experiment was done because the recovery of a catalyst was too small to run three rounds of experiments. Instead of 100 ml of dye half of the quantity was used with 15 mg of catalyst instead of 30 mg. Before running that experiment one time run catalyst from three different times of experiment was dried under dark at room temperature for 10 days.

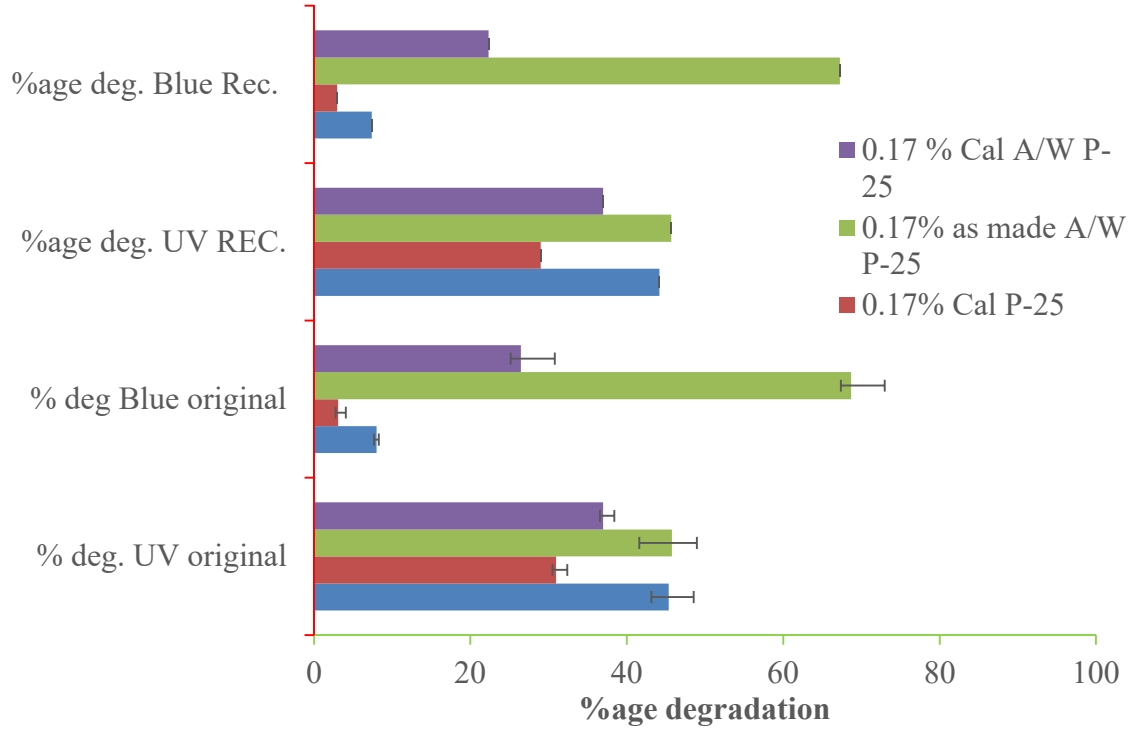

Figure 67: Recycling of catalysts with percentage loading 0.17.

The above graph illustrates that there is no significance difference so the activity of the catalyst remain intact after one round of reaction. Specially, acid washed support showed similar results which may indicate that SO_4^{2-} or Sulphur containing species are in strong contact with the support.

Conclusion

The photocatalytic activity of several Au_9 clusters based on Titanium dioxide materials were evaluated by using photo degradation of an industrial dye Reactive Blue 19 (RB-19) as a model reaction. Initial studies compelled that when using UV-vis spectroscopy as a measure of dye degradation the system did not obey zeroth order, or Langgumuir Hinschelwood kinetics. But it obeys either 1^{st} or 2^{nd} order kinetics for pristine P-25 TiO_2 support and acid washed P-25 TiO_2 respectively. Thus, the extent of degradation in all cases was determined by comparing the absorbance of initial t-0 and t=120 solutions at the absorption maximum of the dye and rate constants coefficients of related reactions.

Initial studies using Aeroxide P-25 as a catalyst were undertaken to determine the effect of Au_9 clusters, percentage clusters loadings, effect of ligands (as made vs calcined), effect of support (pristine P-25 vs acid washed P-25) and degradation under UV and blue light. It was found that the effect of Au_9 increased the photo catalytic degradation under blue irradiation while the only pristine P-25 was totally inactive in that wavelength. Interestingly, not only the rate of degradation increased but also the percentage degradation increased when acid washed P-25 used as catalyst. Au_9 as made clusters were loaded on acid washed P-25, the highest degradation was observed under the blue light with the highest percentage of loading. While the degradation was lowered down in the case of, with respect to same loadings, Au_9 as made or calcined clusters when deposited on the support pristine P-25. The reason may be due to well deposition of Au_9 as made on the surface of acid washed P-25 showing in TEM images and DRS results with clusters signature at ~430nm. It was obvious that the calcined Au_9 were not so effective under blue irradiation for photo catalytic degradation. Although, calcined Au_9 clusters on acid washed P-25 were catalytically less active than even the half of the activity of as made Au_9 on acid washed P-25 but they were far better than non-acid washed calcined clusters under blue. On the other hand, as made Au_9 clusters on pristine P-25 were relatively a little better than Au_9 calcined on pristine P-25 under same blue light. There are multiple reasons theoretically for these results. SO_4^{2-} are lowering the conduction bands of TiO_2 as in all samples of Au_9 clusters deposited on acid-washed P-25, sulfur signals were observed in XPS spectra which corresponded to 1-3% of the samples' total makeup, which may ease the promotion of electron to conduction band from valance band. TGA

shed light onto the significant loss of mass after 200˚C suggesting that SO_4^{2-} ions some are still there for calcined. Even Au_9 may also interact with the visible light under blue but for UV it was found that high proportion of discrete gold clusters (as reported by DRS and XPS) does not necessarily result in a good catalyst. The activity was decrease by post treatment in either UV or blue for such catalysts. The ligands with Au_9 may have electronic transition to interact with visible light. It is thought this can be attributed to the synergetic effect of anchoring /ligands, hinting complex nature of these systems. AAS analysis shows the loadings in each case is very close to estimated values. TEM images show some aggregation in case of pristine support while calcined catalysts show more agglomeration.

Under UV irradiation, both as made of Au_9 clusters with pristine P-25 and acid washed P-25 catalysts and with the different loadings gave almost same results when comparing with each other but surprisingly, less degradation results with respect to pristine P-25, compelling that clusters loadings and presence has inverse effect on degradation. Calcined Au_9 showed even lower down more under UV may be due to agglomeration into larger nanoparticles during calcination inhibiting the UV to reach the surface of titnia. TOC shows that some of the carbon content converting to CO_2 with inorganic constitutes while rest are converting onto smaller organic fragments. By the recycling results is clear that the stability of the 0.17% as made A/W Au_9 cutlers is intact.

4.1 Future Plans

The catalysts would be investigate for degradation under other visible wavelengths as well as mimic to solar light irradiation (UV & visible). Further study on these products should be attempted using high performance liquid chromatography (HPLC), mass spectrometry will shed light on the degradation pathways of the dyes used, as well as the applicability of these degradation reactions to real-world industrial applications. By using some different dyes may also show the mechanism of degradation. However water splitting and liquid fuel generation is the ultimate target for these photo catalysts.

References

1. Abu Bakar, F., J.-Y. Ruzicka, I. Nuramdhani, B. E. Williamson, M. Holzenkaempfer and V. B. Golovko., *Australian Journal of Chemistry* **2015**, 68(3), 471-480.
2. Manual best management practices for pollution prevention in the textile industry. In *EPA/625/R-96/004* September 1996 ed.; U.S. Environmental Protection Agency. **1996**.
3. *Zollinger, H.,* Color chemistry: synthesis, properties and applications of organic dyes and pigments. *2nd ed.; VCH: **1991**.*
4. Catoor, T. European legislation relating to textile dyeing In *Environmental aspects of textile dyeing* Christie, R. M., Ed. Woodhead Publishing Limited: Cambridge, **2007**; pp 1-29.
5. Spagni, A.; Grilli, S.; Casu, S.; Mattioli, D., *International Biodetorioration and Biodegradation* **2010,** *64,* 676-681.
6. Koprivanac, N.; Kusic, H., Hazardous Organic Pollutants in Colored Wastewaters. Nova Science Publishers: New York, **2009**.
7. Mahmoodi, N. M.; Arami, M.*, Journal of Photochemistry and Photobiology B: Biology* **2009,** *94,* 20-24.
8. Akyol, A.; Yatmaz, H. C.; Bayramoglu, M., *Applied Catalysis B-Environmental* **2004,** *54* (1), 19-24.
9. Baldrian, P.; Merhautova, V.; Gabriel, J.; Nerud, F., *Applied Catalysis B: Environmental* **2006,** 66, 258-264.
10. Somensia, C. A.; L, E.; Simionattoa; L, S.; Bertoli; Jr, A. W.; Radetskib, C. M., *Journal of Hazardous Materials* 2010, 175, 235-240.
11. Christie, R. M., *Colour Chemistry.* Royal Society of Chemistry: 2001.
12. Uddin, M. J.; Cesano, F.; Scarano, D.; Bobibo, F.; Agostini, G.; Spoto, G.; Bordiga, S.; Zecchina, A., *Journal of Photochemistry and Photobiology B: Biology* **2008,** *199,* 64-72.
13. *Hashimoto, K.,* Japanese Journal of Applied Physics ***2005,*** 44 *(12), 8269-8285.*
14. Papic, S.; Koprivanac, N.; Bozic, A. L.; Vujevic, D., *Water Environment Research* **2006,** *78* (6), 572.
15. Sung-Suh, H. M.; Choi, J. R.; Hah, H. J.; Koo, S. M.; Bae, Y. C., *Journal of Photochemistry*

and Photobiology A: Chemistry **2004,** *163,* 37-44.

16. Anipsitakis, G. P.; Dionysiou, D. D., *Applied Catalysis B: Environmental* **2004,** *54,* 155-163.
17. Sakthivel, S.; Shankar, M. V.; Palanichamy, M.; Arabindoo, B.; Bahnemann, D. W.; Murugesan, V., *Water Research* **2004,** *38,* 3001-3008.
18. Kumar, P. S. S.; Sivakumar, R.; Anandan, S.; Madhavan, J.; Maruthamuthu, P.; Ashokkumar, M., *Water Research* **2008,** *42,* 4878-4884.
19. Yogi, C.; Kozima, K., *J. Mater Sci.* **2009,** 44, 821-827.
20. Dozzi, M. V.; Prati, L.; Canton, P.; Selli, E., *Physical Chemistry Chemical Physics* **2009,** *11* (33), 7171-7180.
21. Turner, M.; Golovko, V. B., *Nature* **2008,** *07194.*
22. Koenderink, J., *Color for the Science.* The MIT Press: London, **2010.**
23. Broadbent, A. D., Basic Principles of Textile Coloration. Society of Dyers and Colourists: West Yorkshire, England, **2001**.
24. Nassau, K., *The Physics and Chemistry of Color.* 2nd ed.; John Wiley & Sons, Inc.: **2001.**
25. *Shore, J., Classification and general properties of colorants In* Colorants and Auxiliaries Organic Chemistry and Appllication Properties 2ed.; Shore, J., Ed. Society of Dyers and Colourists: West Yorkshire, UK, **2002**, 1, 1-44.
26. Perkampus, Heinz-Helmut., UV-VIS Spectroscopy and Its Applications ISBN 978-3-642-77477-5, **1992.**
27. Atkins, P.; Paula, J. D., *Atkins' Physical Chemistry.* 9 ed.; Oxford University Press: Oxford, **2010**.
28. *Renfrew, A. H. M.,* Reactive Dyes for Textile Fibres: The Chemistry of activated n-bonds as reactive groups and miscellaneous topics. *Society of Dyers and Colourists: Bradford,* **1999**.
29. Clayden, J.; Greeves, N.; Warren, S.; Wothers, P., *Organic Chemistry.* Oxford University Press: Oxford, **2001.**
30. Beech, W. F., *Fibre-Reactive Dyes.* Logos Press Limited: London, **1970.**
31. Hardin, I. R., Chemical treatment of textile dye effluent. In *Environmental aspects of textile dyeing,* Christie, R. M., Ed. Woodhead Publishing Limited: Cambridge, **2007.**

32. Konstantinou, I. K.; Albanis, T. A., *Applied Catalysis B: Environmental* **2004,** *49,* 1-14.

33. Pearce, C. I.; Lloyd, J. R.; Guthrie, J. T., *Dyes and Pigments* **2003,** *58,* 179-196.

34. ONeil, C.; Hawkes, F. R.; Hawkes, D. L.; Lourenco, N. D.; Pinheiro, H. M.; Delee, W., *Journal of Technology and Biotechnology* **1999,** *74,* 1009-1018.

35. Bae, J. S.; Freeman, H. S., *Dyes Pigments* **2007,** *73* (1), 81-85.

36. *Verma, Y.,* Toxicology and Industrial Health ***2011,*** 27 *(1), 41-49.*

37. Gregory, P., Toxicology of textile dyes. In *Environmental aspects of textile dyeing,* Cristie, R. M., Ed. Woodhead Publishing Limited: Cambridge, 2007.

38. Hunger, K., *Chimia* **1994,** *48,* 520-522.

39. Golka, K.; Kopps, S.; Myslak, Z. W., *Toxicology Letters* **2004,** *151,* 203-210.

40. Moller, P.; Wallin, H., *Mutation Research* **2000,** *462,* 13-30.

41. Sichel, S.; Tello, J.; Cara, M. D.; Fernandez-Ibanez, P., *Catalysis Today* **2007,** *129,* 152-160.

42. Fujishiima, A.; Zhang, X., *C. R. Chimie* **2006,** 9, 750-760.

43. Fujishima, A.; Zhang, X.; Tryk, D. A., *International Journal of Hydrogen Energy* **2007,** *32,* 2664-2672.

44. Fujishima, A.; Zhang, X.; Tryk, D. A., *Surface Science Reports* **2008,** *63,* 515-582.

45. Thompson, T. L. and J. J. T. Yates., *Chemical reviews* **2006,** 106(10): 4428.

46. Kozlov, D., D. Bavykin and E. Savinov., *Catalysis Letters* **2003,** 86(4): 169-172.

47. Berger, T., D. Monllor-Satoca, M. Jankulovska, T. Lana-Villarreal and R. Gómez., *Chemphyschem : a European journal of chemical physics and physical chemistry* **2012,** 13(12): 2824.

48. Kominami, H., J. Kato, Y. Takada, Y. Doushi, B. Ohtani, S. Nishimoto, M. Inoue, T. Inui and Y. Kera., *Catalysis Letters* **1997,** 46(3): 235-240.

49. Bagheri, S., N. Muhd Julkapli and S. Bee Abd Hamid., *The Scientific World Journal* **2014**, 2014.

50. Palcheva, R., L. Dimitrov, G. Tyuliev, A. Spojakina and K. Jiratova., *Applied Surface Science* **2013,** 265(0): 309-316.

51. Liang, G., L. He, H. Cheng, W. Li, X. Li, C. Zhang, Y. Yu and F. Zhao., *Journal of Catalysis* **2014,** 309(0): 468-476.

52. Rojas, H., H. Rojas, G. Borda, P. Reyes and J. J. Martínez., *Catalysis today* **2012,** 133-135: 699-705.

53. Shin, H., T.-H. Byun, S. Lee, S.-T. Bae and H. S. Jung., *Journal of Physics and Chemistry of Solids* **2013,** 74(8): 1136-1142.

54. Nalbandian, M. J., K. E. Greenstein, D. Shuai, M. Zhang, Y.-H. Choa, G. F. Parkin, N. V. Myung and D. M. Cwiertny., *Environmental Science & Technology* **2015,** 49(3): 1654-1663.

55. Murdoch, M., G. I. N. Waterhouse, M. A. Nadeem, J. B. Metson, M. A. Keane, R. F. Howe, J. Llorca and H. Idriss., *Nature Chemistry* **2011,** 3(6): 489.

56. *Diebold, U.,* Surface Science Reports ***2003,*** 48, *53-229.*

57. Sclafani, A.; Hermann, J. M., *J. Phys. Chem.* **1996,** *100,* 13655-13661.

58. Fusi, M.; Maccallini, E.; Caruso, T.; Casari, C. S.; Bassi, A. L.; Bottani, C. E.; Rudolf, P.; Prince, K. C.; Agustino, R. G., *Surface Science Reports* **2011,** *605,* 333-340.

59. Sapra, S.; Sarma, D. D., Electronic Structure and Spectroscopy of Semiconductor. Nanocrystals. In the Chemistry of nanomaterials: Synthesis, Propeties and Applications, Rao, C. N . R; Muller, A.; Cheetham, A. K., Wiley –Vch :Weinheeim 2004; pp 371-404.

60. Chen, X., *Chin J Catal* **2009,** *30* (8), 839-851.

61. Yan-Fei, H.; Gang, J.; Da-Qiao, M.; Fan-Jie, K., *Acta Physico-Chimica Sinica* **2010,** *26* (6), 1664-1668.

62. Meng-Hsiung, W.; Chuan, C.; Shin-Pon, J., *Chin J Catal* **2009,** *30* (5), 384-390.

63. Barginsky, L., *Physica E.* **2000,** 5, 142-152.

64. Braginsky, L.; Skhlover, V., *Eur. Phys. J. D.* **1999,** 9, 627-630.

65. Lee, S., C. Fan, T. Wu and S. L. Anderson., *The Journal of Chemical Physics* **2005,** 123(12): 124710

66. Wu, Y.; Liu, H.; Zhang, J.; Chen, F., *J. Phys. Chem.* **2009,** *113,* 14689-14695.

67. Luttrell, T., S. Halpegamage, J. Tao, A. Kramer, E. Sutter and M. Batzill., *Sci Rep* **2014,** 4: 4043.

68. Lu, H., J. Kou, J. Fan, Y. Chen, X. Zhou and F. Wu., *The Journal of chemical physics* **2013,** 139(6): 064705-064706.

69. Yang, Y.; Zhong, H.; Tian, C., *Res Chem Intermed* **2011,** 37, 91-102.

70. Ahmed, S.; Rasul, M. G.; Martens, W. N.; Brown, R.; Hashib, M. A., *Water Air Soil Pollut.* **2011,** *215,* 3-29.

71. *Gratzel, M.,* Journal of Photochemistry andPhotobiology A: Chemistry **2004,** 164, *3-14.*

72. Campbel, W. M.; Burrell, A. K.; Officer, D. L.; Joley, K. W., *Coordination Chemistry Reviews* 2004, *248* (1363-1379).

73. Zheng, X.; Zhang, J.; Peng, L.; Yang, X.; Cao, W., *J. Mater Sci.* **2011,** 46, 5071-5078.

74. Sari, S.; Shishodia, P. K.; Mehra, R. M., *Journal of Renewable and sustainable energy* **2010,** *2,* 043103

75. Burda, C.; Lou, Y.; Chen, X., *Nanoletters* **2003,** *3* (8), 1049-1052.

76. Scuderi, M. V. Brundo, K. Bergum, M. Zimbone, R. Sanz, M. A. Buccheri, F. Simone, G. Nicotra, B. G. Svensson, M. G. Grimaldi and V. Privitera., *Nanoscale* **2014, 6**(19): 11189-11195.

77. Subramanian, V., E. E. Wolf and P. V. Kamat., *Journal of the American Chemical Society* **2004,** 126(15): 4943-4950.

78. Meyer, R., C. Lemire, S. K. Shaikhutdinov and H. J. Freund., *Gold Bulletin* **2004,** 37(1-2): 72-124.

79. Padikkaparambil, S., B. Narayanan, Z. Yaakob, S. Viswanathan and S. M. Tasirin.,*International Journal of Photoenergy* **2013,** 2013: 10.

80. Li, G. and R. Jin., *Accounts of Chemical Research* **2013,** 46(8): 1749.

81. Anderson, D. P., J. F. Alvino, A. Gentleman, H. A. Qahtani, L. Thomsen, M. I. J. Polson, G. F. Metha, V. B. Golovko and G. G. Andersson., *Physical chemistry chemical physics* **2013,** 15(11): 3917.

82. Anderson, D. P., R. H. Adnan, J. F. Alvino, O. Shipper, B. Donoeva, J.-Y. Ruzicka, H. Al Qahtani, H. H. Harris, B. Cowie, J. B. Aitken, V. B. Golovko, G. F. Metha and G. G. Andersson., *Physical chemistry chemical physics* **2013,** 15(35): 14806.

83. Ruzicka, J. Y., F. Abu Bakar, C. Hoeck, R. Adnan, C. McNicoll, T. Kemmitt, B. C. Cowie, G. F. Metha, G. G. Andersson and V. B. Golovko., *Journal of physical chemistry C,* **2015,** 119(43): 24465-24474.

84. *Hermann, J.-M.,* Appl. Catal. B: Environ ***2010.***

85. Chen, X.; Mao, S. S., *Chem. Rev.* **2007,** *107,* 2891-2959.

86. akpan, U. G.; Hameed, B. H., *Journal of Hazardous Materials* **2009,** *170,* 520-529.

87. Primo, A., A. Corma and H. Garcia., *Physical Chemistry Chemical Physics* **2011,** 13(3): 886-910.

88. Ohno, T.; Sakurawa, K.; Tokieda, K.; Matsumura, M., Journal of Catalysis **2001,** 203, 82-86

89. Hurum, D. C.; Agrios, A. G.; Gray, K. A.; Rajh, T.; Thurnauer, M. C., J. Phys. Chem. **2003,** 107, 4545-4549.

90. Lachheb, H.; Puzenat, E.; Houas, A.; Ksibi, M.; Elaloui, E.; Guillard, C.; Hermann, J.-H., *Appl. Catal. B: Environment* **2002**, 39, 75-90.

91. Lee, D. K.; Cho, I. C.; Lee, G. S.; Kim, S. C.; Kim, D. S.; Yang, Y. K., *Separation and Purification Technology* **2004,** 34*,* 43-50.

92. Park, S.-K. and H. Shin. *Journal of Nanoscience and Nanotechnology* **2014** 14(10): 8122-8128.

93. Nishikiori, H., M. Hayashibe and T. Fujii. *Catalysts*. **2013,** 3, 363-377.

94. He, Z.; Lin, L.; Song, S.; Xia, M.; Xu, L.; Ying, H.; Chen, J. *Separation and Purification Technology* **2008,** *62,* 376-381.

95. Tabrizian, E., Amoozadeh A. and Rahmani S. *RSC Adv.* **2016,** *6(26)*, 21854-21864.

96. K. Juodkazis, J. Juodkazyte, V. Jasulaitiene, A. Lukinskas and B. Sebeka,. *Electrochem. Communication.,* **2000**, 2, 503–507

97. B. Koslowski, H. G. Boyen, C. Wilderotter, G. Ka¨stle, P. Ziemann, R. Wahrenberg and P. Oelhafen. *Surfase. Science.*, **2001**,475, 1–10.

98. V. Borman, M. Pushkin, V. Tronin and V. Troyan,J. *Expermental Theoretical Physics,* **2010**, 110, 1005–1025.

99. Zafeiratos S. and Kennou S.*Surface. Science.*, **1999**, 443, 238–244.

100. Muggli D. S., Ding L. *Applied Catalysis B: Environmental,* **2001,** 32, 181–194.

101. Adnan R. A., Gunther G., Andersson G. G., Polson M. J. J., Metha G. F. and Golovko V. B. *Catalyst Science Technology,* **2015,** 5,1323.

102. Balasubramanian R. , R. Guo R., A. J. Mills A. J. and R. W. Murray R. W., *Journal American Chemical. Society,* **2005**, 127, 8126–8132.

103. Kamat P. V. *Journal Physical Chemistr*y *B*, **2002**, 106, 7729–7744.

104. S. Link S. and El-Sayed M. A. *Annual . Review Physical Chemistry*, **2003,** 54, 331–366.

105. Gunter P. L. J., Niemantsverdriet J. W, Ribeiro F. H. and Somorjai G. A.,*Catalyts Review: Science Engineering*, **1997**, 39, 77–168.

106. Ribeiro F. H., Somorjai G. A., G. Wedler B. C., Gates C. T., Campbell, C. Xu, D. W. Goodman, A. Zecchina, D. Scarano, S. Bordiga, A. Cimino, F. S. Stone, Y. Iwasawa, M. A. Barteau, J. M. Vohs and J. P. Vigneron, *Handbook of Heterogeneous Catalysis,* **2008**, 771–908.

107. Colón G., Hidalgo M. C. and Nav´ıo J. A. *Applied Catalysis B: Environmental* **2003,** 45, 39–50.

108. Barraud E., Bosc F., Edwards D, Keller N, and Keller V. *Journal of Catalysis,* **2005,** 235, 318–326.

109. Datye, A. K.; Riegel, G.; Bolton, J. R.; Huang, M.; Prairie, M. R., *Journal of Solid State* **1995,** 115*,* 236-239.

110. Deng H., Qiu Y. and Yang S. *Journal of Materials Chemistry*, **2009**,19, 976-982.

111. Garcia M. A. S., Silvestre D. M, Nomura C. S and Rossi L. M. *Journal of the Brazilian Chemical Society,* **2015,** 26.

112. Siddique M., Khan R., Khan A. F. and Farooq R. *Journal Chemical Society of Pakistan.*, **2014,** 36, 1.

113. Hidalgo M. C., Maicu M., Jose A. Navıo J. A., and Colo G. *Journal of Physical Chemistry C,* **2009,** 113, 12840-12847.

114. Valden M., X. Lai and D. W. Goodman, *Science,* **1998**, 281, 1647–1650.

Appendix:

XPS Peak Fits of Au_9 on Acid-Washed P25 Titania

0.17% w/w

As-Prepared

Before Heating **After Heating**

Before Heating			**After Heating**		
Peak	Position (eV)	FWHM (eV)	Peak	Position (eV)	FWHM (eV)
LBP – 7/2	85.13	1.945	LBP – 7/2	84.61	1.666
LBP – 5/2	88.80	1.945	LBP – 5/2	88.28	1.666
Silicon Satellite	89.72	1.577	HBP – 7/2	86.03	1.666
Silicon Satellite	91.42	1.577	HBP – 5/2	89.7	1.666
			Silicon Satellite	90.10	1.75
			Silicon Satellite	91.80	1.75

0.17% w/w

Vacuum-Calcined

Before Heating **After Heating**

Before Heating			**After Heating**		
Peak	Position (eV)	FWHM (eV)	Peak	Position (eV)	FWHM (eV)
LBP – 7/2	84.08	1.903	LBP – 7/2	84.67	1.665
LBP – 5/2	87.75	1.903	LBP – 5/2	88.34	1.665
HBP – 7/2	86.15	1.903	Silicon	91.61	1.18

			Satellite		
HBP – 5/2	89.82	1.903	Silicon Satellite	89.91	1.18
Silicon Satellite	91.55	1.773			
Silicon Satellite	89.85	1.773			

Note – fitting the spectrum of the sample after heating with a second doublet afforded negligible improvement on the goodness of the fit, and so was excluded.

0.34% w/w

<u>As-Prepared</u>

Before Heating **After Heating**

Before Heating			**After Heating**		
Peak	Position (eV)	FWHM (eV)	Peak	Position (eV)	FWHM (eV)
LBP – 7/2	85.22	2.038	LBP – 7/2	84.85	1.801
LBP – 5/2	88.89	2.038	LBP – 5/2	88.52	1.801
Silicon Satellite	91.31	1.653	HBP – 7/2	86.16	1.358
Silicon Satellite	89.61	1.653	HBP – 5/2	89.83	1.358
			Silicon Satellite	91.81	1.625
			Silicon Satellite	90.11	1.625

0.34% w/w

Vacuum-Calcined

Before Heating **After Heating**

Before Heating			**After Heating**		
Peak	Position (eV)	FWHM (eV)	Peak	Position (eV)	FWHM (eV)
LBP – 7/2	83.99	1.882	LBP – 7/2	84.39	1.677
LBP – 5/2	87.66	1.882	LBP – 5/2	88.06	1.677
HBP – 7/2	85.91	1.882	HBP – 7/2	86.22	1.677
HBP – 5/2	89.58	1.882	HBP – 5/2	89.89	1.677
Silicon Satellite	91.31	1.212	Silicon Satellite	92.01	1.812
Silicon Satellite	89.61	1.212	Silicon Satellite	90.31	1.812

0.5% w/w

As-Prepared # 1

Before Heating **After Heating**

Before Heating			**After Heating**		
Peak	Position (eV)	FWHM (eV)	Peak	Position (eV)	FWHM (eV)
LBP – 7/2	85.31	1.862	LBP – 7/2	85.38	2.012
LBP – 5/2	88.98	1.862	LBP – 5/2	89.05	2.012
Silicon Satellite	91.41	1.274	Silicon Satellite	91.49	1.837
Silicon Satellite	89.71	1.274	Silicon Satellite	89.79	1.837

0.5% w/w

As-Prepared # 2

Before Heating **After Heating**

Before Heating			**After Heating**		
Peak	Position (eV)	FWHM (eV)	Peak	Position (eV)	FWHM (eV)
LBP – 7/2	85.24	1.651	LBP – 7/2	84.38	1.373
LBP – 5/2	88.91	1.651	LBP – 5/2	88.05	1.373
Silicon Satellite	91.26	1.208	HBP – 7/2	85.87	1.576
Silicon Satellite	89.56	1.208	HBP – 5/2	89.54	1.576
			Silicon Satellite	91.71	1.373
			Silicon Satellite	90.01	1.373

0.5% w/w

Vacuum-Calcined # 1

Before Heating **After Heating**

Before Heating			**After Heating**		
Peak	Position (eV)	FWHM (eV)	Peak	Position (eV)	FWHM (eV)
LBP – 7/2	84.15	1.623	LBP – 7/2	84.43	1.593
LBP – 5/2	87.82	1.623	LBP – 5/2	88.1	1.593
HBP – 7/2	85.55	1.623	HBP – 7/2	85.85	1.593
HBP – 5/2	89.22	1.623	HBP – 5/2	89.52	1.593
Silicon Satellite	91.36	1.5	Silicon Satellite	91.36	1.434
Silicon Satellite	89.66	1.5	Silicon Satellite	89.66	1.593

0.5% w/w

Vacuum-Calcined # 2

Before Heating **After Heating**

Before Heating			**After Heating**		
Peak	Position (eV)	FWHM (eV)	Peak	Position (eV)	FWHM (eV)
LBP – 7/2	85.64	1.592	LBP – 7/2	84.53	1.639
LBP – 5/2	89.31	1.592	LBP – 5/2	88.2	1.639
HBP – 7/2	84.11	1.592	HBP – 7/2	86.09	1.639

HBP – 5/2	87.78	1.592	HBP – 5/2	89.76	1.639
Silicon Satellite	91.25	1.307			

0.5% w/w

Vacuum-Calcined # 3

Before Heating **After Heating**

Before Heating			**After Heating**		
Peak	Position (eV)	FWHM (eV)	Peak	Position (eV)	FWHM (eV)
LBP – 7/2	84.27	1.647	LBP – 7/2	84.42	1.591
LBP – 5/2	87.94	1.647	LBP – 5/2	88.09	1.591
HBP – 7/2	85.77	1.647	HBP – 7/2	85.91	1.591
HBP – 5/2	89.44	1.647	HBP – 5/2	89.58	1.591
Silicon Satellite	91.15	1.116	Silicon Satellite	91.3	1.209
Silicon Satellite	89.25	1.116	Silicon Satellite	89.4	1.209

XPS Peak Fits of Au_9 on Bare P25 Titania

0.17% w/w

As-Prepared

Before Heating **After Heating**

Before Heating			**After Heating**		
Peak	Position (eV)	FWHM (eV)	Peak	Position (eV)	FWHM (eV)
LBP – 7/2	83.16	2.239	LBP – 7/2	87.95	2.759
LBP – 5/2	86.83	2.239	LBP – 5/2	91.62	2.759

HBP – 7/2	86.08	2	HBP – 7/2	85.09	1.358
HBP – 5/2	89.75	2	HBP – 5/2	88.76	1.358

Note: As no silicon peak was detected, silicon satellite peaks are excluded.

0.17% w/w

Vacuum-Calcined

Before Heating **After Heating**

Before Heating			**After Heating**		
Peak	Position (eV)	FWHM (eV)	Peak	Position (eV)	FWHM (eV)
LBP – 7/2	83.63	2.247	LBP – 7/2	83.56	0.746
LBP – 5/2	87.3	2.247	LBP – 5/2	87.23	0.746
HBP – 7/2	86.62	2.935	HBP – 7/2	85.6	3.954
HBP – 5/2	90.29	2.935	HBP – 5/2	89.27	3.954

Note: As no silicon peak was detected, silicon satellite peaks are excluded.

0.34%

As-Prepared

Before Heating **After Heating**

Before Heating			**After Heating**		
Peak	Position (eV)	FWHM (eV)	Peak	Position (eV)	FWHM (eV)
LBP – 7/2	84.02	2.606	LBP – 7/2	84.05	2.639
LBP – 5/2	87.69	2.606	LBP – 5/2	87.72	2.639

HBP – 7/2	87.13	2.606	HBP – 7/2	87.13	3.348
HBP – 5/2	90.8	2.606	HBP – 5/2	90.8	3.348

Note: As no silicon peak was detected, silicon satellite peaks are excluded.

0.5%

<u>As-Prepared #1</u>

Before Heating **After Heating**

Before Heating			**After Heating**		
Peak	Position (eV)	FWHM (eV)	Peak	Position (eV)	FWHM (eV)
LBP – 7/2	83.93	2.487	LBP – 7/2	85.37	5
LBP – 5/2	87.6	2.487	LBP – 5/2	89.04	5
HBP – 7/2	87.46	3.468			
HBP – 5/2	91.13	3.468			

Note: As no silicon peak was detected, silicon satellite peaks are excluded.

Note: When fitting the after-heated spectrum, no HBP could be successfully fit at a binding energy below 88 eV, and so was excluded.

0.5%

<u>As-Prepared #2</u>

Before Heating **After Heating**

Before Heating			**After Heating**		
Peak	Position	FWHM (eV)	Peak	Position	FWHM (eV)

	(eV)			(eV)	
LBP – 7/2	85.12	3.021	LBP – 7/2	84.7	1.417
LBP – 5/2	88.79	3.021	LBP – 5/2	88.37	1.417
HBP – 7/2	86.61	3.936	HBP – 7/2	85.28	3
HBP – 5/2	90.28	3.936	HBP – 5/2	88.95	3

Note: As no silicon peak was detected, silicon satellite peaks are excluded.

Kinetics Studies

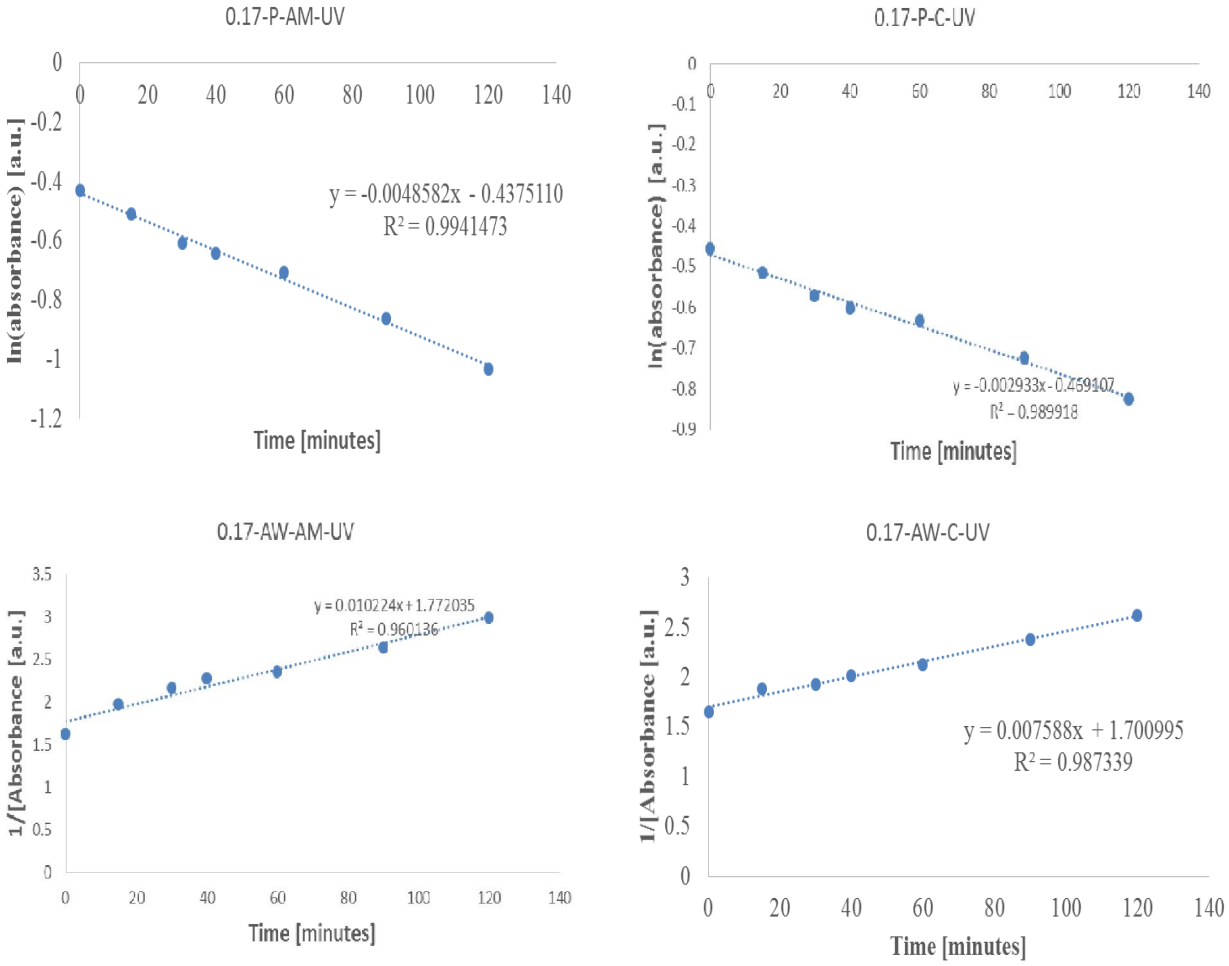

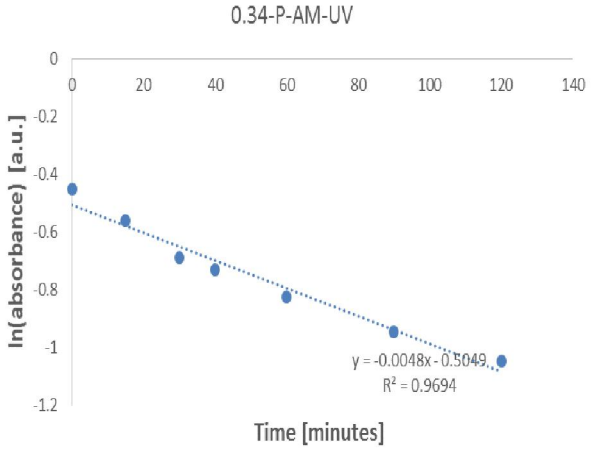
0.34-P-AM-UV
ln(absorbance) [a.u.]
Time [minutes]
y = -0.0048x - 0.5049
R² = 0.9694

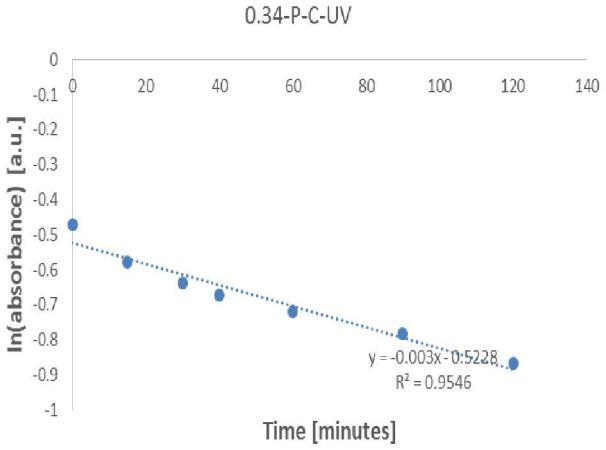
0.34-P-C-UV
ln(absorbance) [a.u.]
Time [minutes]
y = -0.003x - 0.5228
R² = 0.9546

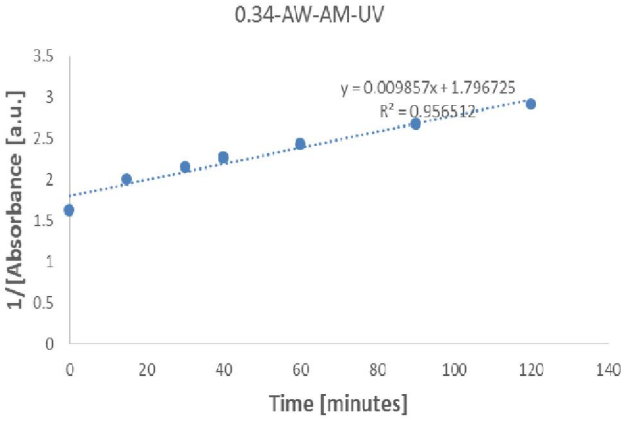
0.34-AW-AM-UV
1/[Absorbance [a.u.]
Time [minutes]
y = 0.009857x + 1.796725
R² = 0.956512

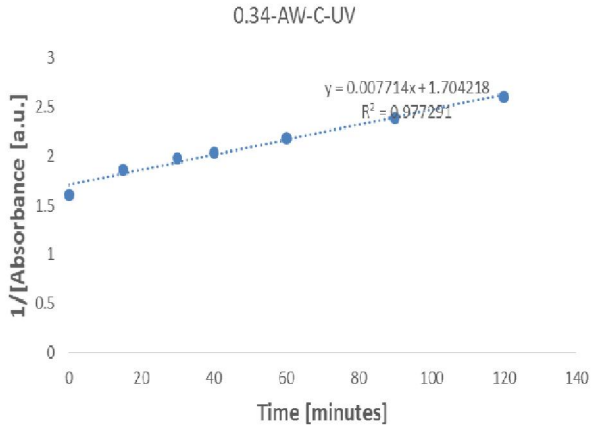
0.34-AW-C-UV
1/[Absorbance [a.u.]
Time [minutes]
y = 0.007714x + 1.704218
R² = 0.977291

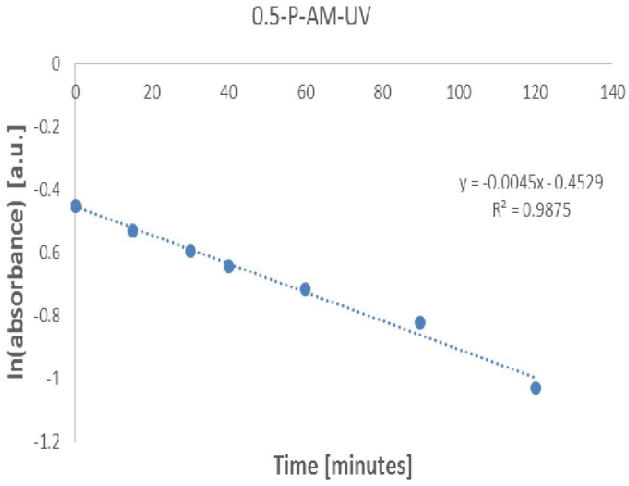
0.5-P-AM-UV
ln(absorbance) [a.u.]
Time [minutes]
y = -0.0045x - 0.4529
R² = 0.9875

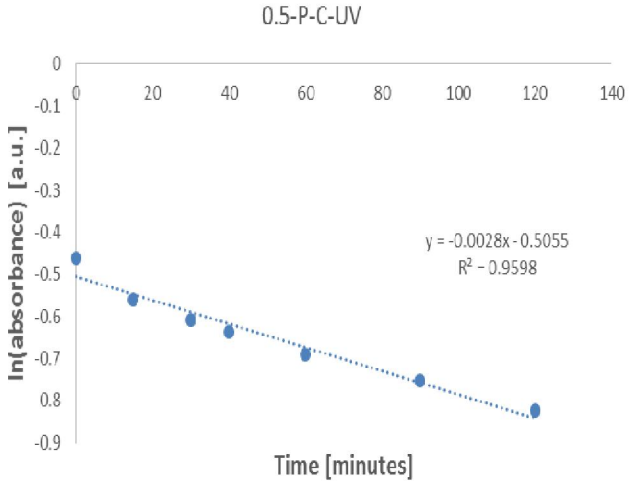
0.5-P-C-UV
ln(absorbance) [a.u.]
Time [minutes]
y = -0.0028x - 0.5055
R² = 0.9598

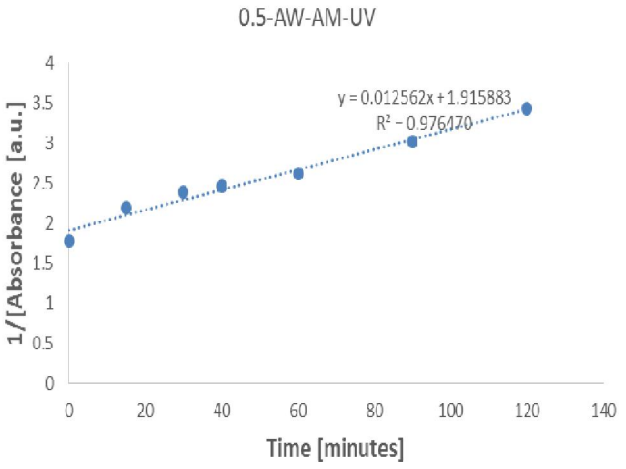
0.5-AW-AM-UV
y = 0.012562x + 1.915883
R² = 0.976470
1/[Absorbance [a.u.]
Time [minutes]

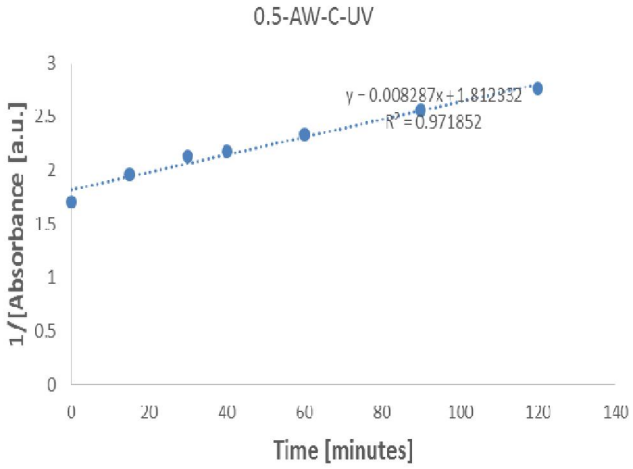
0.5-AW-C-UV
y = 0.008287x + 1.812332
R² = 0.971852
1/[Absorbance [a.u.]
Time [minutes]

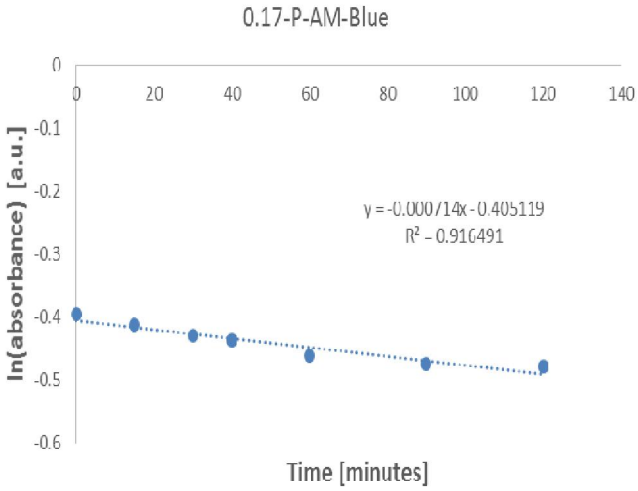
0.17-P-AM-Blue
y = -0.000714x - 0.405119
R² = 0.916491
ln(absorbance) [a.u.]
Time [minutes]

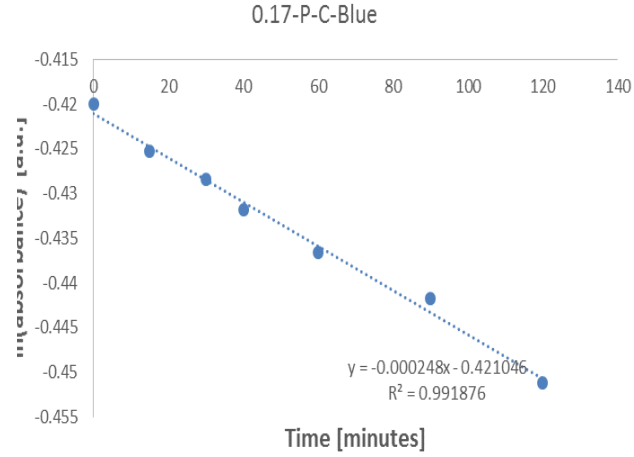
0.17-P-C-Blue
y = -0.000248x - 0.421046
R² = 0.991876
Time [minutes]

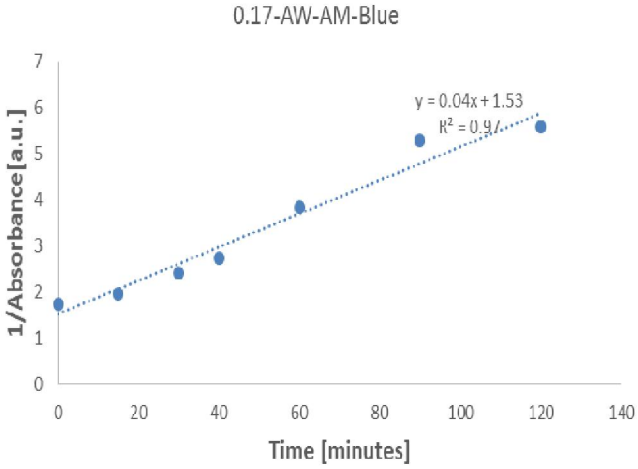
0.17-AW-AM-Blue
y = 0.04x + 1.53
1/Absorbance[a.u.]
Time [minutes]

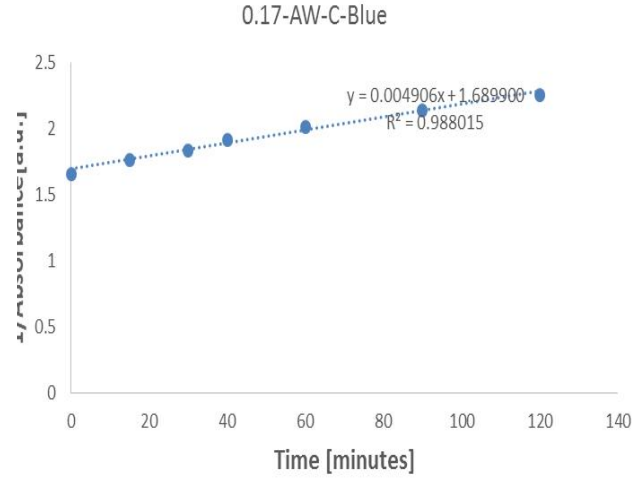
0.17-AW-C-Blue
y = 0.004906x + 1.689900
R² = 0.988015
Time [minutes]

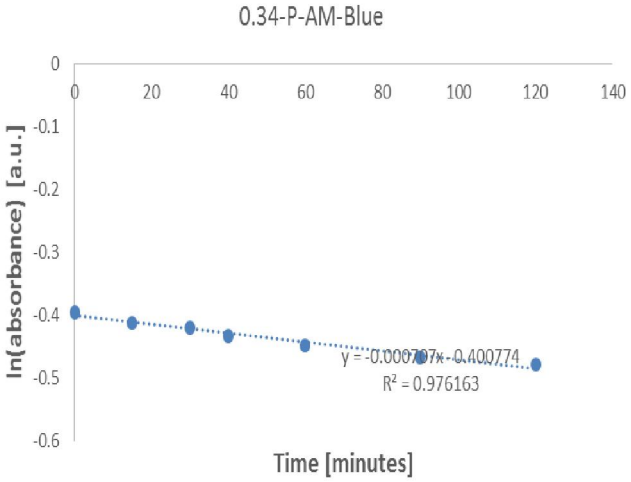
0.34-P-AM-Blue
ln(absorbance) [a.u.]
Time [minutes]
y = -0.000797x - 0.400774
R² = 0.976163

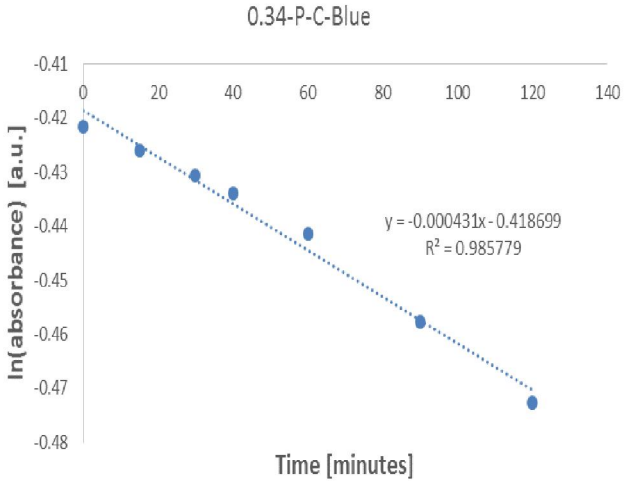
0.34-P-C-Blue
ln(absorbance) [a.u.]
Time [minutes]
y = -0.000431x - 0.418699
R² = 0.985779

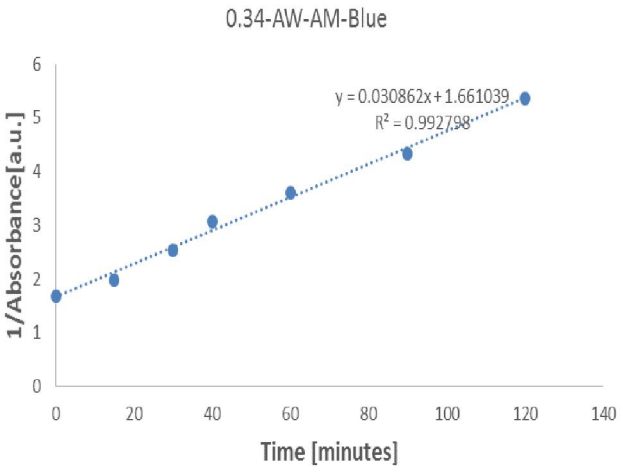
0.34-AW-AM-Blue
1/Absorbance[a.u.]
Time [minutes]
y = 0.030862x + 1.661039
R² = 0.992798

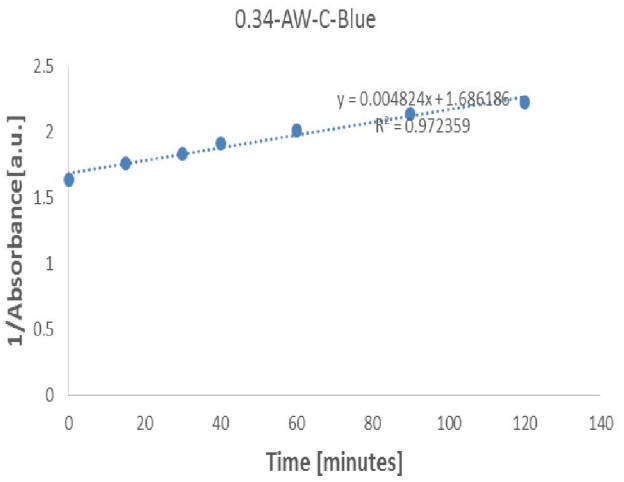
0.34-AW-C-Blue
1/Absorbance[a.u.]
Time [minutes]
y = 0.004824x + 1.686186
R² = 0.972359

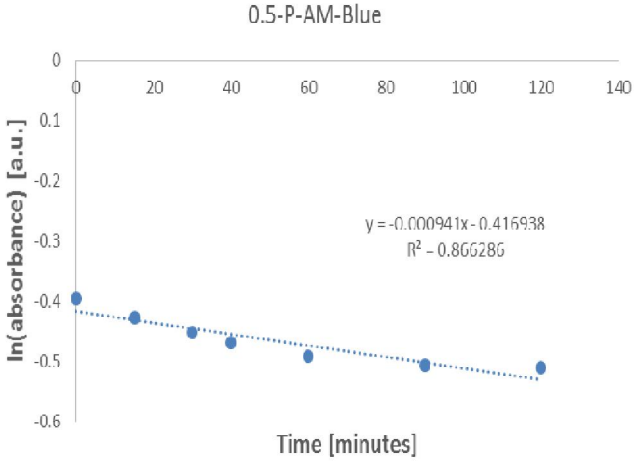
0.5-P-AM-Blue
ln(absorbance) [a.u.]
Time [minutes]
y = -0.000941x - 0.416938
R² = 0.866286

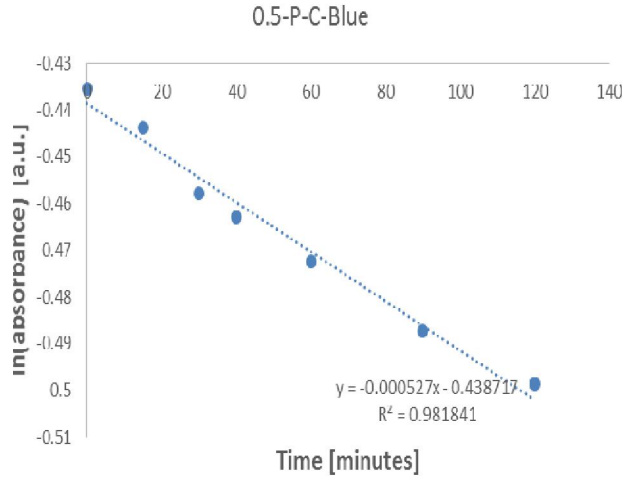
0.5-P-C-Blue
ln(absorbance) [a.u.]
Time [minutes]
y = -0.000527x - 0.438717
R² = 0.981841

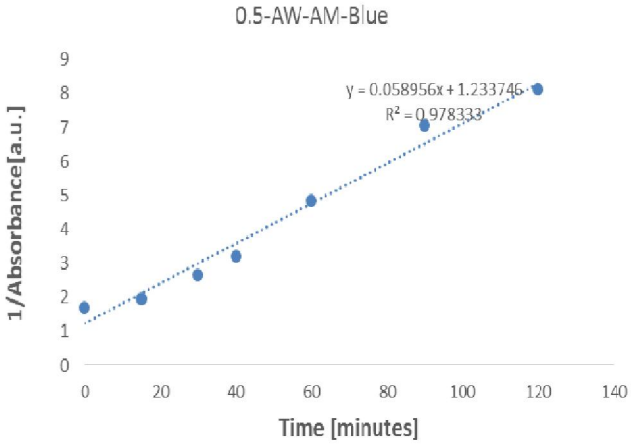
0.5-AW-AM-Blue
y = 0.058956x + 1.233746
R² = 0.978333
1/Absorbance[a.u.]
Time [minutes]
0
1
2
3
4
5
6
7
8
9
0
20
40
60
80
100
120
140

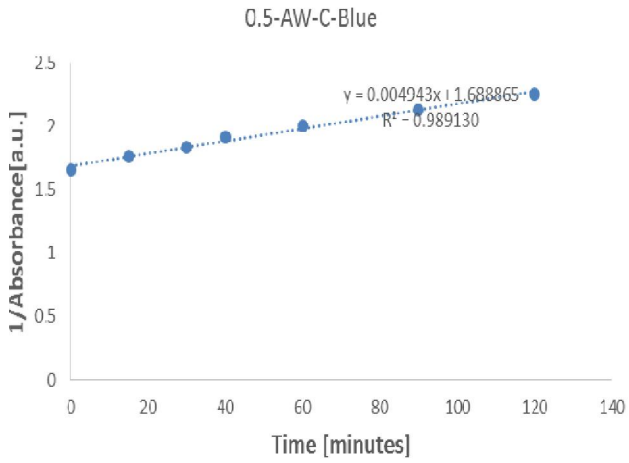
0.5-AW-C-Blue
y = 0.004943x + 1.688865
R² = 0.989130
1/Absorbance[a.u.]
Time [minutes]
0
0.5
1
1.5
2
2.5
0
20
40
60
80
100
120
140